AD-A034 490 EMMANUEL COLL BOSTON MASS F/G 20/14
STUDY AND ANALYSIS OF TOTAL ELECTRON CONTENT AND SCINTILLATION --ETC(U)
OCT 76 S BASU, C J CANTOR, J JOHANSON F19628-76-C-0003
UNCLASSIFIED SCIENTIFIC-1 AFGL-TR-76-0260 NL

1 OF 2
AD A034490

AFGL-TR-76-0260

STUDY AND ANALYSIS OF TOTAL ELECTRON CONTENT AND SCINTILLATION DATA

Santimay Basu
Charles J. Cantor
James Johanson
Eileen MacKenzie
M. Patricia Hagan

The Trustees of Emmanuel College
400 The Fenway
Boston, Massachusetts 02115

October 1976

Scientific Report No. 1

Approved for public release; distribution unlimited.

AIR FORCE GEOPHYSICS LABORATORY
AIR FORCE SYSTEMS COMMAND
UNITED STATES AIR FORCE
HANSCOM AFB, MASSACHUSETTS 01731

MIL-STD-847A
31 January 1973

UNCLASSIFIED
SECURITY CLASSIFICATION OF THIS PAGE (When Data Entered)

(19) REPORT DOCUMENTATION PAGE	READ INSTRUCTIONS BEFORE COMPLETING FORM
(18) 1. REPORT NUMBER: AFGL-TR-76-0260 ✓	2. GOVT ACCESSION NO. 3. RECIPIENT'S CATALOG NUMBER (14)
(6) 4. TITLE (and Subtitle): Study and Analysis of Total Electron Content and Scintillation Data, ✓	5. TYPE OF REPORT & PERIOD COVERED: Scientific [redacted] 1 ✓ 01JUL75 - 30JUN76
	6. PERFORMING ORG. REPORT NUMBER
(10) 7. AUTHOR(s): Santimay Basu, Eileen MacKenzie, Charles J. Cantor, M. Patricia Hagan, James Johanson	8. CONTRACT OR GRANT NUMBER(s): F19628-76-C-0003 NEW (15)
9. PERFORMING ORGANIZATION NAME AND ADDRESS: Emmanuel College, 400 The Fenway, Boston MA 02115 ✓ (16)	10. PROGRAM ELEMENT, PROJECT, TASK AREA & WORK UNIT NUMBERS: 62101F, 46430103 (17) Φ1
11. CONTROLLING OFFICE NAME AND ADDRESS: Air Force Geophysics Laboratory (PHP), Hanscom AFB MA 01731, Contract Monitor: Herbert E. Whitney (11)	12. REPORT DATE: Oct[redacted]76 (13) 13. NUMBER OF PAGES: 105
14. MONITORING AGENCY NAME & ADDRESS (if different from Controlling Office) (12)	15. SECURITY CLASS. (of this report): Unclassified; 15a. DECLASSIFICATION/DOWNGRADING SCHEDULE

16. DISTRIBUTION STATEMENT (of this Report)

A - Approved for public release; distribution unlimited.

17. DISTRIBUTION STATEMENT (of the abstract entered in Block 20, if different from Report)

TECH, OTHER

(9) 18. SUPPLEMENTARY NOTES

Rept. for 1 Jul 75-30 Jun 76

19. KEY WORDS (Continue on reverse side if necessary and identify by block number)

Autocorrelation Studies	Equatorial Electrojet
Computer Programming	Faraday Rotation
Cross Correlation	Group Delay
Dwell Time	Invariant Latitude

(over)

20. ABSTRACT (Continue on reverse side if necessary and identify by block number)

(See reverse side)

DD FORM 1 JAN 73 1473 EDITION OF 1 NOV 65 IS OBSOLETE

UNCLASSIFIED
SECURITY CLASSIFICATION OF THIS PAGE (When Data Entered)

125 950

UNCLASSIFIED
SECURITY CLASSIFICATION OF THIS PAGE(When Data Entered)

19.

Ionosphere	Scattering Domain (weak)
Irregularity Region	Scintillation
$\overline{M}$-Value	Signal Analysis
Model Equations	Spectral Index of Scintillation
Plasmasphere	Sporadic-E (E_{sq})
Power Spectra	Total Electron Content (TEC)
Radar Echoes	Type 1 Irregularities
Scattering Domain (strong)	Type 2 Irregularities

20. ABSTRACT

This report embodies a study of Ionospheric Scintillations as considered from the following aspects:

1) Overall view of scintillations using a large data base, and also the detailed, individual magnetic storm picture. Solar flux level, seasonal variation, invariant latitude, and irregularity region are discussed.

2) Total Electron Content measurements through Faraday Rotation and Group Delay Methods. Results of employment of these techniques are discussed. The $\overline{M}$-factor, for conversion of Faraday Rotation angles is studied, and associated use of it is displayed through a program for which documentation is included.

3) Characteristics of scintillations in the weak and strong scatter regimes. Results on the frequency dependence of scintillations, power spectra, and autocorrelation of amplitude fluctuations are discussed.

4) Daytime VHF scintillations. Type 1, type 2, and E_{sq} irregularities are discussed.

5) A modification to the Signal Analysis Package, previously developed, is described. Application for use on the CDC 6600

E sub sq

UNCLASSIFIED
SECURITY CLASSIFICATION OF THIS PAGE(When Data Entered)

Table of Contents

I.

SCINTILLATIONS

During this period, work was done to focus on both the overall picture of scintillations using a large data base and the detailed, individual magnetic storm picture.

In conjunction with this first aim, a high-latitude model of scintillation has been developed using the observations of the existing data base of Narssarssuaq, Greenland, Goose Bay, Labrador and Sagamore Hill, Massachusetts. The available data consists of:

Narssarssuaq	9/17/68 - 9/1/74	146,700 + samples
Goose Bay	1/1/72 - 12/31/74	71,000 + samples
Sagamore Hill	12/1/69- 11/30/74	148,000 + samples

The model consists of equations which yield scintillations at 137 MHz as a function of local time, magnetic index, solar flux and month of the year.

A validation of this model was attempted using Millstone Hill data obtained by observing scintillations at 400 MHz tracking Transit satellites. The data base for the comparison was that in the publication "The Millstone Hill Radar Propagation Study: Scientific Results " by J. Evans.

Since Evans' data was in the S_4 format at 400 MHz, a conversion using weak scatter relationships must first be made to dB at 137 MHz. This is plotted in Figure 1.

The measured S_4 (400 MHz) as a function of invariant latitude is shown in Figure 2. These values, in three different K_p groupings, at the invariant latitude of Narssarssuaq, Goose Bay and Sagamore Hill, along with the conversion to dB (137 MHz) are shown below.

NSSQ (Λ = 63°)

	S_4 (400 MHz)	dB (137MHz)
$K_p \leq 1+$	.0375	2.5
$2_o \leq K_p \leq 3+$	.05	3.6
$K_p \geq 4_o$	.0775	6.3

Goose Bay (Λ = 60°)

	S_4 (400 MHz)	dB (137 MHz)
$K_p \leq 1+$	.025	1.5
$2_o \leq K_p \leq 3+$	.030	1.9
$K_p \geq 4_o$	.055	4.0

Sagamore Hill (Λ = 54°)

	S_4 (400 MHz)	dB (137 MHz)
$K_p \leq 1+$	.016	.8
$2_o \leq K_p \leq 3+$	.018	1.0
$K_p \geq 4_o$	.021	1.2

This data used by Evans was taken in 1972-1973 and was averaged over local time to include all passes. The model dB values are obtained by using the local time equations developed for each station for 3 particular K_p values. A solar flux level of $S_f = 108$ was used since solar flux in 1972-73 was of this magnitude. The resulting averages over all hours and all months are:

Narssarssuaq (63° Λ)

	dB (137 MHz)	S_4 (400 MHz)
$K_p = .5$	2.5	.0375
$K_p = 2.5$	4.0	.053
$K_p = 5.0$	6.3	.0775

Goose Bay (60° Λ)

	dB (137 MHz)	S_4 (400 MHz)
$K_p = .5$	.3	.012
$K_p = 2.5$	1.6	.026
$K_p = 5.0$	4.8	.063

Sagamore Hill (54° Λ)

	dB (137 MHz)	S_4 (400 MHz)
$K_p = .5$	.55	.014
$K_p = 2.5$	.75	.0155
$K_p = 5.0$	1.23	.022

The model dB values (converted to S_4) are shown as individual points in Figure 2 to facilitate comparison with Evans' data.

The results of Evan's data and the model dB values predicted are in good agreement for both Narssarssuaq and Sagamore Hill. At Goose Bay, the model values are much lower for the low magnetic activity case, somewhat lower for the case K_p=2.5 and higher for the case K_p=5.0.

It is believed that the position of the trough is approximately the invariant latitude of Goose Bay under quiet magnetic conditions, moving farther south as the level of magnetic activity increases. The model data of Goose Bay reflects this picture.

Using this same data base, the seasonal variation of data taken at Narssarssuaq, Greenland, Goose Bay, Labrador, and Sagamore Hill, Massachusetts was also examined. Contour plots have been generated using month of the year versus time of day for each individual station. There is a further breakdown of the data into low and high magnetic index groups. For the Narssarssuaq observations, (Figures 3 and 4) the 350 km. intersection point is 63°Λ. There are striking seasonal contrasts between summer and winter data for both low and high Kp. The December-February period shows uniform mean SI for both low and high Kp with relatively little diurnal pattern although the level is raised for higher magnetic activity. The April-June contours show a strong diurnal pattern with higher mean SI for Kp=4-9. Peak scintillation appears $\sim$ 2300 LST while the lowest levels are noted during the months of April-June at 08-13 LST.

For the Goose Bay observations, Figures 5 and 6, the 350 km. intersection point is 60°Λ. A higher elevation angle shows smaller mean scintillation indices than the Narssarssuaq data. Under quiet magnetic conditions, Kp=0-3, very low mean indices exist for the period of November-January with little diurnal variation. Maximum scintillation occurs in the March-May period with a definite diurnal pattern. The peak values occur ~2100 LST. However, at Goose Bay the higher magnetic activity case is not simply an enhancement of the low Kp case as occurs at Narssarssuaq. For Kp=4-9, minimum SI occurs for the period December-February with a small diurnal variation which reaches a peak ~1-2 hours after magnetic midnight. The maximum activity occurs in the months of July-August with peak values also occurring ~ 1-2 hours after magnetic midnight. The seasonal maximum and minimum though distinguishable, are not as sharply defined as at Narssarssuaq.

The seasonal pattern for Sagamore Hill (at an intersection of 53°Λ) differs from that of the higher latitude stations. The irregularities are mainly confined to the hours of darkness for both low and high magnetic activity, with the peak daily values occurring ~1-3 hours after magnetic midnight, (Fig. 7&8) For Kp=0-3, the seasonal minimum occurs in May-August; for Kp=4-9, it occurs in April-June. The seasonal maximum appears to take place during the equinoctial months; February-April and September-November, with an extension of the highest contours throughout the period July-April when Kp is high.

These Sagamore Hill observations are felt to be mid-latitude for the Kp indices considered while both Narssarssuaq and Goose Bay show the sensitivity to magnetic variations characteristic of high latitude stations.

For a more complete view of scintillations, a detailed picture examining individual magnetic storms is needed in addition to the overall picture provided by seasonal contours and the model. To this end, a magnetic storm atlas has been proposed including all the magnetic storms in the period November 1971-December 1972, as noted in the atlas produced by Mendillo and Klobuchar (1974). As prototype, data was collected for the magnetic storm of October 18-19, 1972.

On October 18, 1972 at 1746 UT, a magnetic storm commenced. The magnetic index, K_p, very low prior to the storm, reached K_p=3 at SSC, peaked at K_p=5 ∿ 0000 UT October 19, then fell to K_p=3 again ∿ 1500 UT on October 19.

Figure 9 is a plot of the 15-minute scintillation index as observed at Narssarssuaq, Goose Bay, Sagamore Hill and College. Narssarssuaq and Goose Bay exhibit a slightly delayed storm rise at 2030 and 2200 UT October 18 respectively. College scintillation responds with medium scintillation ∿ 0830 UT October 19, while Sagamore Hill shows only a sharp burst of scintillation ∿ 2330 UT October 18.

In Figure 10 is seen the Narssarssuaq and Ottawa magnetograms, and the Dst. Both magnetograms show moderate disturbance levels, peaking in the period 0000-1200 UT October 19. The Dst reaches a maximum value of -75 γ at 0900 UT October 19. This, combined with a moderate K_p index, points to the irregularity region developing slowly from a quiet day picture to a

moderately expanded version and then fading again. Thus, the College data does not show moderate scintillation activity until the irregularity region becomes developed enough to reach the latitude of its intersection point. Also, the College SI seems to show a seasonal response pattern, with the equinox response to magnetic storms differing from the winter dramatic disturbance pattern.

The total electron content plots of Narssarssuaq, Goose Bay and Sagamore Hill of October 18-19 (Fig. 11) reveal only slightly enhanced values at SSC on October 18. Nighttime TEC values show the increased TEC occurring during many nights with magnetic activity. In addition to somewhat higher values, spiky areas of activity are seen in the polarization records.

There is no clear indication in these records of a trough (DMSP pictures are not available for this period). The scintillation boundary, except for a brief period between 2330 UT October 18 and 0030 UT October 19, in the nighttime along the 75th meridian lies between Goose Bay and Sagamore Hill. This short period is seen in the contour map (Figure 12) just prior to 2400 October 19. At the same time, the 50% scintillation contour reaches a minimum of $\sim 56°\Lambda$ $\sim$ 0400 UT October 19. Perhaps the trough lies between the latitudes of Goose Bay and Sagamore Hill, but the synchronous satellite records cannot be used to determine the trough position in this case. The increase in scintillation index at Sagamore Hill at 2330 UT on October 18 is accompanied by an increase in TEC on the Sagamore Hill TEC records.

In addition to the local time component of scintillation shown by magnetic storms, a storm time component can be seen in the scintillation increases occurring during some magnetic storms. Data taken at various stations during the magnetic storms of August 1972 illustrate this.

For large magnetic storms when the plasmapause moves well equatorward of its usual quiettime location, a stormtime component of scintillations is recognizable at many midlatitude stations with invariant latitudes $<60°$. Figures 13 and 14 show the Dst index and scintillations observed at stations of varying invariant latitudes. The Dst index reached peak values $\sim$-100γ on August 4-6 and August 9. The high latitude stations exhibit high SI values during these periods but the stormtime component is more noticeable at the lower latitude stations of Sagamore Hill, Aberystwyth and Lindau. Even though these stations are separated 6 hours in local time. all show scintillation peaks $\sim$ 0400 UT on August 4, 0000 UT on August 5 and 0500 UT on August 6. These occur at times of Dst index increases and large TEC depletions at Sagamore Hill (Mendillo and Klobuchar, 1974). On August 9 $\sim$1200 UT, a similar peak occurs at these stations even though the local time of the stations is in the morning-noon sector.

The joint study of the general patterns of scintillation, when combined with the individual magnetic storm analysis should yield a more accurate picture of scintillation development and occurrence.

LIST OF FIGURES

Fig.13 Dst and Scintillation Index at Sagamore Hill, Narssarssuaq, and Goose Bay on 3-10 August 1972.

Fig.14 Scintillation Index at Narssarssuaq, Wales, Athens, and Lindau on 3-10 August 1972.

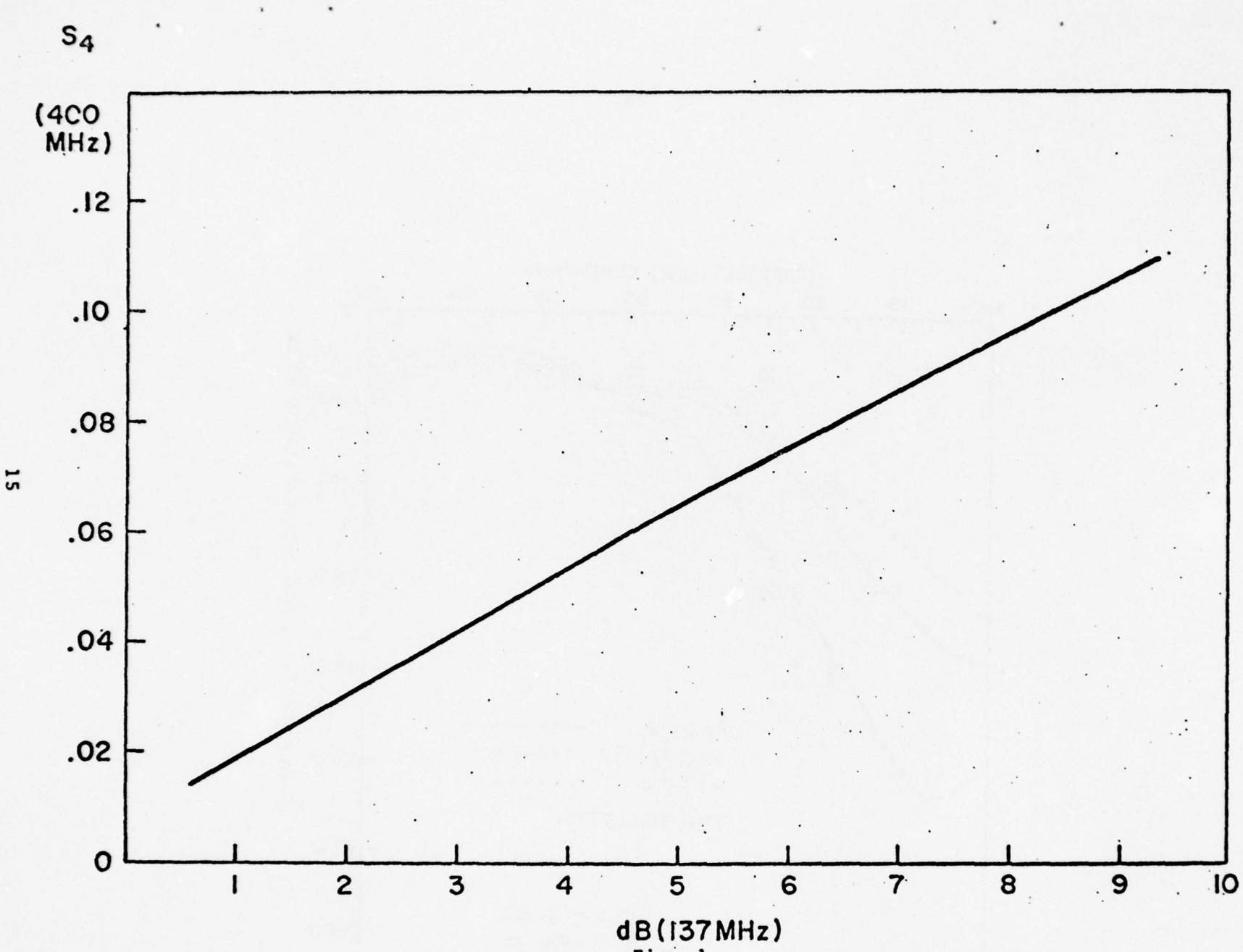

Fig. 1

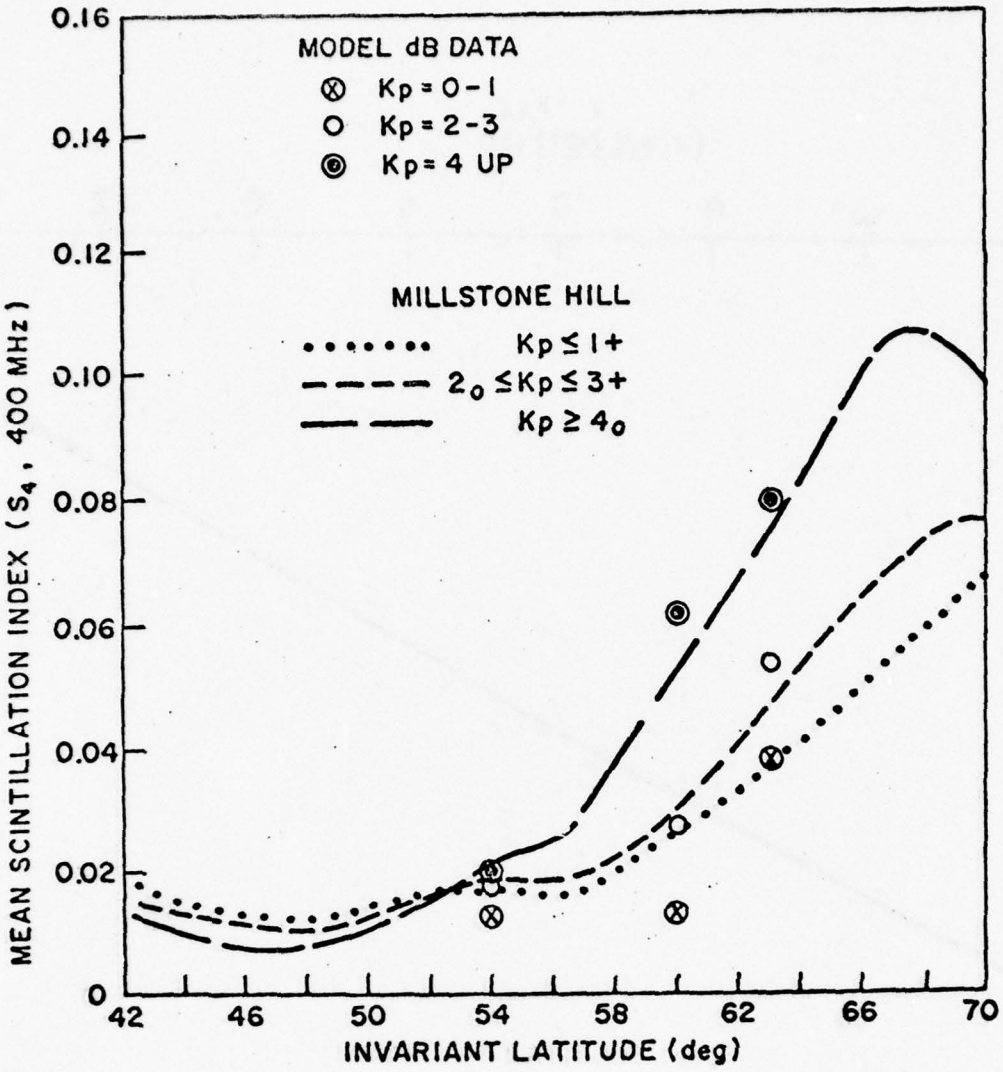
MODEL dB DATA
⊗ Kp = 0-1
O Kp = 2-3
◎ Kp = 4 UP
MILLSTONE HILL
Kp ≤ 1+
2₀ ≤ Kp ≤ 3+
Kp ≥ 4₀
MEAN SCINTILLATION INDEX (S4, 400 MHz)
0.16
0.14
0.12
0.10
0.08
0.06
0.04
0.02
0
42
46
50
54
58
62
66
70
INVARIANT LATITUDE (deg)

Fig. 2

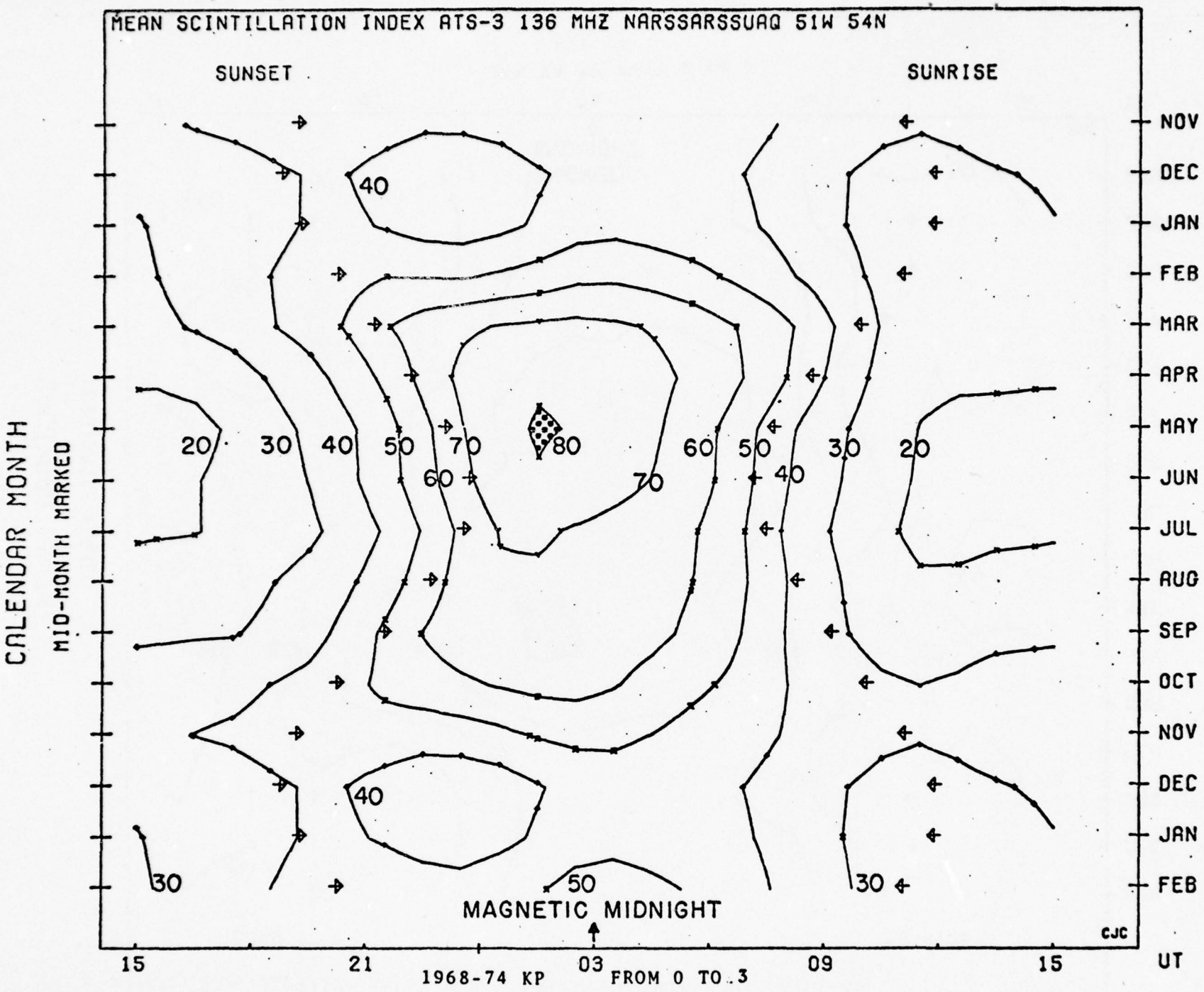
MEAN SCINTILLATION INDEX ATS-3 136 MHZ NARSSARSSUAQ 51W 54N
SUNSET
SUNRISE
CALENDAR MONTH
MID-MONTH MARKED
NOV
DEC
JAN
FEB
MAR
APR
MAY
JUN
JUL
AUG
SEP
OCT
NOV
DEC
JAN
FEB
20
30
40
50
60
70
80
MAGNETIC MIDNIGHT
CJC
15
21
03
09
15
UT
1968-74 KP FROM 0 TO 3

Fig. 3

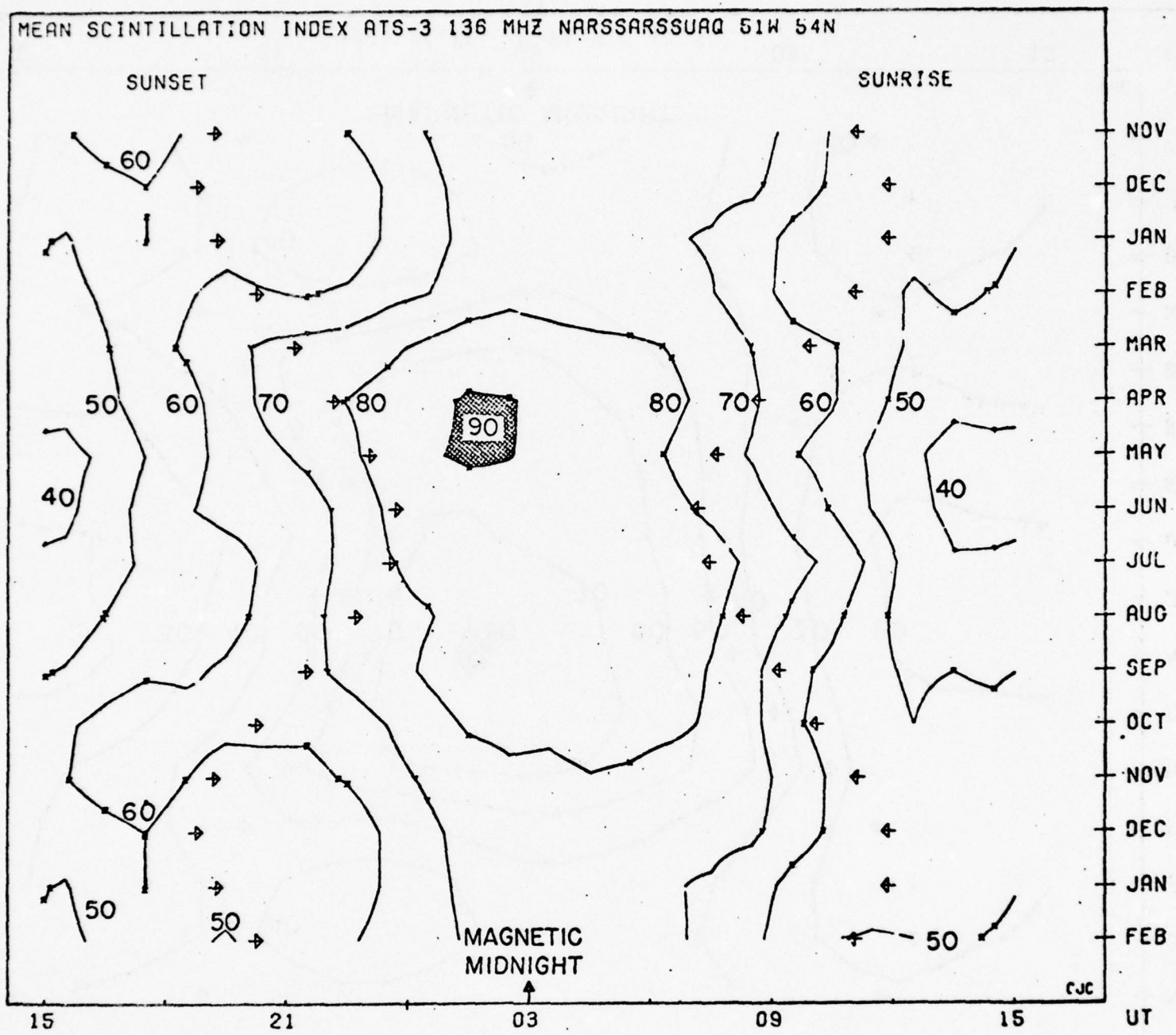

1968-74 KP FROM 4 TO 9

Fig. 4

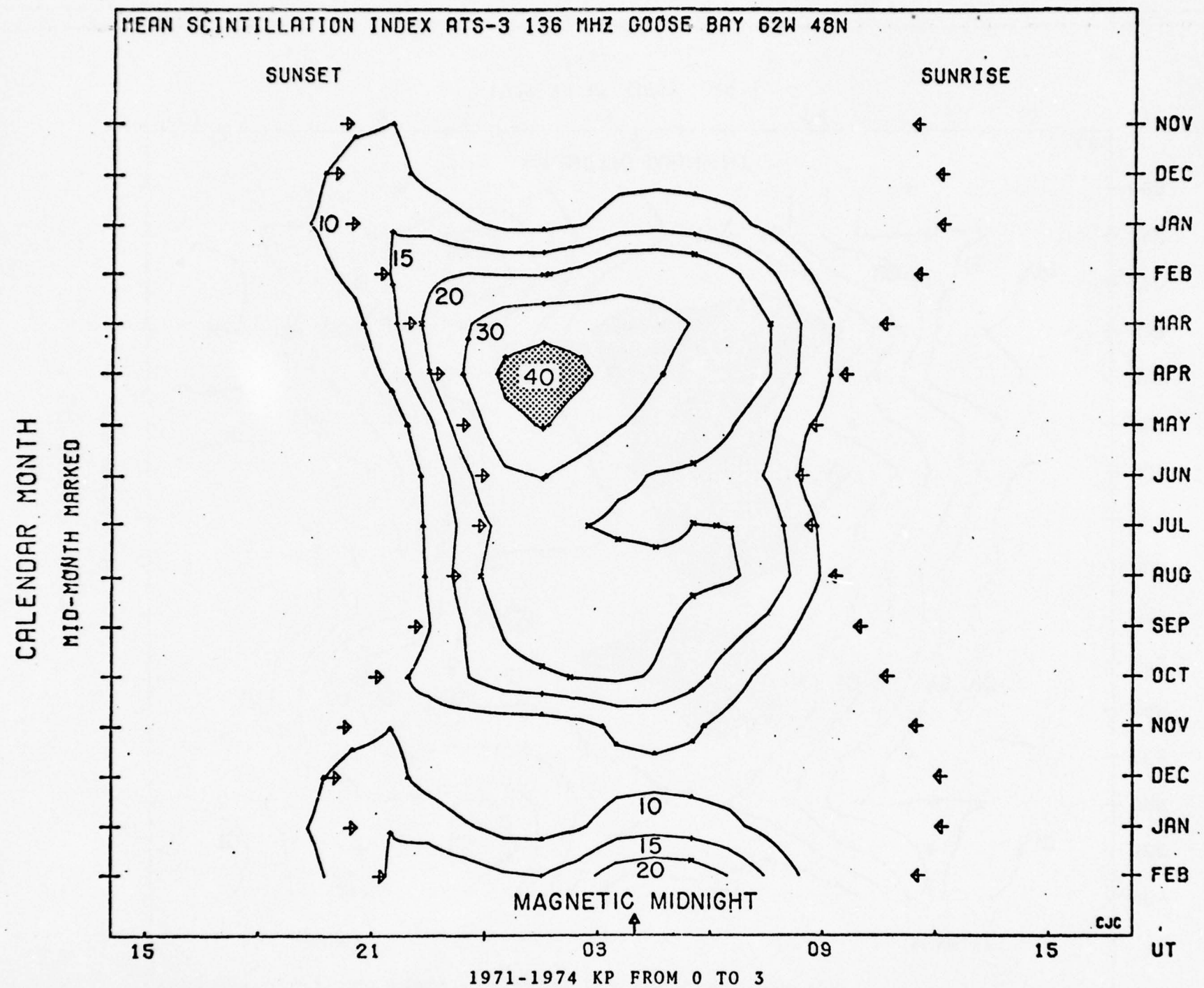
MEAN SCINTILLATION INDEX ATS-3 136 MHZ GOOSE BAY 62W 48N
SUNSET
SUNRISE
10
15
20
30
40
10
15
20
NOV
DEC
JAN
FEB
MAR
APR
MAY
JUN
JUL
AUG
SEP
OCT
NOV
DEC
JAN
FEB
CALENDAR MONTH
MID-MONTH MARKED
MAGNETIC MIDNIGHT
CJC
15
21
03
09
15
UT
1971-1974 KP FROM 0 TO 3

Fig. 5

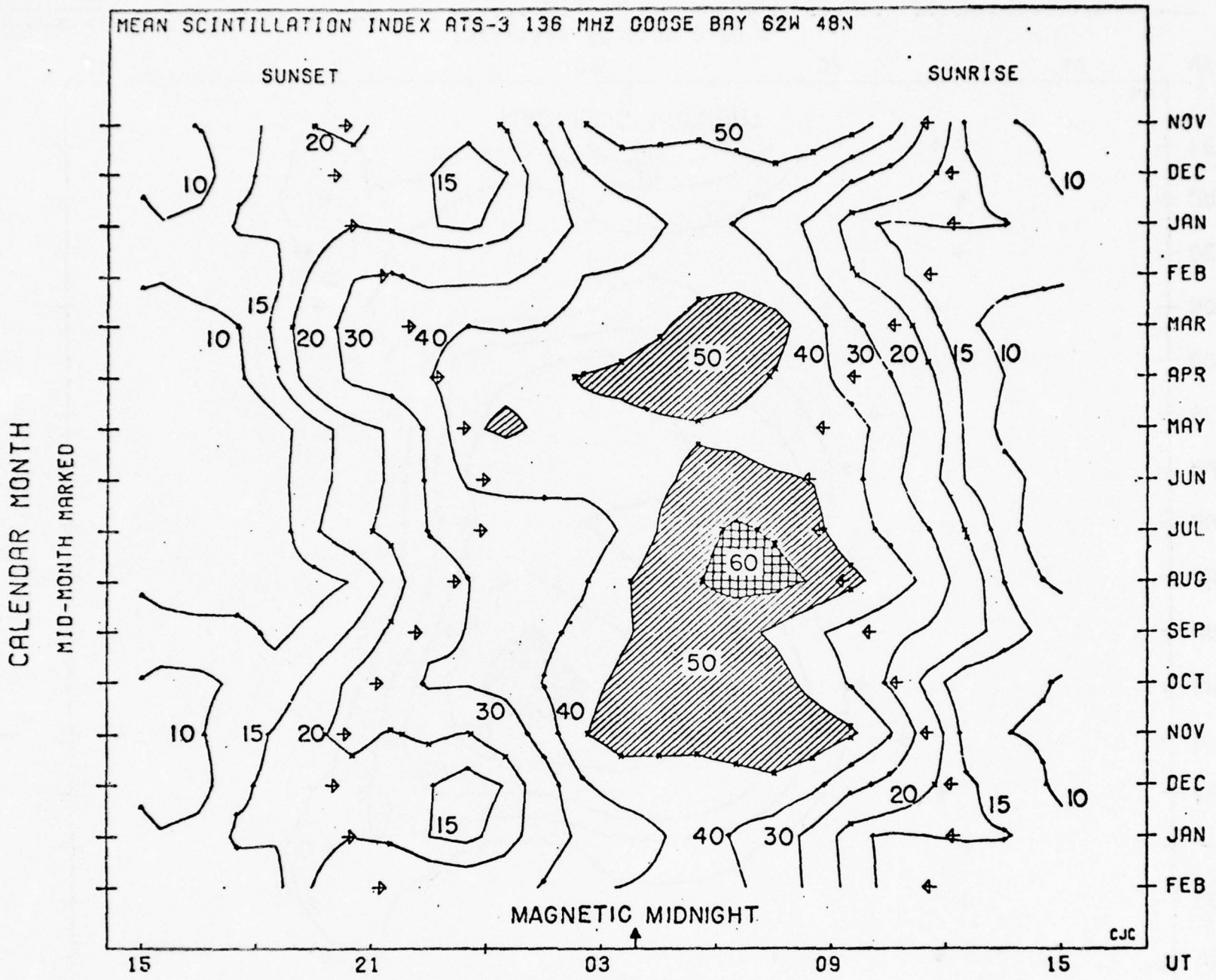
MEAN SCINTILLATION INDEX ATS-3 136 MHZ GOOSE BAY 62W 48N
SUNSET
SUNRISE
CALENDAR MONTH
MID-MONTH MARKED
NOV
DEC
JAN
FEB
MAR
APR
MAY
JUN
JUL
AUG
SEP
OCT
NOV
DEC
JAN
FEB
MAGNETIC MIDNIGHT
CJC
15
21
03
09
15
UT
1971-74 KP FROM 4 TO 9

Fig. 6

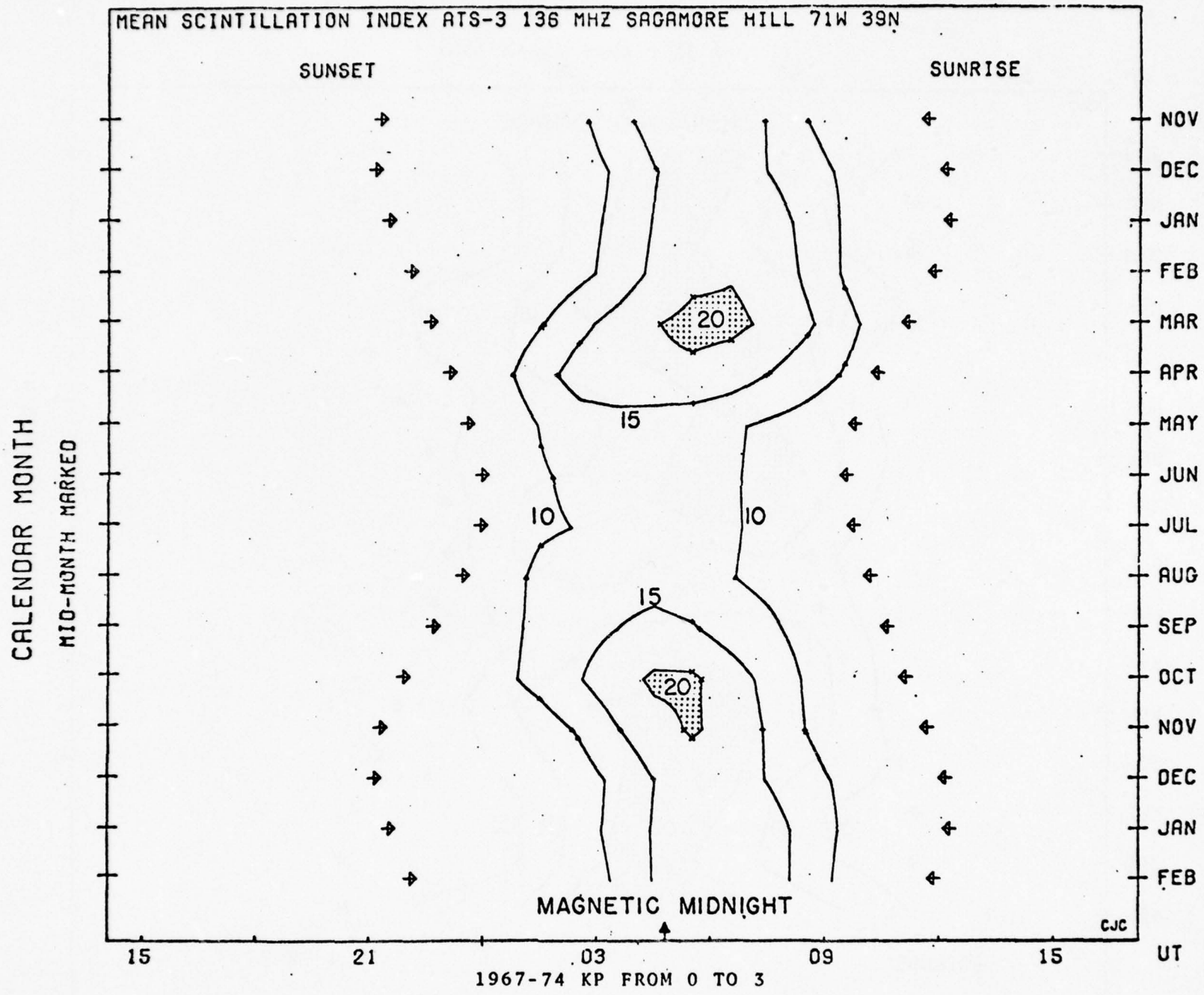
MEAN SCINTILLATION INDEX ATS-3 136 MHZ SAGAMORE HILL 71W 39N
SUNSET
SUNRISE
CALENDAR MONTH
MID-MONTH MARKED
NOV
DEC
JAN
FEB
MAR
APR
MAY
JUN
JUL
AUG
SEP
OCT
NOV
DEC
JAN
FEB
20
15
10
10
15
20
MAGNETIC MIDNIGHT
CJC
15
21
03
09
15
UT
1967-74 KP FROM 0 TO 3

Fig. 7

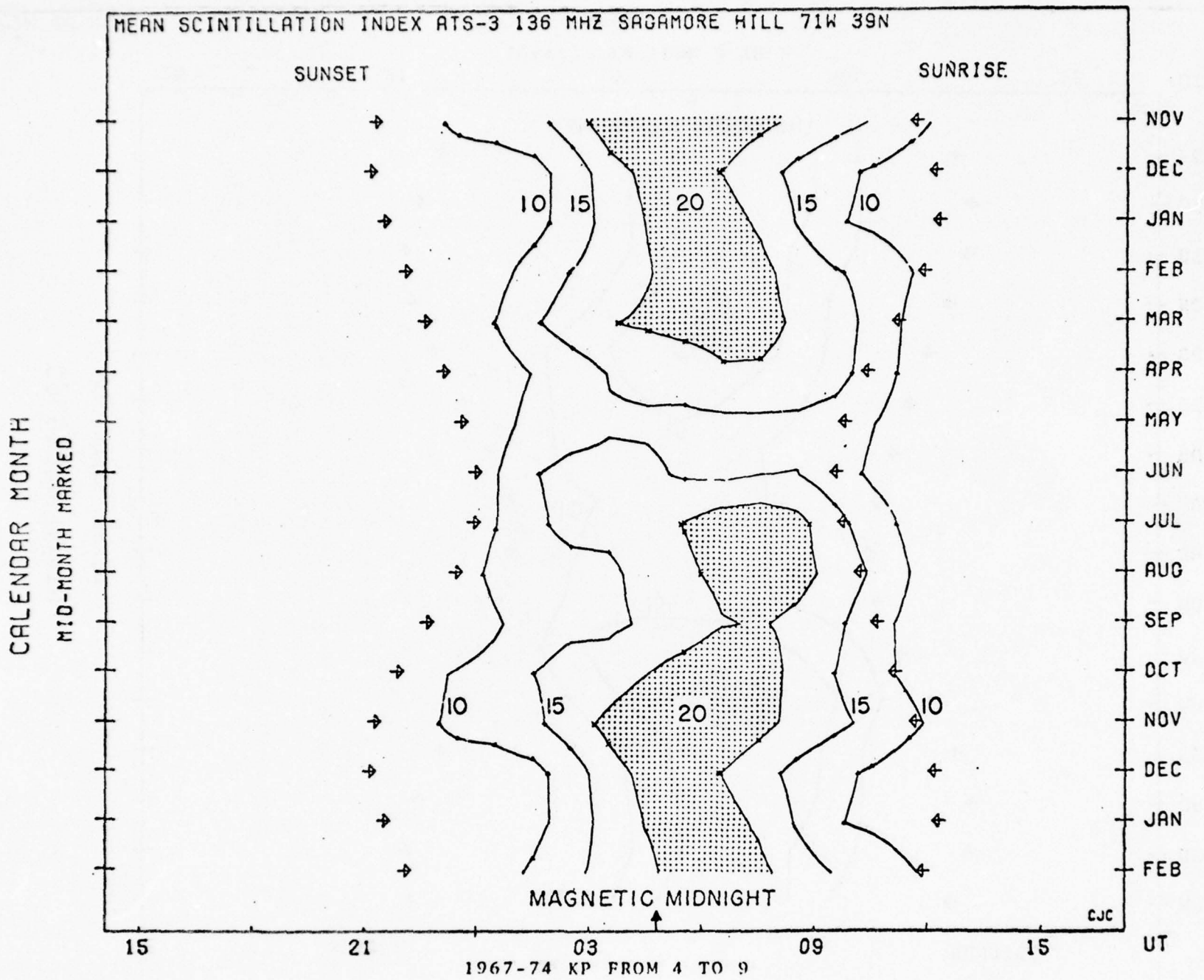
MEAN SCINTILLATION INDEX ATS-3 136 MHZ SAGAMORE HILL 71W 39N
SUNSET
SUNRISE
10
15
20
15
10
10
15
20
15
10
NOV
DEC
JAN
FEB
MAR
APR
MAY
JUN
JUL
AUG
SEP
OCT
NOV
DEC
JAN
FEB
CALENDAR MONTH
MID-MONTH MARKED
MAGNETIC MIDNIGHT
CJC
15
21
03
09
15
UT
1967-74 KP FROM 4 TO 9

Fig. 8

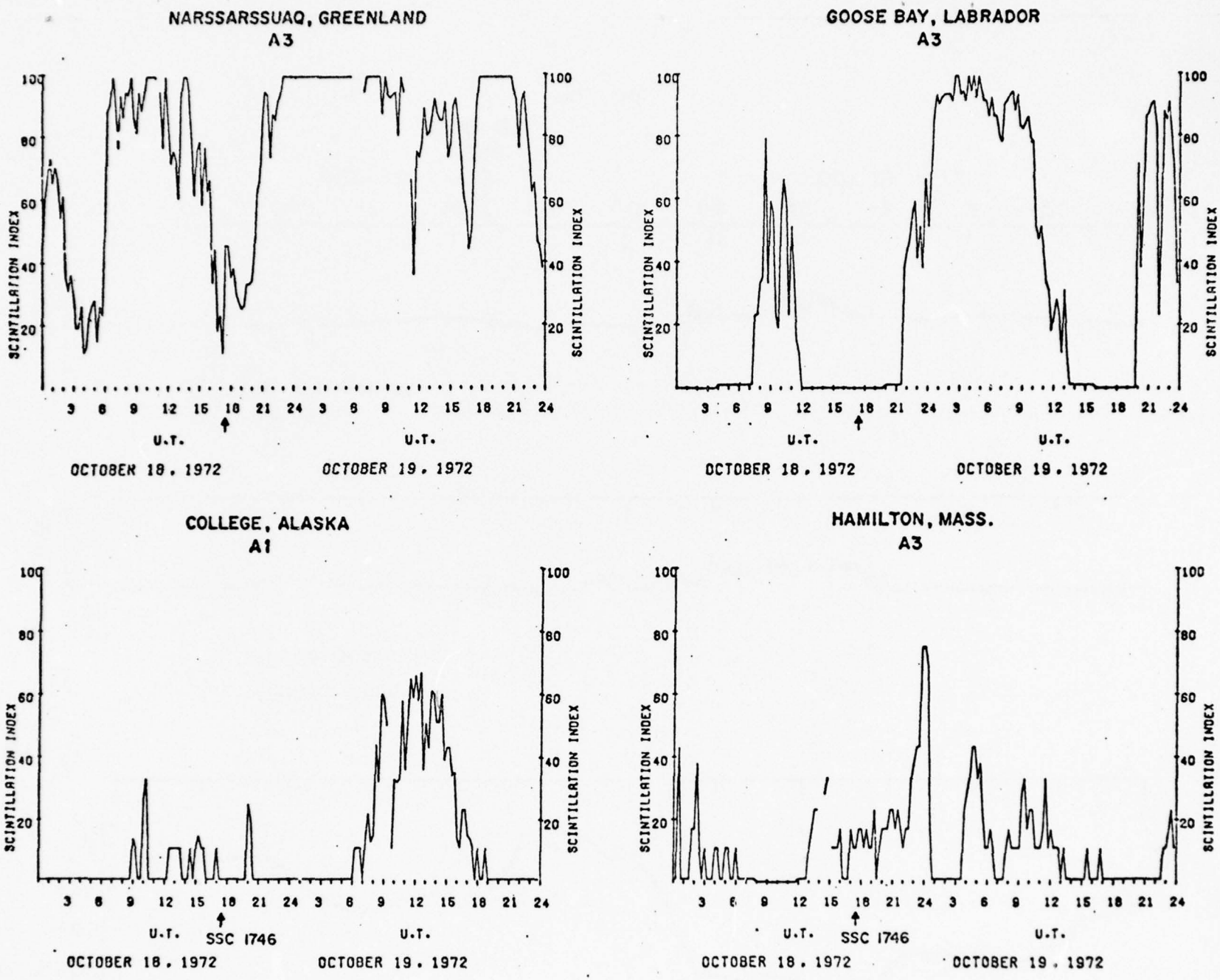
NARSSARSSUAQ, GREENLAND
A3
GOOSE BAY, LABRADOR
A3
COLLEGE, ALASKA
A1
HAMILTON, MASS.
A3
SCINTILLATION INDEX
100
80
60
40
20
3 6 9 12 15 18 21 24 3 6 9 12 15 18 21 24
U.T.
SSC 1746
OCTOBER 18 . 1972
OCTOBER 19 . 1972

Fig. 9

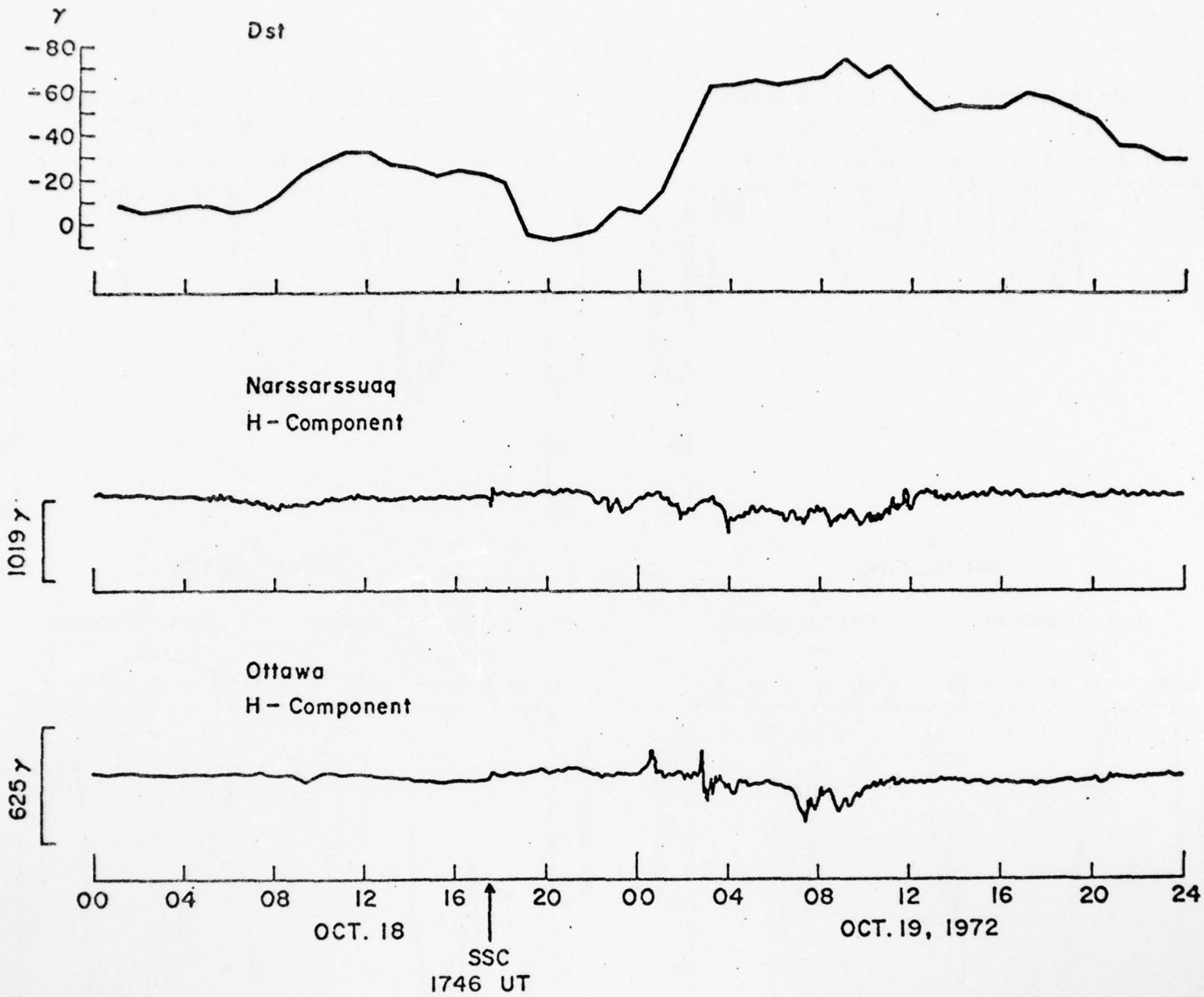
γ
Dst
-80
-60
-40
-20
0
Narssarssuaq
H - Component
1019 γ
Ottawa
H - Component
625 γ
00
04
08
12
16
20
00
04
08
12
16
20
24
OCT. 18
OCT. 19, 1972
SSC
1746 UT

Fig. 10

NARSSARSSUAQ, GREENLAND

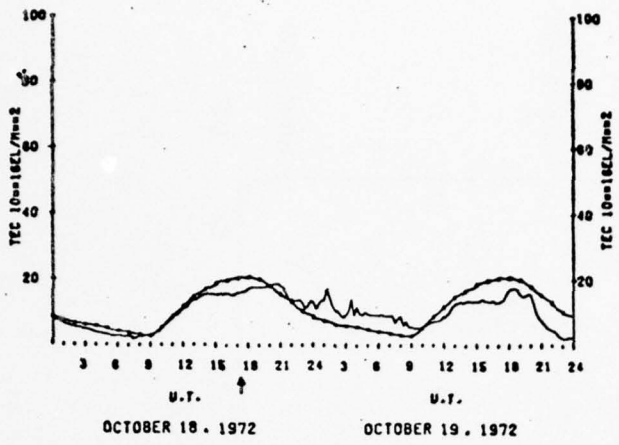

GOOSE BAY, LABRADOR

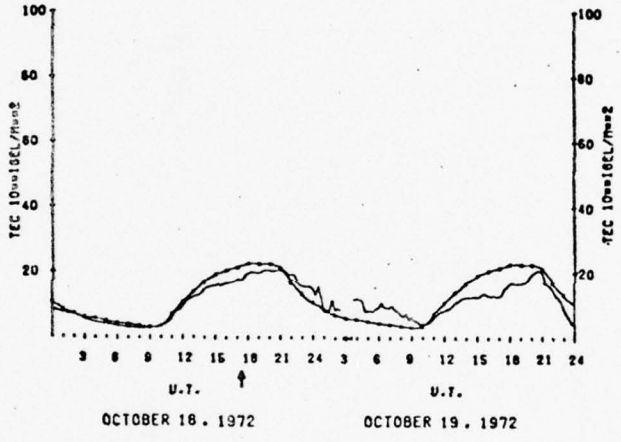

HAMILTON, MASS.

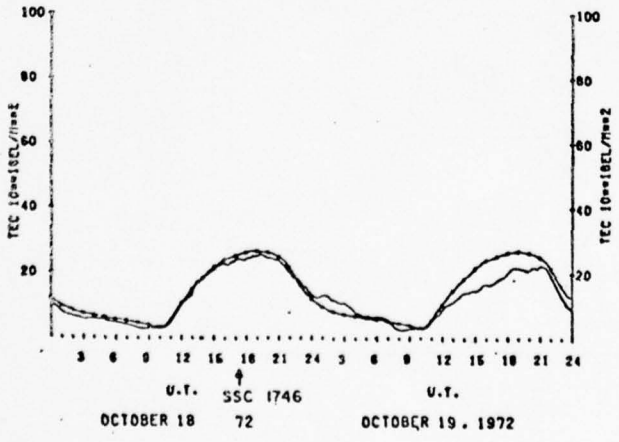

Fig. 11

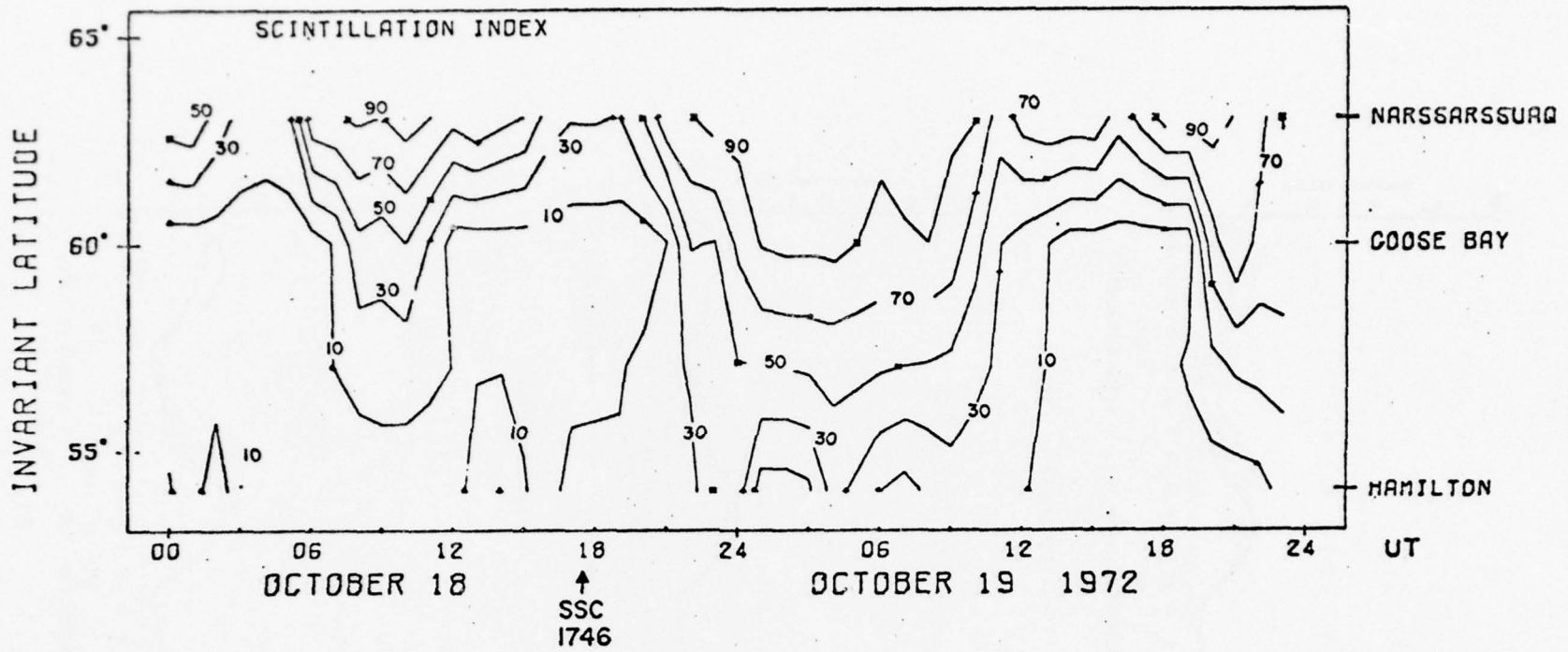
SCINTILLATION INDEX
INVARIANT LATITUDE
65°
60°
55°
NARSSARSSUAQ
GOOSE BAY
HAMILTON
00
06
12
18
24
06
12
18
24
UT
OCTOBER 18
SSC
1746
OCTOBER 19 1972

Fig. 12

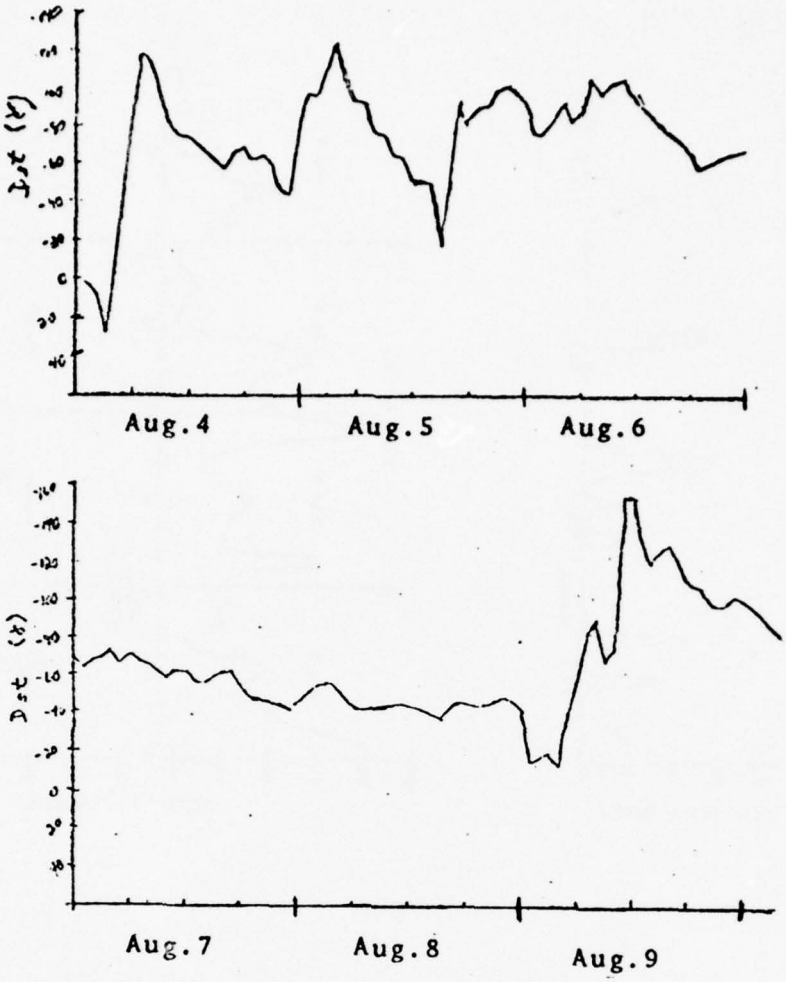
Dst (γ)
Aug. 4
Aug. 5
Aug. 6
Dst (γ)
Aug. 7
Aug. 8
Aug. 9

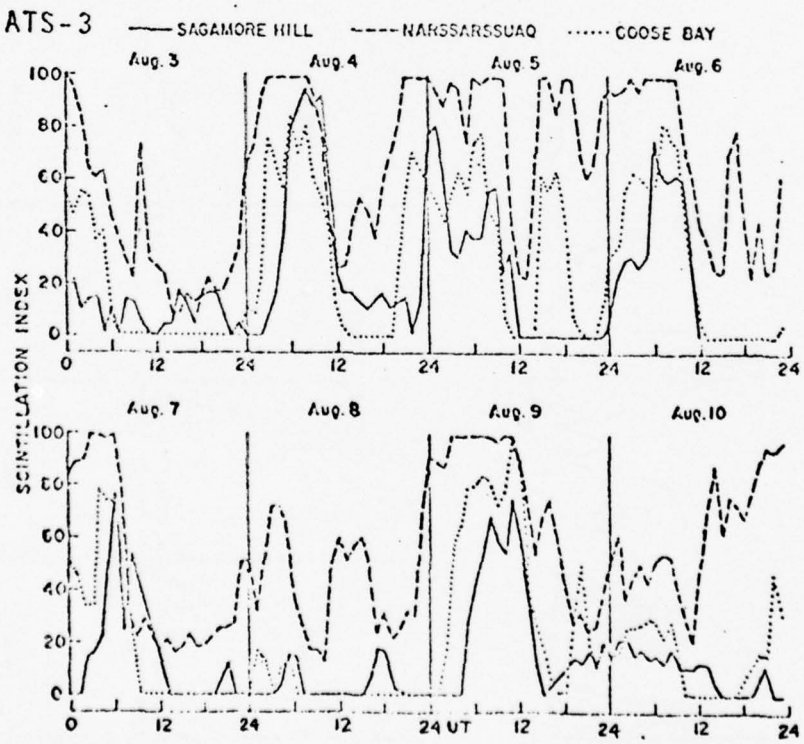
ATS-3
SAGAMORE HILL
NARSSARSSUAQ
GOOSE BAY
Aug. 3
Aug. 4
Aug. 5
Aug. 6
Aug. 7
Aug. 8
Aug. 9
Aug. 10
SCINTILLATION INDEX
UT

Fig. 13

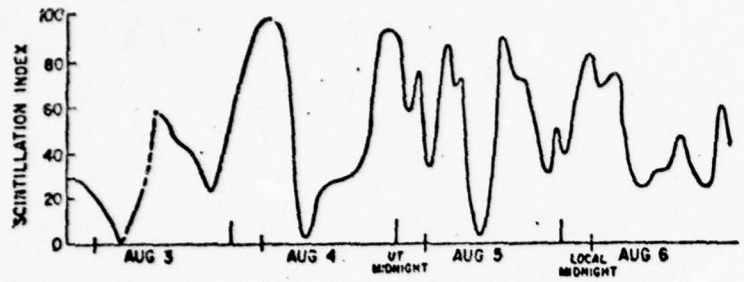

SCINTILLATION INDEX, NARSSARSSUAQ, GREENLAND FOR LES-6

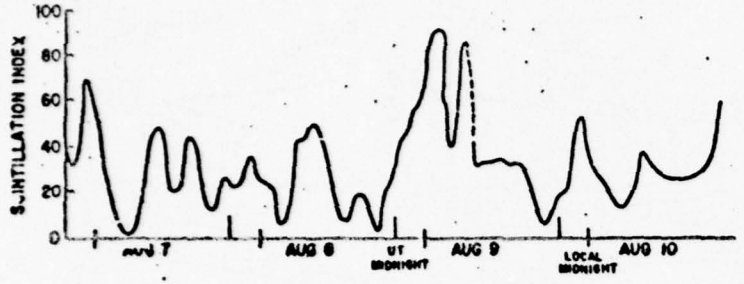

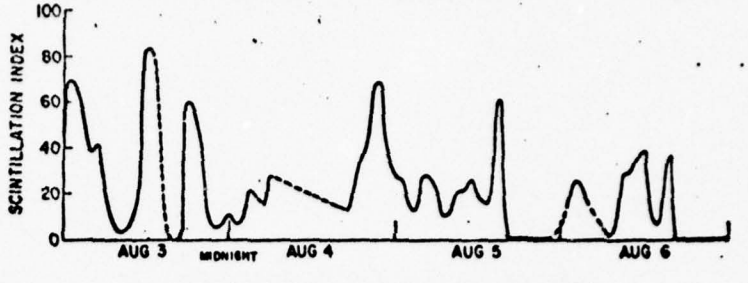

SCINTILLATION INDEX, WALES, FOR I2F2

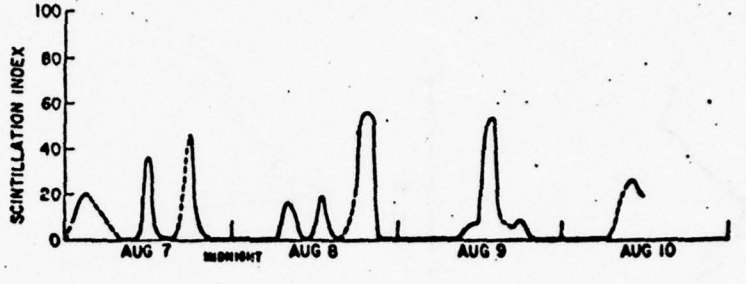

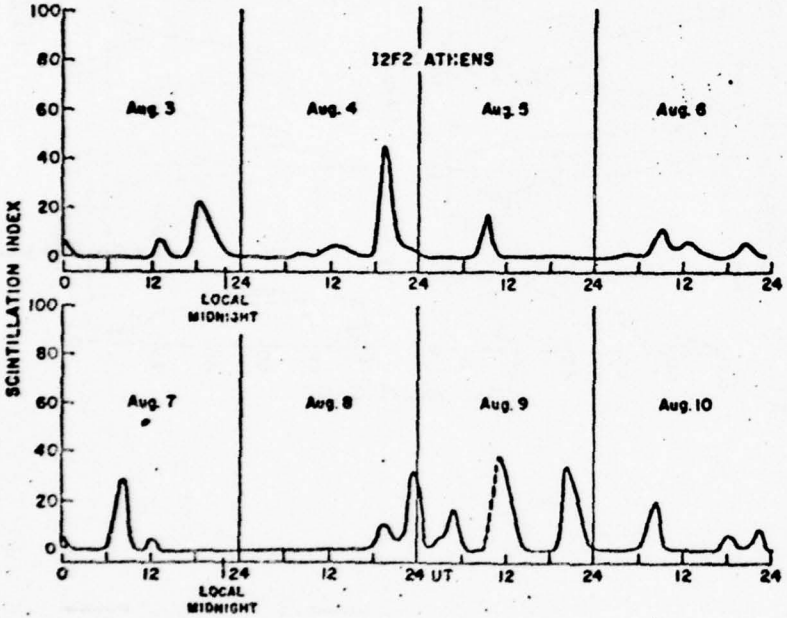

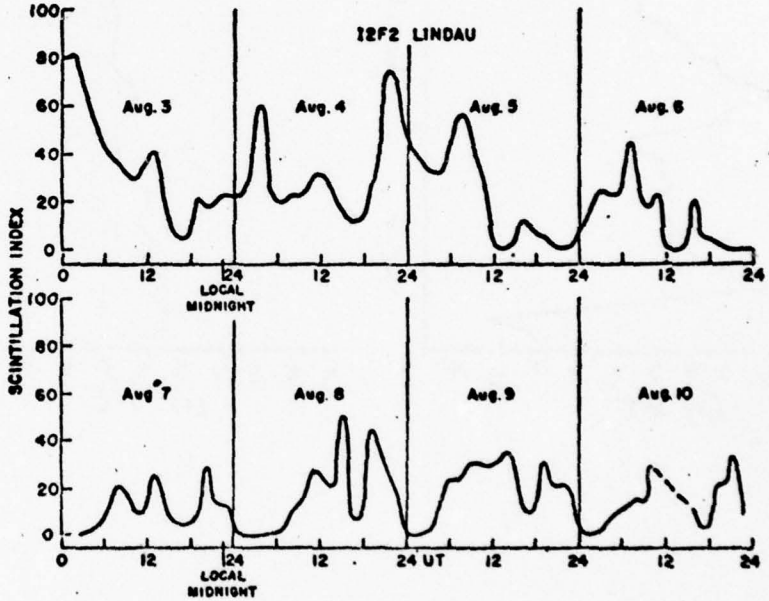

Fig. 14

II.

Total Electron Content Studies

1. Introduction

The total electron content (TEC) is defined as the total number of free, thermal electrons in a vertical column of unit area of ionosphere from the ground to a height well above the peak of ionization. The use of artificial satellite beacons permits continuous monitoring of the integrated electron content of the ionosphere. This is done by measuring the effect of the ionosphere upon radio signals transmitted from the satellite and received at ground stations. TEC measurements have been made by many stations around the globe for many years by employing the Faraday rotation technique. Since the launch of the ATS-6 satellite in 1974 another method of obtaining TEC became available. The Radio Beacon Experiment on board ATS-6 provided the first reliable differential group delay measurements of the ionosphere. The plasmaspheric electron content is the content above the height at which the Faraday rotation of a signal propagating through the ionosphere is negligible and is found by comparing the Faraday and group delay measurements.

2. Faraday Rotation Method

The polarization of a plane polarized VHF radio wave emitted from a geostationary satellite rotates continuously as it propagates through the non-isotropic ionosphere. The total amount of polarization, Ω, encountered between the satellite and the receiving station is given by,

$$\Omega = \frac{k}{f^2} \int_0^h B \cos\theta \sec\chi \, N \, dh$$

where $K = 2.36 \times 10^{-5}$, f= observing frequency in Hertz, B= magnetic field strength in gammas, θ= propagation angle, χ= zenith angle, N= local electron density in el/m^2. If the quantity $B\cos\theta\sec\chi$ is slowly varying with time it may be replaced by its mean value along the propagation path. The equation of total polarization rotation is then simplified to,

$$\Omega = \frac{K\bar{M}}{f^2} N_F$$

where $\bar{M} = \overline{B\cos\theta\sec\chi}$ and $N_F = \int_o^{h_F} N dh$. The height h_F is the height above which the remaining amount of rotation is less than the absolute experimental error.

Several problems occur in the reduction of Faraday rotation data. One is the problem of n-pi ambiguities in the data which is discussed along with general TEC reduction techniques in Cantor et al (1975) . Another is the assurance of absolute rotation values where the orientation of the transmitted VHF wave with respect to the satellite spin axis must be known as well as the reference polarization of the polarimeter. Absolute calibration of all equipment is essential to valid measurements. Klobuchar (1973) has estimated the total polarization rotation measurement error to be not better than $\pm$ 10 degrees.

3. Differential Group Delay Method

An alternative method of measuring the electron content along the line of sight to the satellite is the differential group delay technique. This method has been reviewed by many authors including Evans (1976) and Davies (1976). This technique measures the difference in transit times of two signals propagating through the

ionosphere by comparing the phase of the modulation envelope between the carrier and its sideband at two widely separated frequencies. The ATS-6 satellite carries a multi-frequency beacon and is an ideal source for this type of measurement. Group delay measurements using the ATS-6 beacon have been recorded at Hamilton, Massachusetts during the period June, 1974 through April, 1975.

4. Plasmaspheric Electron Content

The Faraday rotation effect described in Section II is strongly dependent on the earth's magnetic field which is inversely proportional to the cube of the distance from the center of the earth. Also, the electron density decreases exponentially with altitude above the peak density. These two factors together indicate that the Faraday rotation method yields a measure of the electron content of the lower ionosphere, N_F, and is insensitive to electrons encountered in the upper regions of the satellite-station ray path. The group delay method, however, is independent of the magnetic field and gives the integrated electron content, N_T, along the entire ray path. The plasmaspheric content, Np, is found by subtracting N_F from N_T.

The ATS-6 satellite allows for simultaneous measurements of Faraday rotation and group delay along the same ray path. A plot of simultaneous Faraday/group delay data as observed from Hamilton, Massachusetts is shown in Figure 1. The upper plot in Figure 1 shows the monthly median plasmaspheric variation for November, 1974. A scatter plot (Figure 2) for the same period can be used for statistical studies of the plasmaspheric content. Yeh (1976) has found that under normal geomagnetic conditions the plasmaspheric

content exhibits very little diurnal variation and is essentially a constant value. Initial studies of plasmaspheric contents during geomagnetically active periods have produced contradictory results (Soicher, 1976, and Davies et al, 1975). Yeh (1976) and Davies (1976) have reported that the plasmasphere becomes depleted during geomagnetic storms and is steadily replenished by plasma from the ionosphere for several days after sudden commercement. Further studies of storm time effects will yield rates of replenishment of this region.

One of the problems encountered in deriving plasmaspheric contents is that N_p is sometimes of the order of 0.1 N_T, thus very accurate N_T and N_F values are required. A main factor contributing to uncertainies in N_F is due to variations in the $\overline{M}$ value conversion factor. Another consideration is at what height the $\overline{M}$ value should be computed (Yeh, 1976). Variations here are due to uncentainties in the shape of the ionspheric Ne(h) profile.

5. $\overline{M}$- Value Determination

The $\overline{M}$ factor is used to convert Faraday rotation angles in integrated electron contents. For an ideal geostationary satellite in a perfectly synchronous orbit with orbital inclination and eccentricity exactly equal to zero the $\overline{M}$ value is indeed a constant and needs to be determined only once. In real life, even if the ideal orbit is initially achieved it will soon decay due to the perturbing forces if the sun, moon, and variations in the earth's gravitational field.

An inclination in the satellite's orbit results in a diurnal

oscillation in latitude of the sub-satellite point around a mean value of latitude. Any ellipticity in the orbit will produce a similar oscillation in longitude. Several examples of this are shown in Figure 3 and Figure 5. Figure 3 is a plot of the actual hourly variation in latitude and longitude of the sub-satellite position of I2F3 which has an inclination of 6.6 degrees and eccentricity of .002 degrees. The corresponding $\overline{M}$ values for an observer at Lunping, Taiwan are shown in Figure 4. A plot of the sub-satellite position of ATS-3 which has an inclination of 5.9 degrees and eccentricity of .002 degrees appears in Figure 5 and the corresponding $\overline{M}$ values for an observer at Hamilton, Massachusetts are shown in Figure 6. The amplitude of the diurnal variation in $\overline{M}$ value for I2F3 as observed from Lunping is $\pm$ 8.8% from the constant mean value which would traditionally be used in the Faraday computation. The amplitude of the diurnal variation in $\overline{M}$ value for ATS-3 as observed from Hamilton is only $\pm$5.5%. There are several effects to be noted:

1.) For a geostationary satellite observed from a station at middle or high latitudes the relative change in the $\overline{M}$ value with time is smaller than other experimental errors and can be ignored. For observes in or near equatorial regions the relative change in $\overline{M}$ value is large and use of the traditional constant $\overline{M}$ value conversion factor is invalid. An actual value of $\overline{M}$ appropriate to the time of observation must be calculated if one is to obtain a reasonable measure of N_F.

2.) As the inclination of the orbital plane of the satellite increases with time the sub-satellite position will have greater latitudinal oscillations and thus a larger fluctuation in $\overline{M}$ value will occur.

A computer program has been developed which will calculate a satellite's position as a function of time for a given set of orbital elements and will also calculate the corresponding $\overline{M}$ value for an observer at a given station as shown in Table 1. This program is described in more detail in Section VI. The program provides a relatively simple corrective procedure which can be used by the monitoring stations for obtaining more accurate TEC values. This is accomplished by use of a look-up table, an example of which is given in Table 2 and Table 3, which converts Faraday rotation angles expressed in the polarimeter polarization channel strip chart units of pi's and millimeters into corrected TEC values. These tables have been designed to minimize the amount of time and effort that is required of an observer. The conversion tables are currently in use at observing stations in Athens, Greece / Goose Bay, Labrador / Hamilton, Massachusetts / Kennedy Space Flight Center, Florida / Ramey Air Force Base, Puerto Rico / Osan, Korea and Lunping, Taiwan.

Program Support

A satellite ephemeris program, LOKANGL, was developed by the Analysis and Simulation Branch of the Air Force Geophysics Laboratory. Under this Contract (F19628-76-C-0003) the program has been modified and expanded to aid in improving the accuracy of reported TEC values.

OUTPUT: For any given satellite-station pair the program will calculate the satellite's orbit and will produce the sub-satellite and sub-ionospheric latitudes and longitudes, the satellite's right ascension and declination, elevation, azimuth, and range as a function of time as observed from the user specified station. Other output options include:

(1) Position and velocity vectors

(2) Sub-satellite data

(3) Osculating Elements

(4) Table of $\overline{M}$-values as a function of time

(5) Conversion table (TEC (constant $\overline{M}$) to TEC (varying $\overline{M}$))

(6) Faraday rotation to TEC conversion table

Any of these output options may be generated from one of the following input sets:

(1) A 2-card orbital element data set

(2) A 2-card input set of position and velocity vectors

(3) A 5-card SPADATS orbital element data set

The 5-card SPADATS orbital element set has been used exclusively and only this input set will be described in this report.

FUNCTIONAL DESCRIPTION

I. Ephemeris program

NAME	DESCRIPTION
LOKANGL	main program- reads input data- calls necessary routines
CONVRT	reads 2-card element set
DELEM	reads position-velocity vector + converts to SPADATS elements

NAME	DESCRIPTION
DREV	obtains change per revolution in orbital elements
NUMINT	computes changes per rev due to drag by Simpsons rule integration
INTGND	supplies NUMINT with integrands for each integ. step
DENSEL	density model
OSCTMN	converts osculating position-velocity to mean elements
PVTELM	converts position-velocity to orbital elements
MNTOSC	converts elements to osculating position-velocity
ELMTPV	converts elements to position-velocity
SHPRDC	computes short periodic terms
KEPECN	converts mean anomaly to eccentric anomaly
SPSETC	sets constants and program initializations for all routines
SPRFCO	computes refraction correction due to atmosphere
NEW	converts units of output data
CRMXA	prints heading on each output page
SPTRAN	transformation matrix and station coordinates routine
SPROU	prints out BDC and/or binary ephemeris tapes
MULTIP	performs matrix multiplication
JDATE	converts Gregorian date to Julian date-limits Jan 1,1950 to Dec 31,1999
CDATE	converts Julian date to Gregorian date-same limits
WRSTA	reads $\bar{M}$-value and TEC conversion table output options and prints ephemeris predictions
WRTAP	extracts lookangle predictions from binary tape
ANGLE1	reduces an angle to interval $-\pi$ to $+\pi$
ANGLE2	reduces an angle to interval 0 to 2π

II. M-VALUE ROUTINES

NAME	DESCRIPTION
MGEOS	CALLED FROM WRSTA, calculates $\bar{M}$-value as function of satellite position, calls necessary routines
GEO	sets initializations and performs geometric calculations
FIELDG, FIELD	calculate geomagnetic field, updates the POGO coefficients to time of observation, prints $\bar{M}$-value table
HOUR	calculates hour angle
HEADER	prints AFGL header on every page of output
HEAD	prints heading on $\bar{M}$-value table

III. TEC CONVERSION TABLE ROUTINE

NAME	DESCRIPTION
TABLE	produces the following output (1) TEC (constant $\bar{M}$) to TEC (varying $\bar{M}$) conversion table (2) Faraday rotation to TEC conversion table

INPUT

The input which is required by program LOKANGL is of two forms. One is a series of input cards which are to be submitted with the program deck. The other is an input tape (tape 2) on which the POGO (8/69) geomagnetic field coefficients reside. A sample of the control deck is included later in this report.

I. INPUT CARD FORMAT

CARD NO.	COLUMN	FORMAT	UNITS	DESCRIPTION
1	1			"5"= 5 card element set to be used
2	1			"1"= first card of element set
	4-7	A4		satellite name
	46-48	I2		year of orbital elements
	49-51	F3.0		Julian day number of orbital elements
3	1			"2"= second card of element set
	9-13	F5.0		Epoch= fractional part of orb element date; =0.0 if epoch= 0hr U.T.
	23-31	F9.4	degrees	Mean anomaly
	32-40	F9.4	degrees	Right Ascension of ascending node(Ω)
	41-49	F9.4	degrees	Argument of Perigee (ω)
	50-58	F9.4		Eccentricity (e)
	59-67	F9.4	degrees	Inclination (i)
4	9-19	E11.8	revs/day	Mean motion= 1440. (mins/day)/period (mins/rev)= n
	21-31	E11.9	rev/day^2	$\dot{n}/2$
	33-40	E8.5	deg/day	$\dot{\Omega}$
	42-49	E8.5	deg/day	$\dot{\omega}$
	51-58	E8.5		$\dot{e}$/day
	60-67	E8.5	deg/day	$\dot{i}$
5	1			"4" = fourth card of orbital element set
	9-19	E11.8	rev/day^3	$\ddot{n}/6$
	21-31	E11.8	rev/day^4	$\dddot{n}/24$
	33-40	E8.5	rev/day^2	$\ddot{\Omega}/2$
	42-49	E8.5	rev/day^2	$\ddot{\omega}/2$

CARD NO.	COLUMN	FORMAT	UNITS	DESCRIPTION
6	1			"5" = fifth card of orbital element set
	9-19	E11.8	E.R.	Semi-major axis (a) E.R.=earth radii
	21-30	E10.7	E.R./day	$\dot{a}$
	32-41	E10.7	E.R./day^2	$\ddot{a}/2$
7	1-3	I3		number of stations requesting look angle output
	4-6	I3		if number of stations 1, code in column 6: 0= output as function of time 1= output as function of time
8				station parameters
	1-5	I5		I.D. of station
	8	I3		"2" = geodetic system
	9-23	E15.8	degrees	station longitude (+W)
	24-38	E15.8	degrees	station geodetic latitude (+N)
	39-53	E15.8	meters	station height
	61-72	2A6		name of station
9				start and stop times of ephemeris table
	1-15	E15.8	seconds	print interval (t)
	17-18	I2		start month
	20-21	I2		day
	23-24	I2		year (last two digits)
	26-29	F4.1		hour
	31-34	F4.1		minutes
	36-41	F7.3		seconds
	43-44	I2		end month
	46-47	I2		day

CARD NO.	COLUMN	FORMAT	UNITS	DESCRIPTION
9	49-50	F4.1		end year (last two digits)
	52-55	F4.1		hour
	57-60	F4.1		minutes
	62-67	F4.1		seconds
10				print codes all=0 when look angles requested
	2	I2		=0; =1 to print position/velocity vectors
	4	I2		=0; =1 to print sub-satellite position
	6	I2		=0; =1 to print osculating elements
	8	I2		=0; =1 to print station observation data
	9-10	I2		=0; =1 to write binary tape
	11-13	E15.8		=1.0; single correction of range for refraction
11	16	I1		output options for $\bar{M}$-value and Conversion Tables "0"= $\bar{M}$-value table only "1"= $\bar{M}$-value and Faraday to TEC Conversion Tables "2"= all tables
	33-38	F6.2	MHz	operating frequency
	52-55	F4.1	MM	Polarization reference value(millimeters
	60-63	I4		Year of requested $\bar{M}$-value prediction
12	1-3			"END"
	5-6			"OF"
	8-14			"PROBLEM"
13	1			"9" = end of all input

II. INPUT TAPE FORMAT

The POGO (8/69) set of geomagnetic field coefficients must be attached to the local file TAPE2 before program execution. The format for this file is as follows;

CARD NO.	COLUMN	VARIABLE NAME	FORMAT	DESCRIPTION
1	1	J	I1	=0 if coefficients were derived using oblate earth ≠0 if coefficients were derived using spherical earth
1	2	K	I1	=0 if coefficients are Schmidt normalized ≠0 if coefficients are Gauss normalized
1	4-9	TZERO	F6.1	epoch for which coefficients were derived = 1960.0
1	10-72	AID	10A6,A3	Alphabetic identification

Each succeeding card contains the variables N,M, GNM, HNM, GTNM, HTNM, GTTNM, HTTNM, in the following format (2I3,6F11.4) where GNM, HNM, GTNM, HTNM, GTTNM, and HTTNM are the spherical harmonic coefficients in units of gamma (10^{-5} gauss).

$N = n+1$

$M = m+1$

$GNM = g_n^m$ } spherical harmonic coefficients

$HNM = h_n^m$ }

$GTNM = \dot{g}_n^m$ }

$HTNM = \dot{h}_n^m$ } time derivatives at the epoch date

$GTTNM = \ddot{g}_n^m$ }

$HTTNM = \ddot{h}_n^m$ }

Termination of the coefficient set is accomplished by a flag card where N is set equal to zero. A list of the POGO (8/69) coefficient file is given in Table 4 of this report.

EXECUTION REQUIREMENTS

Core memory required = 110 K octal

Compile time = 17.9 decimal seconds

Execution time = 8.7 seconds per station/month

Since this program will be used to produce output tables for many stations each month one would like to minimize the execution requirements. One way of accomplishing this is to store the binary object code as a user-library, thus avoiding the need for compiling the program each time it is use while greatly reducing the operating costs.

TAPE REQUIREMENTS

The following tapes must be included on the program card:

TAPE1 : output tape containing the $\bar{M}$-value and TEC tables

TAPE2 : input tape containing the POGO (8/69) coefficient set

TAPE3 : scratch tape

TAPE4 : scratch tape

TAPE5 : input ; card reader

TAPE6 : output; line printer ; contains ephemeris data

USE OF PROGRAM

In order to use the Faraday to TEC conversion correctly an observer should first verify that the station location, operating frequency, satellite being observed, and reference polarization value match those listed on the computer table headings.

The observer then turns to the page of the conversion tables with the proper pi-value and finds the millimeter reading which matches the polarization channel chart reading. He then scans across the table to find the final TEC value in the column which corresponds to the time of the observation.

For example, referring to the sample output in Table 3 one can easily see that for an observer at Lunping, Taiwan monitoring the satellite IS2F3 which has a nominal longitude of -161.9 degrees east, on a frequency of 136.44 MHz, with a reference polarization value of 13.5 millimeters during the month of September, 1976, a polarization chart reading of 2π, 15 millimeters at 14 hrs universal time corresponds to a TEC value of 13.8×10^{16} el/m^2.

SAMPLE CONTROL DECK

```
JJLOK,T90,CM110000.                                          2535     JOHANSON
ATTACH,JLIB,JMJLIBX2939,ID=JOHANSON.
ATTACH,TAPE2,P0G0X2939,ID=JOHANSON.
LIBRARY(JLIB)
LDSET(PRESET=ZERO)
LOWANGL.
REWIND,TAPE1.
COPY,TAPE1,OUTPUT.
EXIT.
7/8/9
5
1  12F3                                          076127
2          0.0          55.8347  54.0444 298.4900 .0019999    6.61364
3        1.002989,          ,      -.0134    0.0268
4
5        6.6096106
  1  1
   47     -121.17        25.0                                      LUNPING
3600.          09 15 76 00.0 00.0 00.000 09 15 76 23.0 00.0 00.000
 0 0 0 0 01.0
OUTPUT OPTION =1     FREQUENCY =136.44      BETAR =13.5     1976       LUN
END OF PROBLEM
9
6/7/8/9
```

TABLE I

M-VALUE OUTPUT

LOOK ANGLES FOR A GEOSTATIONARY SATELLITE (EQUATORIAL ORBIT) AS A FUNCTION OF SATELLITE LATITUDE AND LONGITUDE.

DATE	STATION	LATITUDE	E.LONGITUDE
SEPTEMBER 15, 1976	TAIWAN	25.00	121.00

TIME (UT)	SUB-SATELLITE LAT	SUB-SATELLITE E.LONG	SUB-IONOSPHERIC LAT	SUB-IONOSPHERIC E.LONG	M	PROP ANGLE	SEC Z	G	ELEV	AZIM	RANGE	HOUR ANGLE HR	HOUR ANGLE MIN	HOUR ANGLE SEC	DECLIN DEG	DECLIN MIN	ALPHA
0 0	4.3	-161.6	23.6	138.5	-29419.	108.6	2.822	3.60	4.7	91.5	41229.	18	19	41	0	39.0	-65.0
1 0	2.8	-161.9	23.1	138.9	-30711.	109.5	2.837	3.95	4.2	92.9	41278.	18	20	6	-0	-50.1	-64.9
2 0	1.2	-162.0	22.6	139.3	-32138.	110.5	2.852	4.34	3.6	94.5	41329.	18	20	38	-2	-30.7	-64.7
3 0	-.6	-162.1	22.0	139.8	-33682.	111.5	2.865	4.71	3.0	96.1	41380.	18	21	10	-4	-16.0	-64.6
4 0	-2.2	-162.2	21.3	140.2	-34925.	112.5	2.876	5.04	2.3	97.7	41431.	18	21	34	-5	-59.1	-64.6
5 0	-3.8	-162.3	20.8	140.7	-36064.	113.4	2.885	5.33	1.7	99.1	41478.	18	21	46	-7	-32.8	-64.5
6 0	-5.1	-162.3	20.2	141.1	-36924.	114.1	2.890	5.55	1.1	100.3	41521.	18	21	41	-8	-50.7	-64.5
7 0	-6.0	-162.2	19.8	141.5	-37457.	114.6	2.893	5.70	.6	101.1	41554.	18	21	20	-9	-47.4	-64.5
8 0	-6.5	-162.1	19.6	141.8	-37693.	114.8	2.894	5.79	.3	101.5	41576.	18	20	47	-10	-19.0	-64.5
9 0	-6.6	-161.9	19.5	141.9	-37626.	114.8	2.895	5.80	.1	101.5	41583.	18	20	9	-10	-23.2	-64.5
10 0	-6.2	-161.8	19.7	142.0	-37239.	114.5	2.895	5.74	.2	101.1	41571.	18	19	33	-9	-59.7	-64.5
11 0	-5.4	-161.7	20.0	141.8	-36536.	114.1	2.894	5.61	.4	100.3	41541.	18	19	6	-9	-10.1	-64.6
12 0	-4.2	-161.6	20.5	141.5	-35550.	113.4	2.892	5.42	.9	99.2	41494.	18	18	52	-7	-58.1	-64.6
13 0	-2.7	-161.6	21.1	141.0	-34350.	112.6	2.887	5.15	1.5	97.9	41433.	18	18	51	-6	-28.4	-64.6
14 0	-1.1	-161.6	21.7	140.4	-33050.	111.6	2.877	4.84	2.3	96.4	41364.	18	19	1	-4	-47.3	-64.7
15 0	.7	-161.7	22.4	139.8	-31734.	110.7	2.863	4.47	3.1	94.8	41293.	18	19	16	-3	-1.6	-64.7
16 0	2.4	-161.7	22.9	139.2	-30504.	109.7	2.845	4.08	3.9	93.3	41228.	18	19	30	-1	-18.6	-64.8
17 0	3.9	-161.8	23.4	138.7	-29453.	108.8	2.827	3.71	4.6	91.9	41174.	18	19	39	0	14.8	-64.9
18 0	5.1	-161.8	23.8	138.2	-28648.	108.1	2.811	3.39	5.1	90.7	41136.	18	19	39	1	32.1	-65.0
19 0	6.0	-161.8	24.1	138.0	-27823.	107.6	2.800	3.13	5.5	89.8	41116.	18	19	30	2	27.9	-65.1
20 0	6.5	-161.7	24.2	137.9	-27364.	107.3	2.794	2.99	5.6	89.3	41115.	18	19	17	2	58.3	-65.2
21 0	6.6	-161.7	24.2	137.9	-27310.	107.2	2.795	2.99	5.6	89.3	41130.	18	19	5	3	1.2	-65.2
22 0	6.2	-161.6	24.1	138.0	-27670.	107.4	2.802	3.10	5.4	89.6	41159.	18	18	58	2	36.4	-65.1
23 0	5.4	-161.6	23.9	138.3	-28414.	107.9	2.813	3.32	5.1	90.4	41198.	18	19	1	1	45.8	-65.1

FOR A SATELLITE AT THE EQUATOR...

	0.0	-161.9	22.1	139.8	-33035.	111.1	2.865	4.60	3.0	95.5	41426.	18	20	6	-3	-41.7	-64.7

NSAT=I2F3 FREQ= 136.440 DETAT= 7.00 DETAR= 13.5

TABLE 2

TEC CONVERSION TABLE OUTPUT

CONVERSION TABLES FROM REFERENCE POLARIZATION CHANNEL CHART READINGS TO FINAL T.E.C. VALUES

********** WARNING **********

MAKE CERTAIN THAT STATION, SATELLITE, FREQUENCY, MONTH, AND REFERENCE POLARIZATION VALUE ARE CORRECT BEFORE USING THESE TABLES.

****

TO OBTAIN THE REFERENCE POLARIZATION VALUE:

1. INITIALLY ADJUST THE POLARIZATION CHANNELS FOR 45 MILLIMETERS (DIVISIONS) DEFLECTION.
2. CONNECT A SIGNAL GENERATOR INTO R.F. SWITCH INPUT "B" WITH INPUT "A" TERMINATED WITH WITH A MATCHED LOAD.
3. READ REFERENCE POLARIZATION VALUE ON POLARIZATION REFERENCE CHANNEL.

DIFFERENCES BETWEEN THE ACTUAL REFERENCE POLARIZATION VALUE AND THAT LISTED IN THE TABLE HEADINGS CAN BE ACCOMODATED BY ONE OF THE FOLLOWING:

1. TAKE THE DIFFERENCE BETWEEN THE ACTUAL REFERENCE POLARIZATION VALUE MINUS THE COMPUTER LISTED VALUE. ADD THIS VALUE TO THE FINAL CHART READINGS BEFORE LOOKING UP FINAL T.E.C. IN THE FOLLOWING TABLES.
2. NEW TABLES WITH CORRECT VALUES MAY BE OBTAINED FROM AFGL-LIR BY NOTIFYING THEM OF THE CORRECT REFERENCE POLARIZATION VALUE (IN MILLIMETERS).

TABLE 3

FARADAY TO TEC CONVERSION TABLE

DATE: SEPTEMBER 1976 | STATION: TAIWAN | SATELLITE (NOMINAL LONGITUDE): I2F3 -161.9 | FREQUENCY (MHZ): 136.440 | REFERENCE POLARIZATION VALUE (MM): 13.5

CHART RECOGNITION ********

PI	MM	TIME (U.T.) 0	1	2	3	4	5	6	7	8	9	10	11	12	13	14	15	16	17	18	19	20	21	22	23
2	0	13.1	12.5	12.0	11.5	11.0	10.7	10.4	10.3	10.2	10.2	10.3	10.5	10.7	11.0	11.4	11.9	12.4	12.9	13.4	13.8	14.0	14.1	13.9	13.5
2	1	13.2	12.7	12.1	11.6	11.2	10.8	10.6	10.4	10.4	10.4	10.5	10.5	10.9	11.2	11.6	12.0	12.5	13.1	13.6	14.0	14.2	14.3	14.1	13.7
2	2	13.4	12.9	12.3	11.8	11.3	11.0	10.7	10.6	10.5	10.5	10.6	10.8	11.0	11.3	11.7	12.2	12.7	13.3	13.8	14.2	14.4	14.5	14.3	13.9
2	3	13.6	13.1	12.5	11.9	11.5	11.1	10.9	10.7	10.6	10.7	10.8	10.9	11.2	11.5	11.9	12.4	12.9	13.5	14.0	14.4	14.6	14.7	14.5	14.1
2	4	13.9	13.2	12.6	12.1	11.6	11.3	11.0	10.9	10.8	10.8	10.9	11.1	11.3	11.6	12.0	12.5	13.1	13.6	14.2	14.6	14.8	14.9	14.7	14.3
2	5	14.0	13.4	12.8	12.3	11.8	11.4	11.2	11.0	10.9	11.0	11.1	11.2	11.5	11.8	12.2	12.7	13.3	13.8	14.4	14.8	15.0	15.1	14.9	14.5
2	6	14.2	13.5	13.0	12.4	12.0	11.6	11.3	11.2	11.1	11.1	11.2	11.4	11.6	12.0	12.4	12.9	13.4	14.0	14.6	15.0	15.2	15.3	15.1	14.7
2	7	14.4	13.8	13.2	12.6	12.1	11.7	11.5	11.3	11.2	11.3	11.3	11.5	11.8	12.1	12.5	13.0	13.6	14.2	14.8	15.2	15.4	15.5	15.3	14.9
2	8	14.6	13.9	13.3	12.8	12.3	11.9	11.6	11.4	11.4	11.4	11.5	11.7	11.9	12.3	12.7	13.2	13.8	14.4	14.9	15.4	15.6	15.7	15.5	15.1
2	9	14.7	14.1	13.5	12.9	12.4	12.0	11.8	11.6	11.5	11.5	11.6	11.8	12.1	12.4	12.9	13.4	14.0	14.6	15.1	15.6	15.8	15.9	15.7	15.3
2	10	14.9	14.3	13.7	13.1	12.6	12.2	11.9	11.7	11.7	11.7	11.8	12.0	12.2	12.6	13.0	13.5	14.1	14.8	15.3	15.8	16.0	16.1	15.9	15.5
2	11	15.1	14.5	13.8	13.3	12.7	12.3	12.1	11.9	11.8	11.8	11.9	12.1	12.4	12.7	13.2	13.7	14.3	14.9	15.5	16.0	16.2	16.3	16.1	15.6
2	12	15.3	14.7	14.0	13.4	12.9	12.5	12.2	12.0	12.0	12.0	12.1	12.3	12.5	12.9	13.3	13.9	14.5	15.1	15.7	16.2	16.4	16.5	16.3	15.8
2	13	15.5	14.8	14.2	13.6	13.1	12.7	12.4	12.2	12.1	12.1	12.2	12.4	12.7	13.1	13.5	14.1	14.7	15.3	15.9	16.4	16.6	16.7	16.5	16.0
2	14	15.7	15.0	14.4	13.7	13.2	12.8	12.5	12.3	12.3	12.3	12.4	12.6	12.8	13.2	13.7	14.2	14.9	15.5	16.1	16.6	16.8	16.9	16.7	16.2
2	15	15.8	15.2	14.5	13.9	13.4	13.0	12.7	12.5	12.4	12.4	12.5	12.7	13.0	13.4	13.5	14.4	15.0	15.7	16.3	16.8	17.0	17.1	16.9	16.4
2	16	16.1	15.4	14.7	14.1	13.5	13.1	12.8	12.6	12.5	12.6	12.7	12.9	13.2	13.5	14.0	14.6	15.2	15.9	16.5	17.0	17.2	17.3	17.1	16.8
2	17	16.2	15.6	14.9	14.2	13.7	13.3	13.0	12.8	12.7	12.7	12.8	13.0	13.3	13.7	14.2	14.7	15.4	16.1	16.7	17.2	17.5	17.5	17.3	16.8
2	18	16.4	15.7	15.0	14.4	13.9	13.4	13.1	12.9	12.8	12.9	13.0	13.2	13.5	13.8	14.3	14.9	15.6	16.2	16.9	17.4	17.7	17.7	17.5	17.0
2	19	16.5	15.9	15.2	14.6	14.0	13.6	13.3	13.1	13.0	13.0	13.1	13.3	13.6	14.0	14.5	15.1	15.7	16.4	17.1	17.6	17.9	17.9	17.7	17.2
2	20	16.6	16.1	15.4	14.7	14.2	13.7	13.4	13.2	13.1	13.2	13.3	13.5	13.8	14.2	14.7	15.2	15.9	16.6	17.3	17.8	18.1	18.1	17.9	17.4
2	21	17.0	16.3	15.6	14.9	14.3	13.9	13.6	13.4	13.3	13.3	13.4	13.6	13.9	14.3	14.8	15.4	16.1	16.8	17.4	18.0	18.3	18.3	18.1	17.6
2	22	17.2	16.5	15.7	15.1	14.5	14.0	13.7	13.5	13.4	13.4	13.6	13.8	14.1	14.5	15.0	15.6	16.3	17.0	17.6	18.2	18.5	18.5	18.3	17.8
2	23	17.4	16.6	15.9	15.2	14.6	14.2	13.9	13.7	13.6	13.6	13.7	13.9	14.2	14.6	15.1	15.8	16.4	17.2	17.8	18.4	18.7	18.7	18.5	18.0
2	24	17.5	16.8	16.1	15.4	14.8	14.3	14.1	13.8	13.7	13.7	13.9	14.1	14.4	14.8	15.3	15.9	16.5	17.3	18.0	18.5	18.9	18.9	18.7	18.2
2	25	17.7	17.0	16.2	15.6	15.0	14.5	14.2	13.9	13.9	13.9	14.0	14.2	14.5	14.9	15.5	16.1	16.8	17.5	18.2	18.7	19.1	19.1	18.9	18.4
2	26	17.9	17.2	16.4	15.7	15.1	14.6	14.3	14.1	14.0	14.0	14.2	14.4	14.7	15.1	15.6	16.3	17.0	17.7	18.4	18.9	19.3	19.3	19.1	18.6
2	27	18.1	17.4	16.6	15.9	15.3	14.8	14.4	14.2	14.2	14.2	14.3	14.5	14.8	15.3	15.8	16.4	17.2	17.9	18.6	19.1	19.5	19.5	19.2	18.7
2	28	18.3	17.5	16.8	16.0	15.4	14.9	14.6	14.4	14.3	14.3	14.4	14.7	15.0	15.4	16.0	16.6	17.3	18.1	18.9	19.3	19.7	19.7	19.4	18.9
2	29	18.5	17.7	16.9	16.2	15.6	15.1	14.7	14.5	14.4	14.5	14.6	14.8	15.1	15.6	16.1	16.8	17.5	18.3	19.0	19.5	19.9	19.9	19.6	19.1
2	30	18.7	17.9	17.1	16.4	15.7	15.3	14.9	14.7	14.6	14.6	14.7	15.0	15.3	15.7	16.3	16.9	17.7	18.5	19.2	19.7	20.1	20.1	19.9	19.3
2	31	18.9	18.1	17.3	16.5	15.9	15.4	15.1	14.8	14.7	14.8	14.9	15.1	15.4	15.9	16.4	17.1	17.9	18.6	19.4	19.9	20.3	20.3	20.0	19.5
2	32	19.0	18.3	17.4	16.7	16.1	15.6	15.2	15.0	14.9	14.9	15.0	15.3	15.6	16.0	16.6	17.3	18.0	18.8	19.6	20.1	20.5	20.5	20.2	19.7
2	33	19.2	18.4	17.6	16.9	16.2	15.7	15.3	15.1	15.0	15.1	15.2	15.4	15.8	16.2	16.8	17.5	18.2	19.0	19.7	20.3	20.7	20.7	20.4	19.9
2	34	19.4	18.6	17.8	17.0	16.4	15.9	15.5	15.3	15.2	15.2	15.3	15.5	15.9	16.4	16.9	17.6	18.4	19.2	19.9	20.5	20.9	20.9	20.6	20.1
2	35	19.5	18.8	18.0	17.2	16.6	16.0	15.6	15.4	15.3	15.3	15.5	15.7	16.1	16.5	17.1	17.8	18.6	19.4	20.1	20.7	21.1	21.1	20.8	20.3
2	36	19.6	19.0	18.1	17.4	16.7	16.2	15.8	15.6	15.5	15.5	15.6	15.9	16.2	16.7	17.3	18.0	18.8	19.6	20.3	20.9	21.3	21.3	21.0	20.5
2	37	20.0	19.1	18.2	17.5	16.8	16.3	15.9	15.7	15.6	15.6	15.8	16.0	16.4	16.8	17.4	18.1	18.9	19.8	20.5	21.1	21.5	21.5	21.2	20.7
2	38	20.2	19.3	18.5	17.7	17.0	16.5	16.1	15.9	15.8	15.9	15.9	16.2	16.6	17.0	17.6	18.3	19.2	19.9	20.7	21.3	21.7	21.7	21.4	20.9
2	39	20.4	19.5	18.6	17.8	17.2	16.6	16.2	16.0	15.9	15.9	16.1	16.3	16.7	17.1	17.8	18.5	19.3	20.1	20.9	21.5	21.9	21.9	21.6	21.1
2	40	20.5	19.7	18.8	18.0	17.3	16.8	16.4	16.2	16.1	16.1	16.2	16.5	16.8	17.3	17.9	18.6	19.5	20.3	21.1	21.7	22.1	22.1	21.8	21.3
2	41	20.7	19.9	19.0	18.2	17.5	16.9	16.5	16.3	16.2	16.2	16.4	16.6	17.0	17.5	18.1	18.8	19.6	20.5	21.3	21.9	22.3	22.3	22.0	21.5
2	42	20.9	20.0	19.2	18.3	17.6	17.1	16.7	16.4	16.3	16.3	16.4	16.6	16.8	17.1	17.6	18.2	19.0	19.8	20.7	21.5	22.1	22.5	22.2	21.7
2	43	21.1	20.2	19.3	18.5	17.8	17.2	16.8	16.6	16.5	16.5	16.7	16.9	17.3	17.8	18.4	19.2	20.0	20.9	21.7	22.3	22.7	22.7	22.4	21.8
2	44	21.3	20.4	19.5	18.7	18.0	17.4	17.0	16.7	16.6	16.7	16.8	17.1	17.4	17.9	18.6	19.3	20.2	21.0	21.9	22.5	22.9	22.9	22.6	22.0

TABLE 4

POGO (E/69) COEFFICIENT SET

00	1960.0	POGO(E/69)					
2	1	-30470.8320	-0.0	26.8223	-0.0	-0.0	-0.0
2	2	-2170.2336	5757.0859	10.0325	2.2485	-0.0	-0.0
3	1	-1542.4851	-0.0	-23.6564	-0.0	-0.0	-0.0
3	2	2589.3350	-1979.3044	1.4984	-6.8426	-0.0	-0.0
3	3	1555.9304	266.0750	7.9161	-28.3228	-0.0	-0.0
4	1	1333.3594	-0.0	-7.2364	-0.0	-0.0	-0.0
4	2	-1982.5684	-424.8779	-11.4175	4.4887	-0.0	-0.0
4	3	1292.1541	241.6939	0.8416	-0.9585	-0.0	-0.0
4	4	833.6372	-173.5776	3.2653	1.7665	-0.0	-0.0
5	1	564.6553	-0.0	-1.5687	-0.0	-0.0	-0.0
5	2	810.7571	134.4438	-1.1772	3.6897	-0.0	-0.0
5	3	506.8203	-303.6641	-5.3583	5.6356	-0.0	-0.0
5	4	-357.8083	19.3989	1.0208	-1.0901	-0.0	-0.0
5	5	224.7370	-276.3591	8.3387	-2.0537	-0.0	-0.0
6	1	-237.4645	-0.0	3.5940	-0.0	-0.0	-0.0
6	2	356.5618	5.0910	0.5769	2.3359	-0.0	-0.0
6	3	249.7766	107.9608	-0.2723	4.0147	-0.0	-0.0
6	4	-14.3464	-107.2727	-3.2611	-4.2427	-0.0	-0.0
6	6	-75.7366	117.0901	5.0440	-5.0275	-0.0	-0.0
6	5	-149.7288	-108.2535	-1.0817	0.6315	-0.0	-0.0
6	6	-75.7366	117.0901	5.0440	-5.0275	-0.0	-0.0
7	1	44.7689	-0.0	0.1186	-0.0	-0.0	-0.0
7	2	59.3998	-7.6247	0.3830	-0.6497	-0.0	-0.0
7	3	-3.6751	118.1291	2.3535	-2.3806	-0.0	-0.0
7	4	-232.3608	58.3039	1.2792	2.4867	-0.0	-0.0
7	5	9.5710	-18.1037	-2.7692	-1.6966	-0.0	-0.0
7	6	1.9681	-27.0357	0.0831	2.3390	-0.0	-0.0
7	7	-83.0814	0.1058	-1.2965	-2.5932	-0.0	-0.0
8	1	79.2588	-0.0	-1.5993	-0.0	-0.0	-0.0
8	2	-51.5829	-54.4392	-0.2631	-1.6805	-0.0	-0.0
8	3	-0.2746	-21.2277	0.7227	-1.1414	-0.0	-0.0
8	4	8.9470	-7.6602	0.8573	0.5781	-0.0	-0.0
8	5	-33.4966	5.5250	0.8359	1.2319	-0.0	-0.0
8	6	-3.2699	15.0556	-0.5747	0.9359	-0.0	-0.0
8	7	10.0034	-23.6011	1.0100	0.4034	-0.0	-0.0
8	8	3.9274	-27.8326	-1.3952	0.6037	-0.0	-0.0
9	1	9.9028	-0.0	0.1883	-0.0	-0.0	-0.0
9	2	3.1867	9.8124	0.2709	0.0110	-0.0	-0.0
9	3	-5.6134	-16.2345	0.3290	0.3866	-0.0	-0.0
9	4	-16.5215	9.9281	0.8273	-1.0603	-0.0	-0.0
9	5	-3.2876	-18.8907	0.4170	-0.0866	-0.0	-0.0
9	6	4.5906	10.6028	-0.0007	-0.4919	-0.0	-0.0
9	7	-11.5698	20.6160	0.4934	0.5618	-0.0	-0.0
9	6	4.9906	10.6028	-0.0007	-0.4919	-0.0	-0.0
9	7	-11.9698	20.6160	0.4934	0.5618	-0.0	-0.0
9	8	10.1946	-0.1734	0.7337	-0.6709	-0.0	-0.0
9	9	18.6983	-20.7399	-1.4755	-0.0795	-0.0	-0.0
10	1	9.5694	-0.0	0.1661	-0.0	-0.0	-0.0
10	2	5.3443	-25.3560	-0.0791	0.4840	-0.0	-0.0
10	3	3.0948	12.8425	-0.4572	0.4232	-0.0	-0.0
10	4	-11.9937	3.1355	-0.0917	0.1703	-0.0	-0.0
10	5	15.2921	-2.4809	-0.3723	-0.4054	-0.0	-0.0
10	6	0.7382	-2.0734	-0.0282	-0.2177	-0.0	-0.0
10	7	0.8367	7.2521	-0.4837	0.2051	-0.0	-0.0
10	8	0.3897	12.7127	0.5370	0.0107	-0.0	-0.0
10	9	6.2269	4.6771	-0.1324	-1.1328	-0.0	-0.0
10	10	-3.7603	0.7433	-0.3251	0.1563	-0.0	-0.0
11	1	-1.6855	0.0	-0.0265	0.0	0.0	0.0
11	2	-2.2307	2.8873	-0.0756	-0.1371	0.0	0.0
11	3	1.2560	3.4969	0.1663	-0.3725	0.0	0.0
11	4	1.5793	-0.6889	-0.0662	0.5148	0.0	0.0
11	5	-2.1523	6.6194	-0.1231	-0.0206	0.0	0.0
11	6	9.3095	-5.0403	-0.3321	0.0435	0.0	0.0
11	7	8.6777	1.0199	-0.3308	-0.1912	0.0	0.0
11	8	0.2722	-2.8203	-0.2116	0.0687	0.0	0.0
11	9	-2.3784	2.1396	0.2742	0.3963	0.0	0.0
11	10	-0.0938	4.2055	0.4915	-0.5333	0.0	0.0
11	11	5.2727	-8.7786	-0.7501	0.3076	0.0	0.0
00							

LIST OF FIGURES

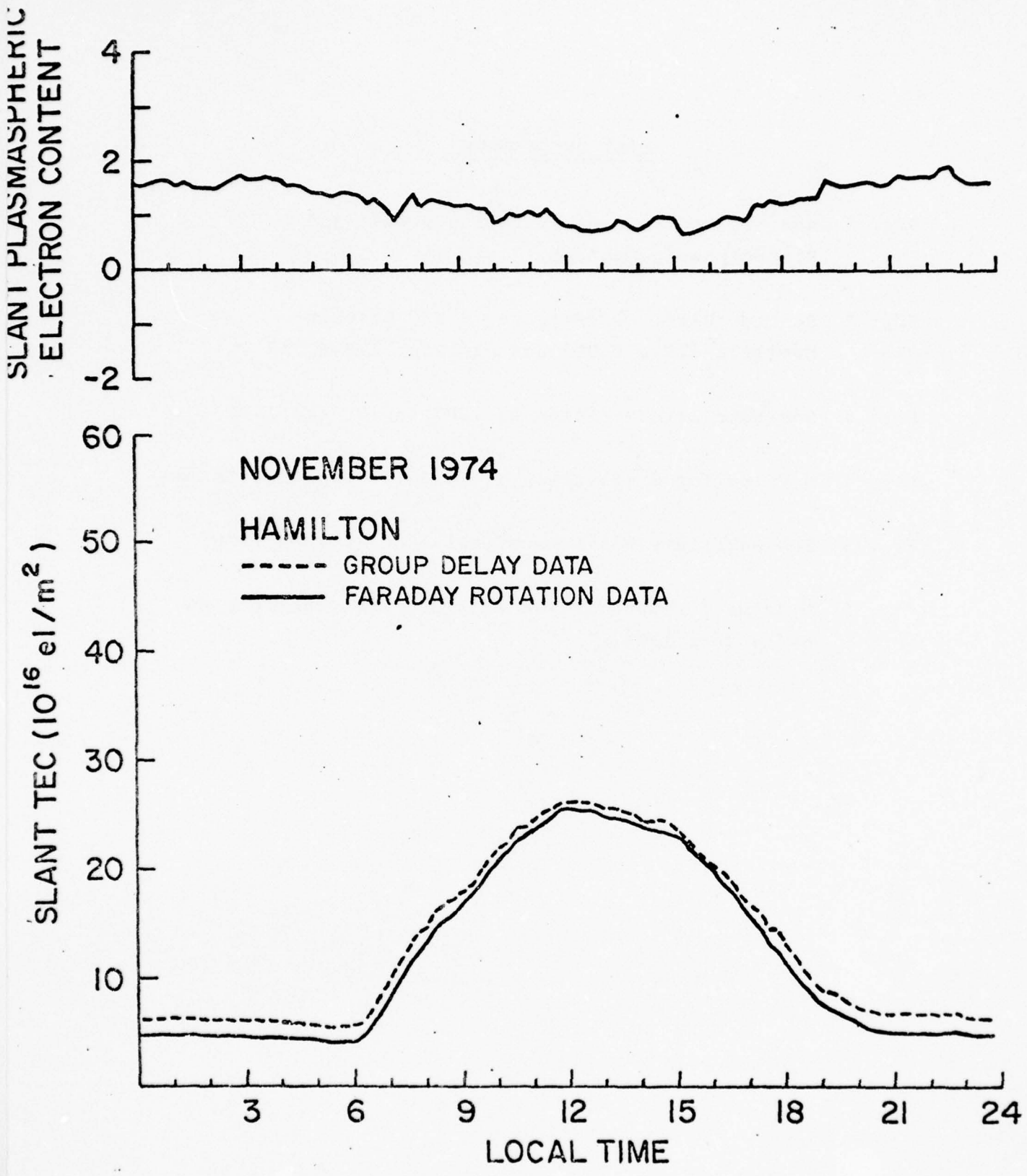
SLANT PLASMASPHERIC ELECTRON CONTENT
4
2
0
-2
NOVEMBER 1974
HAMILTON
GROUP DELAY DATA
FARADAY ROTATION DATA
SLANT TEC (10^{16} el/m^2)
60
50
40
30
20
10
3
6
9
12
15
18
21
24
LOCAL TIME

Fig. 1

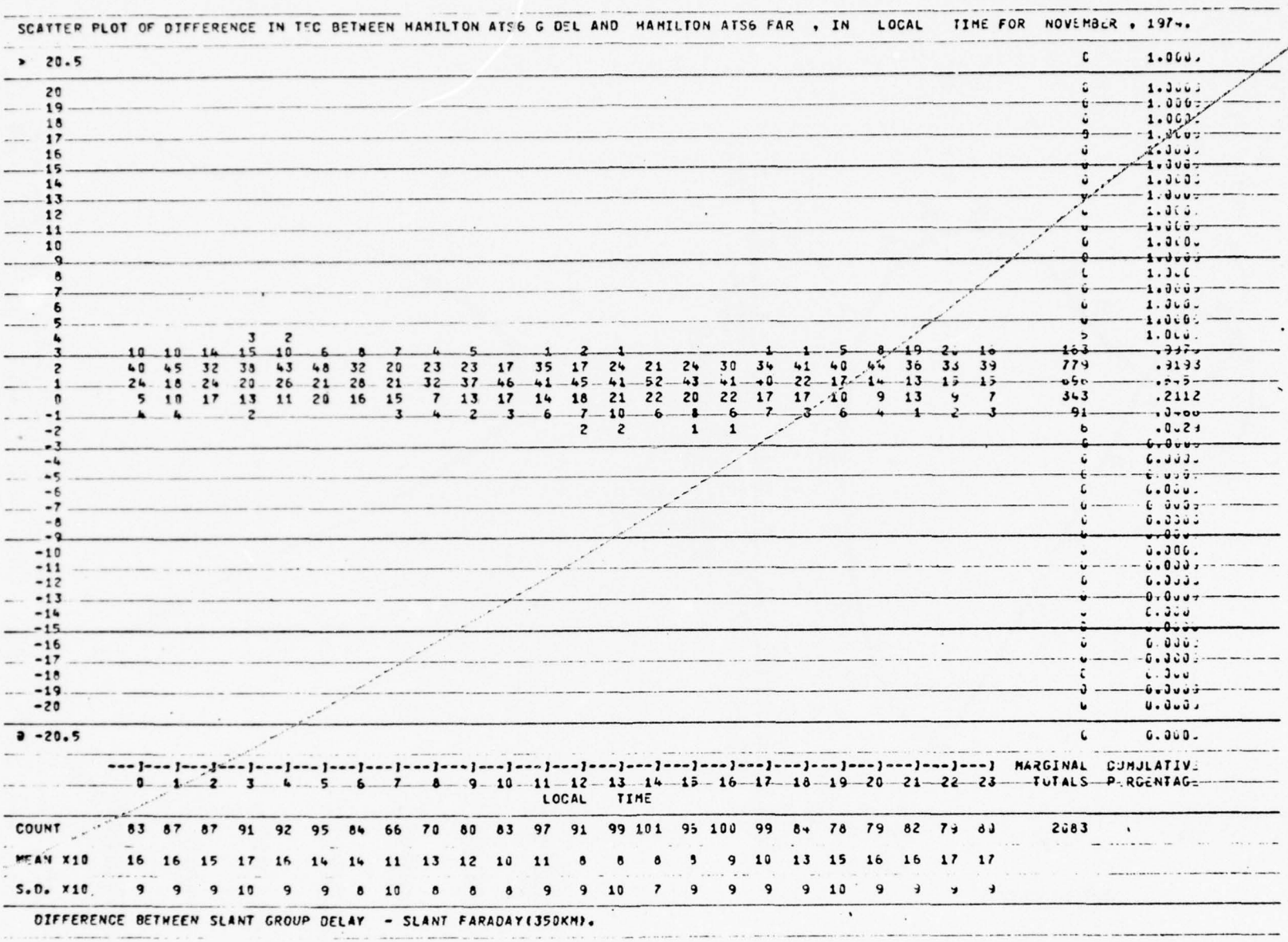
SCATTER PLOT OF DIFFERENCE IN TEC BETWEEN HAMILTON ATS6 G DEL AND HAMILTON ATS6 FAR , IN LOCAL TIME FOR NOVEMBER , 197-.
LOCAL TIME
MARGINAL TOTALS
CUMULATIVE PERCENTAGE
COUNT
MEAN X10
S.D. X10
DIFFERENCE BETWEEN SLANT GROUP DELAY - SLANT FARADAY(350KM).

Fig. 2

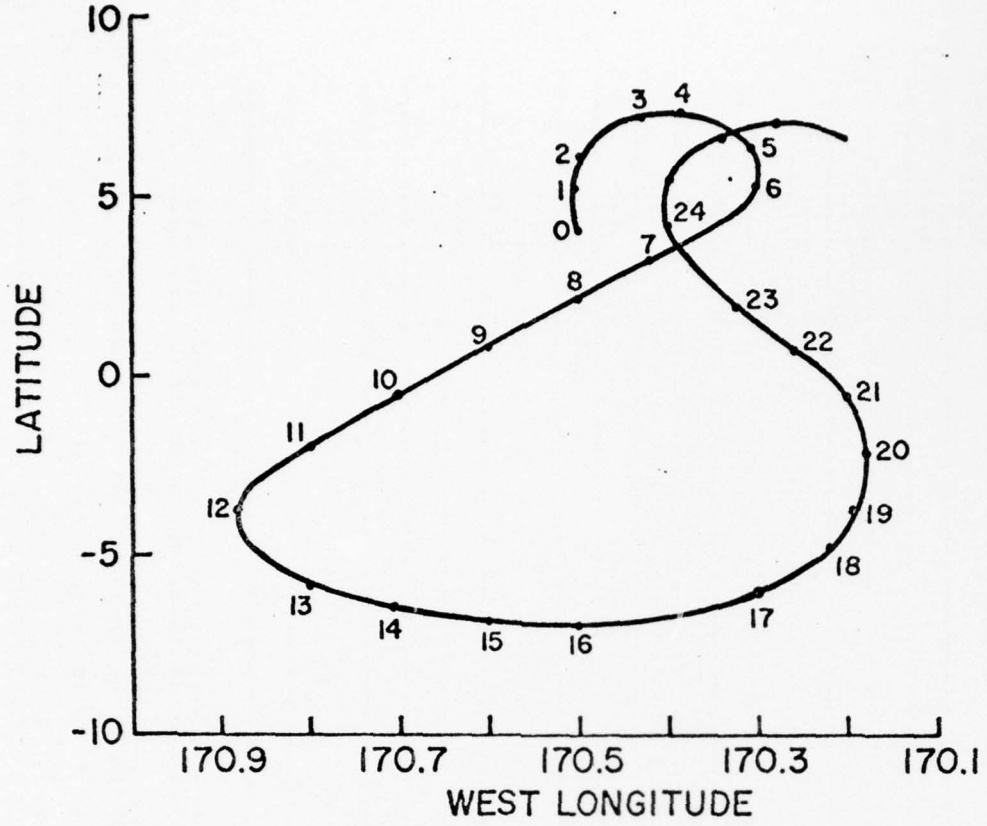
10
5
0
-5
-10
LATITUDE
170.9
170.7
170.5
170.3
170.1
WEST LONGITUDE
0
1
2
3
4
5
6
7
8
9
10
11
12
13
14
15
16
17
18
19
20
21
22
23
24

Fig. 3

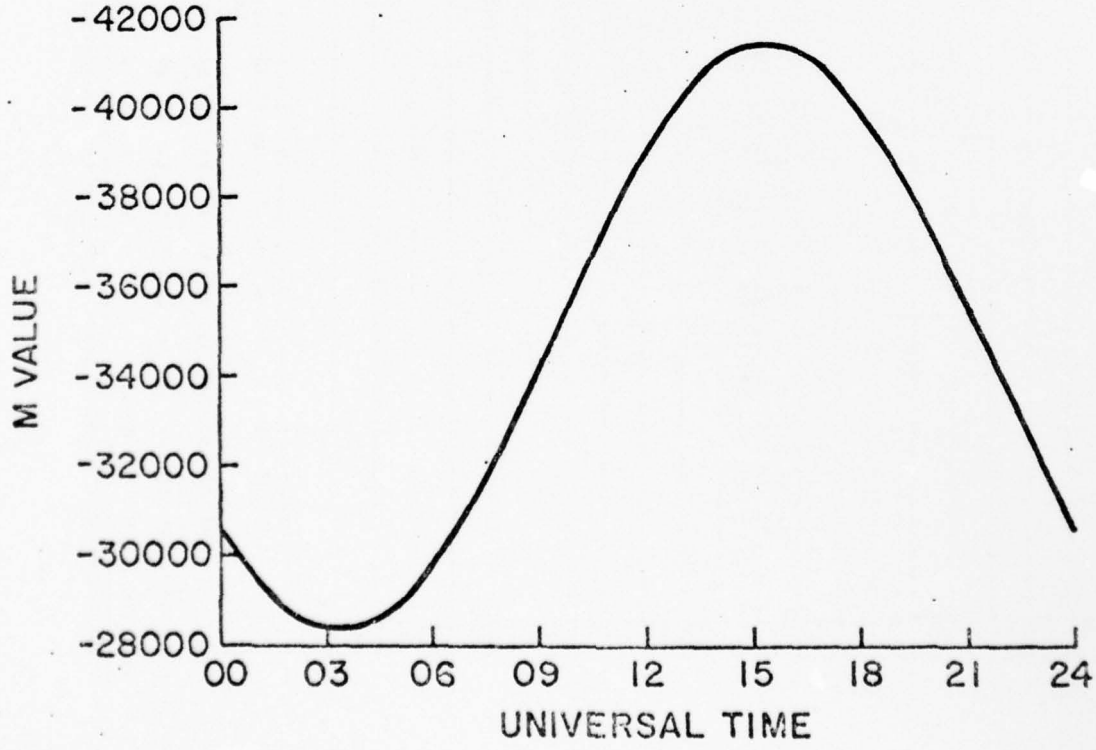
-42000
-40000
-38000
-36000
-34000
-32000
-30000
-28000
M VALUE
00
03
06
09
12
15
18
21
24
UNIVERSAL TIME

Fig. 4

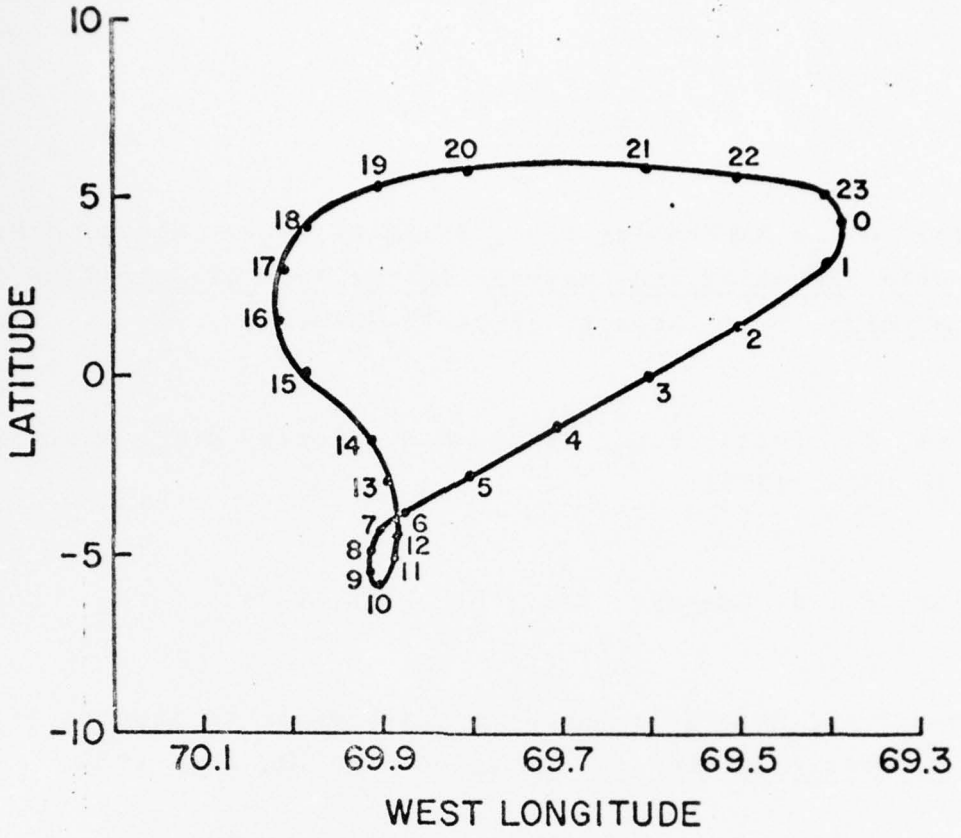
10
5
0
-5
-10
LATITUDE
70.1
69.9
69.7
69.5
69.3
WEST LONGITUDE
0
1
2
3
4
5
6
7
8
9
10
11
12
13
14
15
16
17
18
19
20
21
22
23

Fig. 5

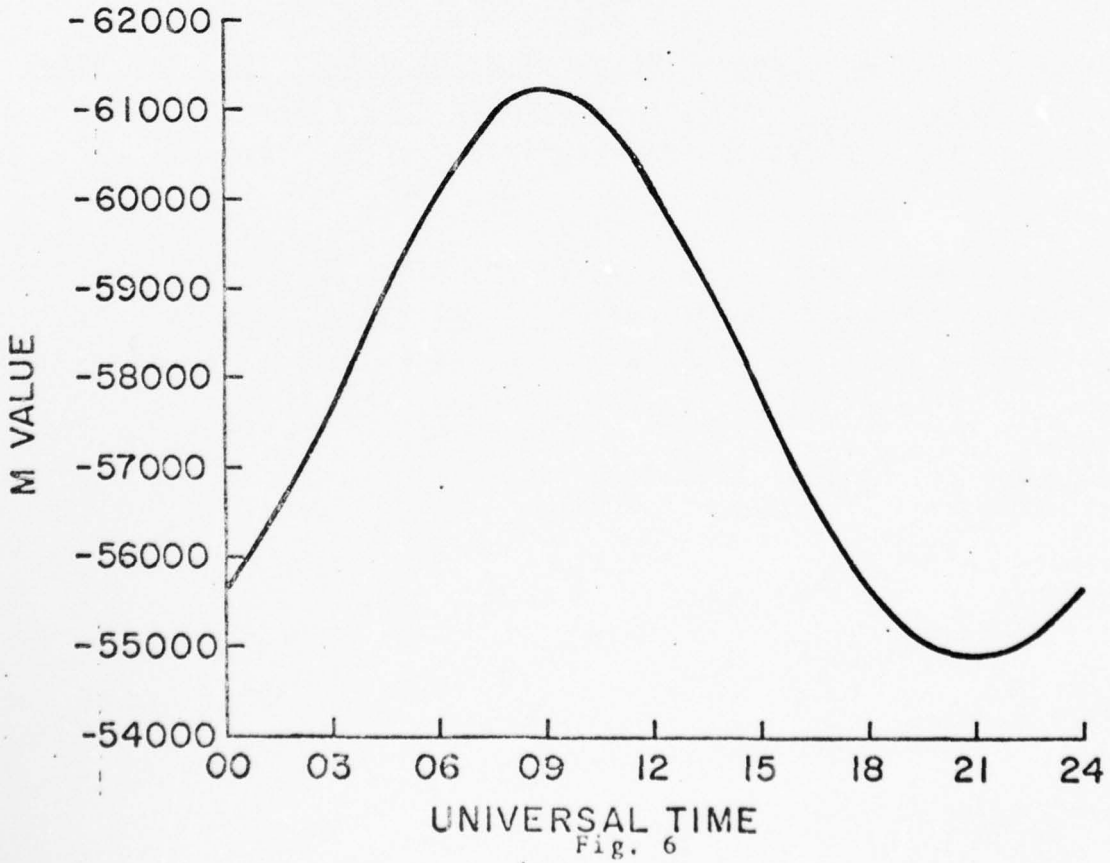
-62000
-61000
-60000
-59000
-58000
-57000
-56000
-55000
-54000
M VALUE
00
03
06
09
12
15
18
21
24
UNIVERSAL TIME

Fig. 6

REFERENCES

Cantor, C.J., MacKenzie, E.M., Vesprini, R.L., Hagan, M.P., Data Reduction and Analysis in the Area of Satellite Studies, Final Report, AFCRL-TR-75-0493, 1975.

Davies, K., Fritz, R.B., Grubb, R.N., Jones, J.E., Radio Sci., 10, 785, 1975.

Davies, K., J. Geophys. Res., 81, 2825, 1976.

Evans, J.V., Satellite Beacon Contributions to Studies of the Structure of the Ionosphere, Boston MA, June 1976.

Klobuchar, J.A., et al., Total Electron Content Studies of the Ionosphere, AFCRL-TR-73-0098, 1973.

Koster, J.R., Ionospheric Research Using Satellites, The Total Electron Content of the Ionosphere Over Legon for the Year 1972, AFCRL-TR-74-0414, 1973.

Poletti-Liuzzi, D.A., Yeh, K.C., Lin, C.H., Simulation and Measurement of the Plasmaspheric Electron Content, Proceedings of COSPAR Satellite Beacon Symposium, 1976.

Soicher, H., Nature, 259, 33, 1976.

III.

SIGNAL STATISTICS OF IONOSPHERIC SCINTILLATION IN THE WEAK AND STRONG SCATTER REGIMES

1. INTRODUCTION

For a successful design of ground to space communication links, a knowledge of ionospheric scintillations at a desired frequency as well as the fine structure of the fluctuations is required. At mid-latitudes where the amplitude fluctuations are small, ground based scintillation measurements in conjunction with the well-developed weak scattering theories allow predictive systems of scintillations to be successfully built. On the other hand, in the equatorial region, where strong irregularities extend over several hundred kilometers, amplitude fluctuations as large as 25 dB in the VHF range and even 2 dB at frequencies as high as 6 GHz are often observed. The deleterious effects of such intense scintillations on communication links are indeed very formidable. In view of the paucity of experimental data defining the structure of ionospheric scintillations in the strong scatter regime and the fact that scattering theories in this domain are not fully developed, it has not been possible to develop a successful predictive system of scintillations in the equatorial region for use in communication engineering.

In this report, we present such a study of the characteristics of ionospheric scintillation in the weak and strong scatter regimes. Results on the frequency dependence of scintillations, power spectra and autocorrelation intervals of amplitude fluctuations in the two scattering domains are discussed.

2. OBSERVATIONAL MATERIAL AND METHOD OF ANALYSIS

The study has been based on simultaneous amplitude scintillation measurements of 137 and 360 MHz transmissions from ATS-6 carried out at Huancayo, Peru. The data used in the study correspond to a high level of scintillation activity and were recorded over the interval 2215-2400 LT on Nov. 1, 1974 and 2018-2333 LT on Nov. 4, 1974. In order to study the behavior of the wavelength dependence of scintillation, low fluctuation level scintillation data obtained at Sagamore Hill Radio Observatory, Hamilton, Mass., have also been used. Sagamore Hill data were obtained from ATS-5 transmissions at 137 and 412 MHz on April 12 and May 18, 1973. The data were recorded on FM analog tape which was later digitized at the rate of 6 samples/second. From each 15-minute data block from Huancayo and every 5-minute block from Sagamore Hill, the S_4 index of scintillation has been derived which is defined as the second moment of intensity normalized to the average intensity. The 137 and 360 MHz scintillation data recorded at Huancayo have also been processed to obtain the autocorrelation intervals and the power spectrum of scintillations by the use of FFT algorithm.

3. FREQUENCY DEPENDENCE OF SCINTILLATION IN THE WEAK AND STRONG SCATTER REGIMES

From channel modelling considerations there is considerable interest in the study of frequency dependence of scintillation as it provides an estimate of scintillation at a desired frequency by extrapolating scintillation measurements at another frequency. Recent in-situ measurements at F-region heights indicate that the power spectral density of the irregularity wavenumber spectrum exhibits a power law form with one-dimensional spectral index $\alpha_1 \sim 2$. The dependence of three-dimensional irregularity power spectral density $\Phi_N(k)$ on the irregularity wavenumber k may thus be represented as;

$$\Phi_N(k) = k^{-p} \qquad (1)$$

where $p = \alpha_1 + 2 \sim 4$ for F-region irregularities.

It has been shown that in the weak scatter limit or small amplitude fluctuations, the above form of irregularity spectrum yields a frequency dependence of S_4 index of scintillation as;

$$S_4 \propto f^{-(p+2)/4} \propto f^{-\eta} \qquad (2)$$

Thus the exponent η for the frequency dependence of scintillation is related to the spectral index p of three-dimensional irregularity wavenumber spectrum as;

$$\eta = \frac{p+2}{4} \qquad (3)$$

For F-region irregularities if we assume that $p \approx 4$ the exponent for wavelength dependence η is expected to have a value of about 1.5 for weak scintillations.

Based on Sagamore Hill observations of 137 and 412 MHz scintillations of ATS-5 transmissions on April 12 and May 18, 1973, we obtained the exponent η. In order to examine if the

weak scatter conditions are violated we studied the variation of η with S_4 index at 137 MHz, corresponding to the lower limit of the frequency pair. Most of the observation points pertained to $S_4 < 0.4$ at 137 MHz conforming to weak scatter limit. The data of April 12, 1973 yielded a median value of $\eta \sim 1.2$ while May 18, 1973 data yields $\eta \sim 1.5$. These values of η correspond to spectral indices varying between 3.8 to 4.0 which is very close to that obtained from in-situ measurements of F-region irregularity power spectrum.

The frequency dependence of scintillation in the regime of strong amplitude fluctuations was studied by the use of scintillation measurements at Huancayo with ATS-6 transmissions at 137 and 360 MHz. It may be observed that the exponent η progressively decreases with increasing S_4 in the strong scatter regime. For $S_4 > 0.9$, $\eta \sim 0$, indicating thereby that scintillations become invariant of wavelength for very strong scattering.

Numerical solutions to the problem of multiple scattering indicate that scintillations gradually saturate as scattering conditions become stronger. In the case of our two frequency (137/360 MHz) observations, scintillations saturate first at lower frequency while the scintillation index of the higher frequency still registers an increase with increasing strength of scattering. This explains the observed progressive decrease of η index with S_4. Finally, when the scattering becomes so strong as to drive both 137 and 360 MHz to the saturated scintillation regime, frequency-independent scintillation ($\eta \approx 0$) should result. The experimental results may thus be explained in the framework of multiple scatter theories.

4. POWER SPECTRUM SCINTILLATIONS IN THE WEAK AND MULTIPLE SCATTER REGIMES

The power spectrum of scintillations in the equatorial region was studied and its variation with scintillation activity was examined.

Figures 2 and 3 illustrate the characteristics of power spectrum of scintillations at 137 and 360 MHz over two 15-minute intervals. The spectra in Figure 2 were obtained when the S_4 indices at 137 and 360 MHz were 0.36 and 0.13 respectively and the case therefore corresponds to weak scatter conditions. The noise and frequency resolution error bars as computed at 0.1 Hz are indicated in the diagram. The spectral structure around 1 Hz corresponds to satellite spin modulation. It may be observed that the spectra are characterized by a relatively flat portion and then a linear roll-off portion. The spectral slopes of the roll-off portions correspond to $f^{-3.6\pm0.5}$ and $f^{-2.3\pm0.5}$. If we consider the spectral slope to be approximately 3, then from weak scatter theory an irregularity power spectral index of 4 is obtained in agreement with in-situ measurements of F region irregularities

Figure 3 illustrates the power spectrum of scintillations when multiple scatter conditions prevailed at both frequencies, the S_4 indices at 137 and 360 MHz being 0.95 and 0.84 respectively. The marked variation of the spectral features in this case as compared to that under weak scatter domain, illustrated in the previous diagram, is evident. The flat portion of the spectrum extends to much higher frequency and the slopes of the roll-off portions become very steep as strong scattering is

encountered. The frequency extension of the flat portion indicates that the noise band becomes more white in the strong scatter case and is more red in the weak scatter condition.

A close examination reveals that the limiting frequency of the flat portion is higher at 137 MHz as compared to 360 MHz. The results were confirmed independently by determining directly the autocorrelation intervals at the two frequencies. That the autocorrelation interval is shorter at lower frequency as compared to the higher frequency is opposite to what is expected under weak scatter theory.

From a knowledge of irregularity velocity, the autocorrelation intervals may be transferred to autocorrelation distance. This result has important implications in space diversity systems. We find that for combating weak scintillations the space diversity at lower frequencies is to be larger than that required at higher frequency but the reverse situation will hold when strong scintillations are encountered.

LIST OF FIGURES

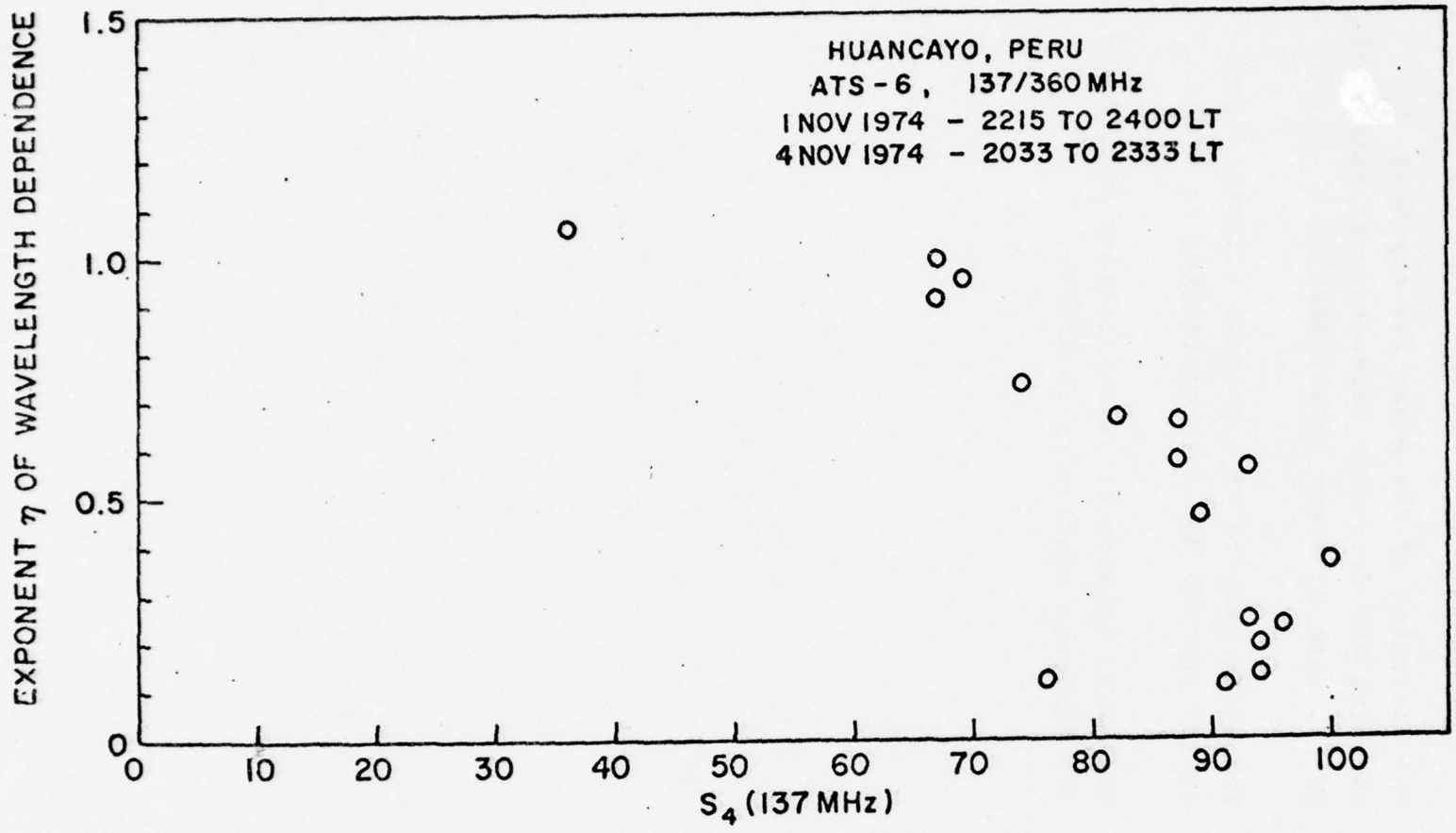
HUANCAYO, PERU
ATS-6, 137/360 MHz
1 NOV 1974 - 2215 TO 2400 LT
4 NOV 1974 - 2033 TO 2333 LT
EXPONENT η OF WAVELENGTH DEPENDENCE
1.5
1.0
0.5
0
0
10
20
30
40
50
60
70
80
90
100
S4 (137 MHz)

Fig. 1

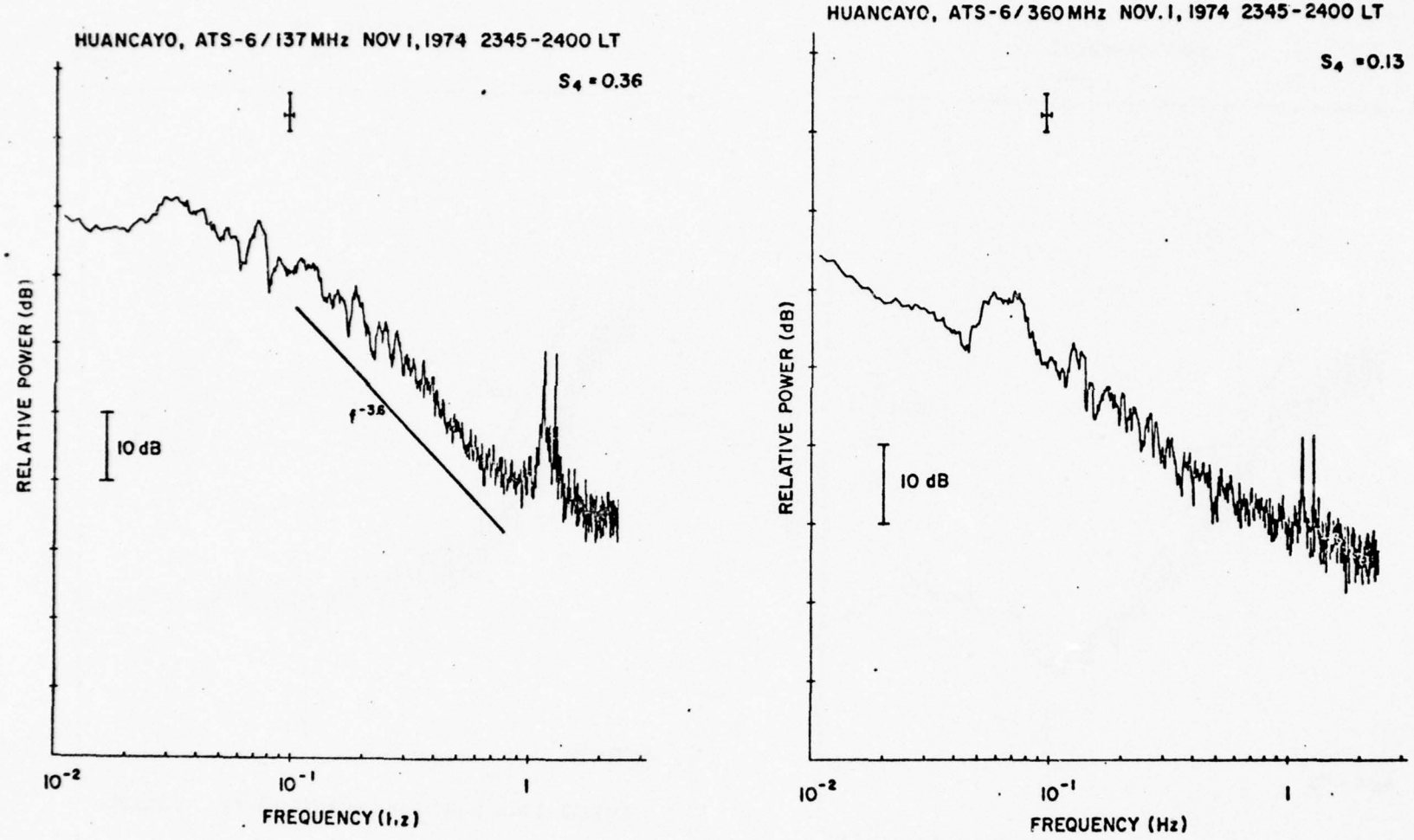
HUANCAYO, ATS-6/137 MHz NOV 1, 1974 2345-2400 LT
S_4 = 0.36
RELATIVE POWER (dB)
10 dB
$f^{-3.6}$
10^{-2}
10^{-1}
1
FREQUENCY (Hz)
HUANCAYO, ATS-6/360 MHz NOV. 1, 1974 2345-2400 LT
S_4 = 0.13
RELATIVE POWER (dB)
10 dB
10^{-2}
10^{-1}
1
FREQUENCY (Hz)

Fig. 2

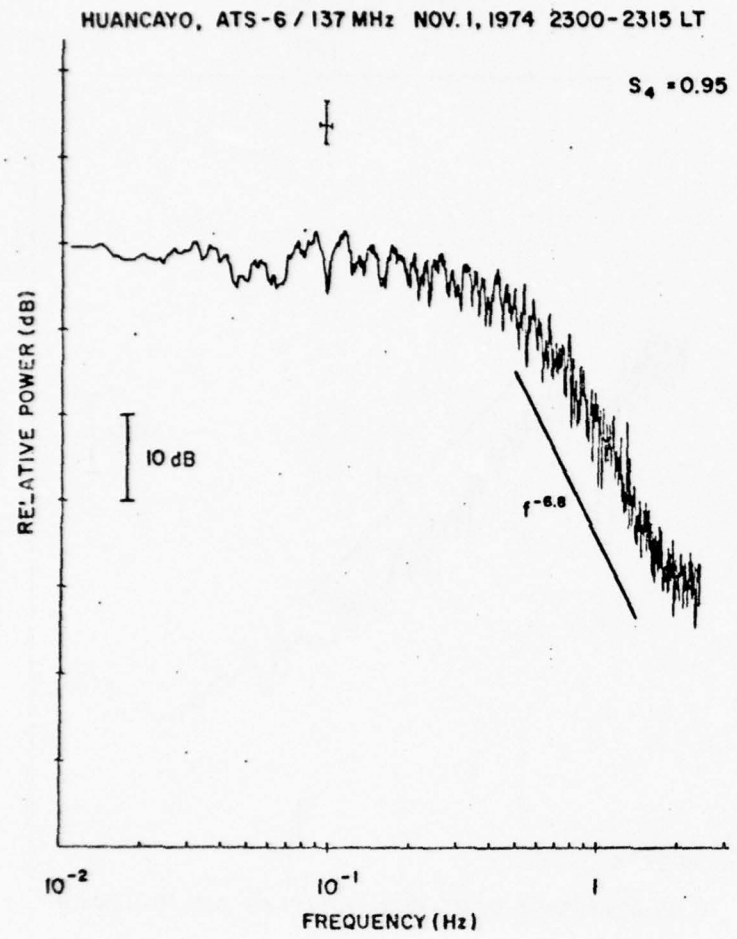
HUANCAYO, ATS-6 / 137 MHz NOV. 1, 1974 2300-2315 LT
S_4 = 0.95
10 dB
$f^{-6.8}$
RELATIVE POWER (dB)
10^{-2}
10^{-1}
1
FREQUENCY (Hz)

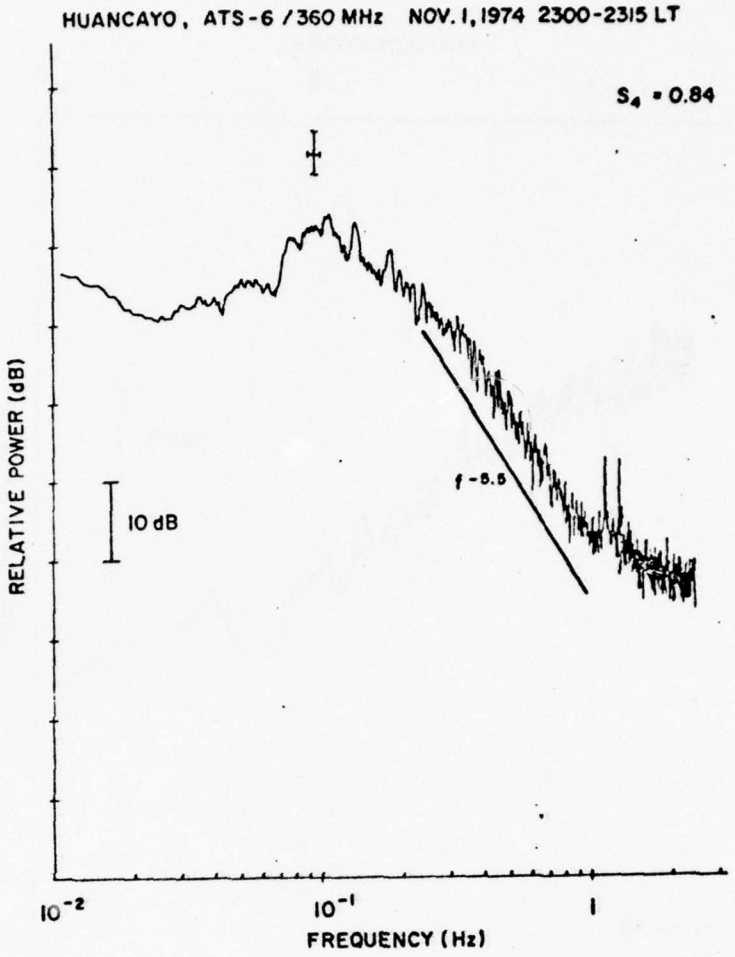
HUANCAYO, ATS-6 / 360 MHz NOV. 1, 1974 2300-2315 LT
S_4 = 0.84
10 dB
$f^{-5.5}$
RELATIVE POWER (dB)
10^{-2}
10^{-1}
1
FREQUENCY (Hz)

Fig. 3

IV.

ON THE NATURE OF ELECTROJET IRREGULARITIES RESPONSIBLE FOR DAYTIME VHF SCINTILLATIONS

1. INTRODUCTION

Scintillation measurements made at Huancayo, Peru by the use of 41 and 140 MHz transmissions of ATS-6 indicate that scintillation is almost a regularly occurring phenomenon during daytime near the magnetic equator. In view of the much lower level of daytime scintillation as compared to nighttime, the characteristics of daytime scintillation have remained unexplored whereas equatorial nighttime scintillation has been extensively studied. The most viable portion of the equatorial ionosphere where plasma density irregularities are generated during daytime corresponds to the electrojet region which is to be associated with the observed daytime scintillations.

The nature of electron density irregularities with meter wavelength present in the equatorial electrojet has been extensively explored, experimentally, by the radar spectral techniques and theoretically in the light of plasma instability mechanisms. These studies reveal the existence of two distinct types of meter wave irregularities, namely, types 1 and 2. Type 1 irregularities are considered to be generated by a modified two-stream instability when the electron drift velocity relative to the ions exceeds the ion-acoustic velocity of about 360 m/sec. Type 2 irregularities, on the other hand, are generated by gradient drift instability mechanism when the electron drift velocity exceeds a velocity of about 30 m/sec in a region of steep density gradient.

In view of the fact that a backscatter radar is sensitive to half the transmitted wavelength, sweep frequency radars have been operated over the frequency range of 15-150 MHz to study the

electrojet irregularities with wavelengths ranging between 10m - 1m. These studies indicate that the long wave irregularities correspond to type 2 generated by gradient drift instability mechanism whereas short wave irregularities correspond to type 1 being generated by two-stream instability mechanism. In an effort to extend the study of electrojet irregularities to wavelengths longer than those explored by radar measurements, the features of equatorial sporadic-E (E_{sq}) in relation to radar measurements have been recently explored. The sporadic-E signature on ionograms corresponds typically to 30-80m irregularity wavelengths. It has been found that the long wave E_{sq} irregularities are related to type 2 meter wave irregularities which are generated by the gradient drift mechanism. This indeed conforms to the theoretical predictions. Recent theoretical studies show that the gradient drift mechanism generates still longer irregularity wavelengths in the kilometer range. From experimental as well as theoretical standpoint there exists considerable interest in exploring the long wavelength end of electrojet irregularities.

The present report based on VHF scintillation measurements and ionograms obtained at Huancayo as well as NOAA oblique VHF radar measurements made at Jicamarca attempts such a study of the characteristics of electrojet irregularities. It is known that scintillations arise from irregularities with wavelengths of the order of Fresnal dimension of the exploring wavelength at the irregularity height. For ATS-6 observations from Huancayo the Fresnel dimensions at 41 and 140 MHz with 110km slant range of the electrojet region correspond to 1km and 0.5km respectively. The study of E_{sq} on ionograms obtained at Huancayo provided

simultaneous information on 30-80m irregularity wavelengths whereas 50 MHz oblique radar backscatter measurements carried out at Jicamarca reveal the existing types of irregularities at 3m wavelength. This study, therefore, covers the wide range of irregularity wavelength from a few meters to about a kilometer in the equatorial electrojet.

2. RESULTS AND DISCUSSIONS

On normal days, the onset of scintillations occur immediately before 0800 LT and continue until about 1800 LT. Around noontime, scintillations attain maximum daytime level which can be as large as 13 dB peak to peak at 41 MHz and a few dB even at 140 MHz. On some occasions, the nighttime F-region scintillation continues through the early morning hours to merge with the daytime scintillation. On these days it is impossible to determine the onset time of daytime scintillation. On some other occasions, the onset of post-sunset F-region scintillation takes place before the daytime scintillation event has ceased completely.

Figure 1 indicates the time intervals over which both the NOAA oblique VHF radar detected electrojet irregularities and scintillations were recorded at Huancayo. On a few days scintillation measurements at 41 MHz only were available and on some others scintillation measurements at 140 MHz only could be made. The shading for these different measurements have been indicated in the diagrams. The breaks in the bar diagrams indicate either no observations were made during the period or no satellite transmission was available. During the period February 1-8, 1975, scintillations are observed only when 50 MHz radar is also able to detect electrojet irregularities. In view of the higher

frequency, scintillations at 140 MHz are detected slightly after the radar detects the presence of electrojet irregularities. Similarly, the cessation of scintillation activity at 140 MHz occurs earlier than the cessation of radar echo. We shall later provide estimates of irregularity amplitudes required to give measurable scintillation at 140 MHz. This will indicate that the irregularity amplitudes need to be larger than some threshold level to give measurable 140 MHz scintillation. It is interesting to note that on February 4, the electrojet irregularities are absent during the major part of the day as indicated by the radar measurements and scintillations are also conspicuous by their absence. The weak irregularities detected by the radar between 1500 and 1800 LT are not sufficiently strong to cause 140 MHz scintillation. Scintillation at 140 MHz observed on February 1 immediately prior to 2000 LT without any associated radar echo is attributed to the post-sunset F region irregularities. On this day, the nighttime scintillation at 140 MHz occurred at 1945 LT and continued until 0445 LT on the next day. Between February 18 and March 5, 1975, scintillation measurements could be made at the lower frequency of 41 MHz and it may be noted that the time synchronism between the radar echo and scintillation is excellent. The weak irregularity amplitudes which become detectable with the radar give rise to immediate scintillation effects at the lower frequency.

The comparative study of radar echoes and VHF scintillation illustrated by Figure 1 indicate that daytime scintillation is caused by electrojet irregularities and that the irregularities with wavelengths of the order of a km (corresponding to Fresnel dimensions) as explored by scintillation measurements co-exist

with the short-wavelength (3m) irregularities detected by the 50 MHz radar.

We shall next illustrate the behavior of q-type sporadic-E (E_{sq}) echoes on February 20 in relation to 41 MHz scintillation and VHF radar echo. Figure 2 shows that both the scintillation activity and radar echo corresponding to type 2 ceased at 1820 LT. The bottom panel of this figure shows the ionogram sequence between 1800 and 1830 LT. The presence of E_{sq} echoes in the first two frames may be observed but in the final frame obtained at 1830 LT, E_{sq} is seen to have disappeared. Such a correlation between these events is found to exist on other days also. It shows that VHF scintillation, type 2 radar echo and E_{sq} echoes appear and disappear together. An extensive study of E_{sq} echoes in relation to type 2 radar echoes has been recently carried out. Our results establish the fact that type 2 irregularities are synchronized not only with the appearance of irregularities at 30-80m wavelengths as viewed by E_{sq} echoes on ionograms but with kilometer wavelength irregularities as well which cause 41 MHz scintillations. Thus this correlative study indicates that type 2 irregularities cover about a 3-decade range in wavelength.

The radar observations provided information on the nature of electrojet irregularities observed at 50 MHz. It has been established that both type 1 and type 2 are equally important in giving 50 MHz radar backscatter echoes whereas at frequencies higher than 50 MHz, type 1 irregularities predominate and radar echoes at lower frequencies are dominated by type 2 irregularities. The present 50 MHz radar observations yield the time

evolution of type 1 and type 2 irregularities and also provide the strength of either type of echo simply as weak or strong. Figure 3 shows the time variation of scintillation index SI at 140 MHz and the evolution of type 1 and type 2 irregularities as observed by the 50 MHz radar. The levels 1 and 2 marked in NOAA radar plots represent respectively the presence of weak or strong type 2 irregularities whereas levels 3 and 4 correspond respectively to weak and strong type 1 irregularities. On February 2, 140 MHz scintillation becomes discernible at 0915 LT when the radar echo reveals the presence of strong type 2 and weak type 1 echo. At 1210 LT when the radar echo indicates the cessation of type 1 irregularities and presence of type 2 irregularities only, the scintillation index does not show any change. This implies that the presence or absence of type 1 irregularities do not introduce any marked variation of the scintillation level indicating thereby that VHF scintillation activity is related to type 2 irregularities.

The lower data set obtained on February 4 shows an unusual day with no electrojet irregularities and consequently no scintillation during the major part of the day. The sporadic appearance of radar echo between 1600-1920 LT corresponding mostly to weak type 2 is not associated with scintillation activity at 140 MHz. The absence of scintillation activity on that day as well as any type 2 irregularities during the major part of the day may be related to a reversal of electric field at E-region heights. On a normal day, the E-region electric field near the magnetic equator is eastward, an upward Hall electric field is generated which in the presence of an upward

plasma density gradient generates type 2 irregularities. The generation of these irregularities is inhibited when the electric field reverses its direction to become westward. The reversal of the electric field, termed as counter-electrojet, has been diagnosed from a decrease in horizontal magnetic field intensity and has been shown to be correlated with the disappearance of E_{sq} echoes and decrease of signal intensity in transequatorial VHF scatter links.

During the development phase of VHF scintillations, a scintillation index (SI) of about 50% at 41 MHz typically corresponds to moderately strong type 2 echoes at meter wavelengths. The SI index of 50% corresponds to the theory based S_4 index of about 0.25. A knowledge of S_4 index allows us to compute the electron density deviation in the irregularities of realistic assumptions can be made regarding the irregularity layer thickness (L), layer height (z) and irregularity power spectrum. The slant range (z) of electrojet region to Huancayo for ATS-6 observations during the period was about 110 km. The thickness (L) of this layer over which the irregularities are assumed to be distributed undiminished in magnitude is considered as 5 km. We have also assumed that the 3-dimensional irregularity power spectrum has a spectral index of 4 in agreement with other experimental and theoretical results. The outer scale of the irregularity has been taken as 2 km in keeping with the numerical studies of type 2 irregularities. We find that S_4 index of 0.25 at 41 MHz may be observed when the electron density deviation of the irregularities is $\Delta N = 6 \times 10^{9} m^{-3}$. This corresponds to irregularity amplitudes of 6% and 3% respectively for ambient

ionization density of 10^{11} and $2\times10^{11}\,m^{-3}$ corresponding to critical frequencies of 3 and 4 MHz. At 140 MHz, similar level of S_4 is attained only if the irregularity amplitudes increase by a factor of about 5. Theoretical studies of type 2 irregularities indicate that when the amplitude of type 2 irregularities in the tens of meter wavelength range attains a level of about 4% under the linear theory of gradient drift instability, shorter wavelength irregularities in the meterwave range may be generated through non linear cascading mechanism. Our computations of irregularity amplitudes based on VHF scintillation measurements indicate that when the r.m.s. irregularity amplitude in the kilometer wavelength range is found to be of the order of 5%, the 50 MHz radar is able to detect simultaneously the presence of type 2 irregularities. The highest level of S_4 index at 41 MHz during daytime is found to be of the order of 0.5, which is found to correspond to an electron density deviation $\Delta N = 1.6\times10^{10}\,m^{-3}$ with the above assumed parameters. This value corresponds to r.m.s. irregularity amplitudes of 16% for ambient ionization density of $10^{11}\,m^{-3}$.

For a power law type of irregularity power spectrum, the scintillation index (S_4) is expected to have a power law variation with frequency. Assuming that such a power law variation exists, we defined the spectral index (η) of scintillation as

$$\eta = \frac{\log\,(S_{4_1}/S_{4_2})}{\log\,(f_2/f_1)}$$

where S_{4_1} and S_{4_2} are the scintillation indices (S_4) at f_1 and f_2

respectively. From simultaneous daytime scintillation measurements at 41 and 140 MHz the spectral index η is obtained. Figure 4 indicates the variation of η with S_4 index at 41 MHz. It is found that for S_4 varying between 0.2 to 0.4, η varies between 0.6 to 1.2. For weak scattering spectral index of scintillation related to the spectral index (p) of the irregularity power spectrum as $\eta = \frac{p+2}{4}$. Thus the results indicate that during the development or decay of type 2 irregularities, the irregularity power spectrum is very flat but attains a spectral index of about 3 when the irregularities are fully developed. It should be emphasized that the Fresnal dimensions of 41 and 140 MHz at the electrojet height corresponds to 0.5 km and 1 km respectively. Thus the derived spectral indices of the irregularities correspond to the above wavelength range which is close to the outer scale of type 2 irregularities.

3. SUMMARY

The study reveals that daytime VHF scintillations are generated when E_{sq} echoes appear on ionograms and 50 MHz radar detects type 2 electrojet irregularities. Since VHF scintillations are sensitive to kilometer wavelength irregularities, E_{sq} monitors 30-80m wavelength irregularities and 50 MHz radar detects 3m wavelength irregularities, it may be concluded that type 2 irregularities covering the wavelength range of a few meters to a few kilometers co-exist. We have also found that during periods when the radar does not detect any electrojet irregularity, neither E_{sq} nor VHF scintillation is observed.

With the time scale of our measurements, it is not possible to locate the time period when non-linear cascading mechanism starts to generate meter wave irregularities, the theoretically predicted time interval being of the order of a second.

We have shown that when type 2 meter wave irregularities and VHF scintillations are simultaneously observed the irregulatity amplitudes ranging between 4% to 16% (for ambient ionization density of $10^{11} m^{-3}$) at kilometer wavelengths are obtained. Further in the wavelength range of 0.5-1 km corresponding to the Fresnal dimensions of scintillation measurements, the spectral index of the irregularity power spectrum indicates a variation with irregularity amplitudes. At low levels of scintillation, the power spectrum is very flat but confirms to a power law spectral exponent of about 3 when fully developed. The observed evolution of irregularity spectrum corresponds to wavelengths in the vicinity of outer scale of type 2 irregularities which is typically assumed to lie in the range of 2-3 km.

LIST OF FIGURES

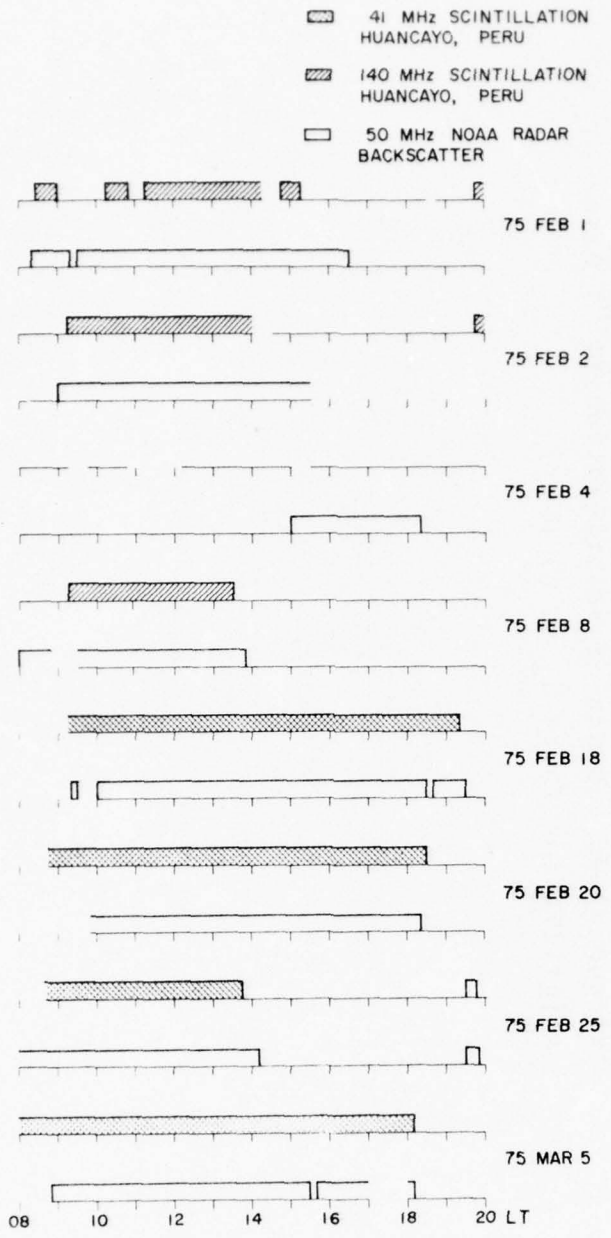
41 MHz SCINTILLATION
HUANCAYO, PERU
140 MHz SCINTILLATION
HUANCAYO, PERU
50 MHz NOAA RADAR
BACKSCATTER
75 FEB 1
75 FEB 2
75 FEB 4
75 FEB 8
75 FEB 18
75 FEB 20
75 FEB 25
75 MAR 5
08
10
12
14
16
18
20 LT

Fig. 1

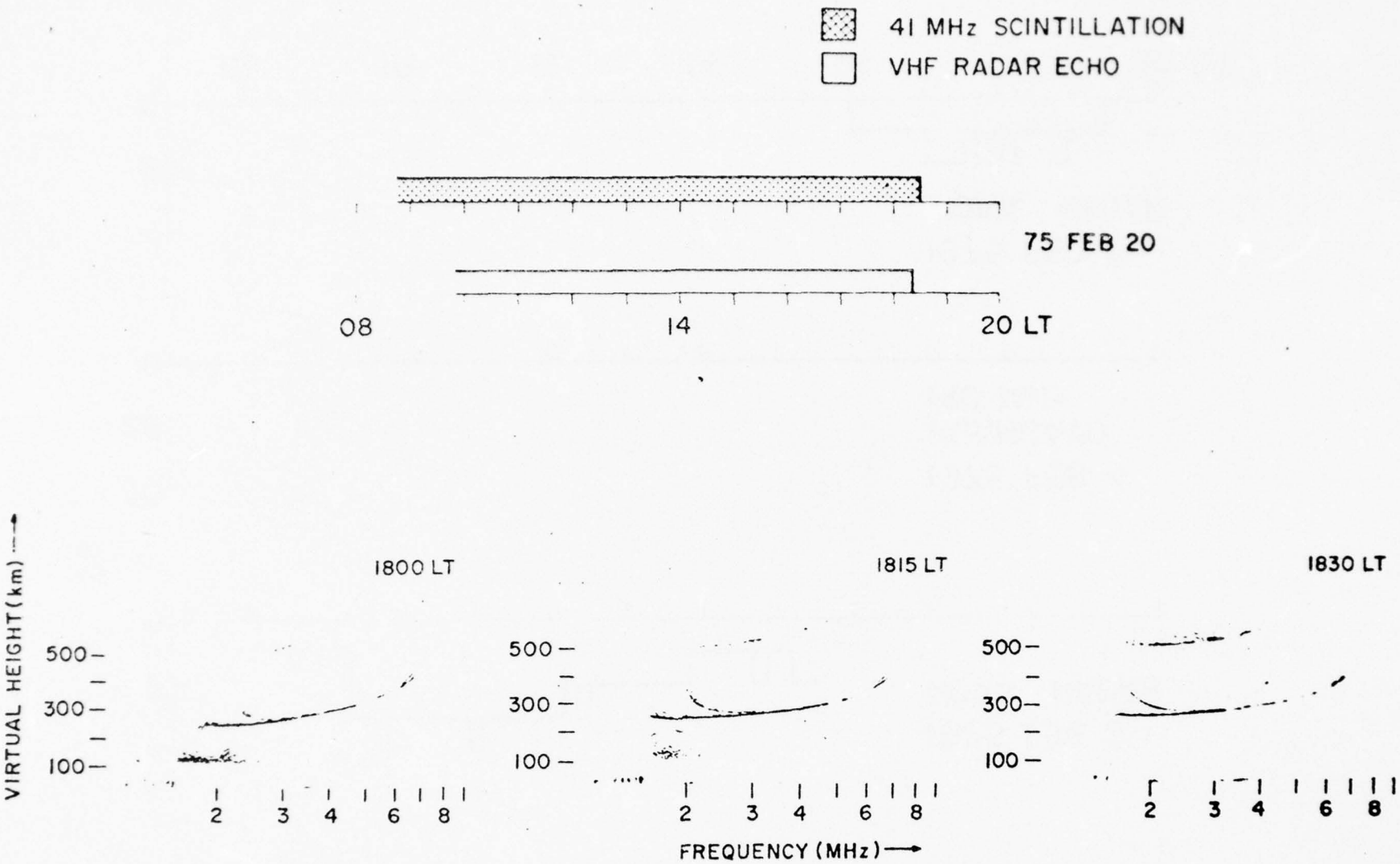
41 MHz SCINTILLATION
VHF RADAR ECHO
75 FEB 20
08
14
20 LT
1800 LT
1815 LT
1830 LT
VIRTUAL HEIGHT (km)
500
300
100
2
3
4
6
8
FREQUENCY (MHz)

Fig. 2

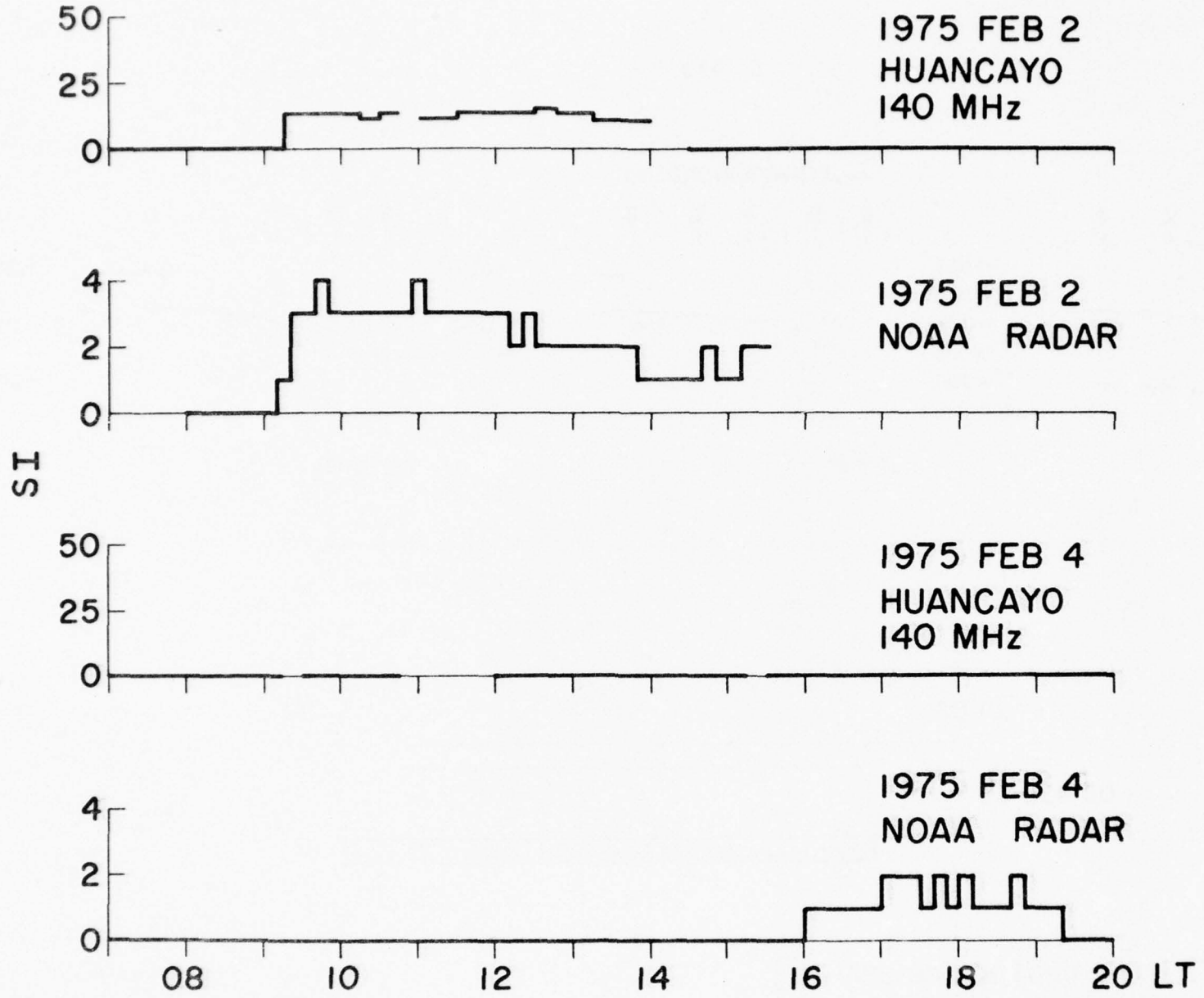
50
25
0
1975 FEB 2
HUANCAYO
140 MHz
4
2
0
1975 FEB 2
NOAA RADAR
IS
50
25
0
1975 FEB 4
HUANCAYO
140 MHz
4
2
0
1975 FEB 4
NOAA RADAR
08
10
12
14
16
18
20 LT

Fig. 3

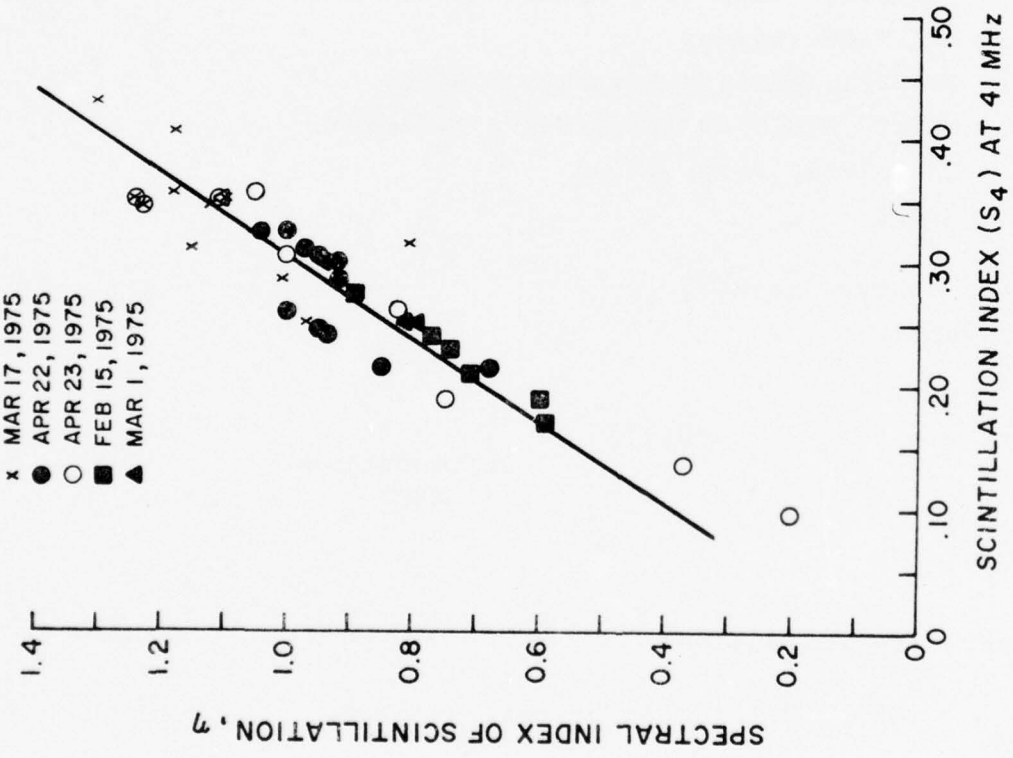
x MAR 17, 1975
● APR 22, 1975
○ APR 23, 1975
■ FEB 15, 1975
▲ MAR 1, 1975
SPECTRAL INDEX OF SCINTILLATION, η
1.4
1.2
1.0
0.8
0.6
0.4
0.2
0
.10
.20
.30
.40
.50
SCINTILLATION INDEX (S_4) AT 41 MHz

Fig. 4

V.

SIGNAL ANALYSIS PACKAGE

The signal analysis package described in a Final Report AFGL-TR-76-0041, has been modified for greater ease of use. Following is a description of the deck setup required to operate this program on the CDC 6600. In all that follows, optional parameters are enclosed in square brackets [ ].

Deck Setup

```
Job Card    Jobname,CM110000,Txxx,TP1.  Job#  Name
            VSN,TAPE1=xxxxxx.
            REQUEST,TAPE1,HY,S(xxxxxx/NORING)
            ATTACH,SIG,SIGNALYSISx3828,ID=CANTOR.
            CALL,I=SIG,P=runoption.
            7/8/9

Calibration control card[s]
control card[s]
Title card
[ [Calibration control card[s]]
  [control card[s]]                  ]   continuation
  Title card                             runs
```

Run option

There are five run options:

ONRED
ONBLACK — ON or OFF for on or offline plot
OFFRED
OFFBLACK — RED or BLACK ink
NOPLOT

Calibration Control Cards

Txx,Cxx,Fxx[T_1,T_2,R_1,R_2][,H][,U]

Tape number xx is floating point (T37, T45.1)
Cal number (C3)
File number (F2)

T_1, T_2 are start and end time of digitization for this file

R_1, R_2 are start and end time (real time of data acquisition for this file)

T_i, R_i are of the form hhmmss

Here cals follow

Update - update cal file

Calibration Cards (H option)

Card 1 - Channel number, identification (I2,A10) - b2360MHZ

Card 2-n - digitized count level, dB level free format separated by blank or comma. Need not be one level per card. Calibrations are entered with high signal first and nondecreasing signal strengths. All dB levels are normalized to 0 dB high signal

Example:
128,0,100,1,90,2 is normalized to

128 0
100 - 1
90 - 2

Calibrations can be added at either end.

Example:
140,-2,135,-1
128,0,100,1,90,2
85,3 is normalized to

140 0
135 - 1
128 - 2
100 - 3
90 - 4
85 - 5

Card n+1 $\left\{\begin{matrix}\text{blank}\\-9\end{matrix}\right\}$ end of $\left\{\begin{matrix}\text{channel}\\\text{calibrations}\end{matrix}\right\}$

If no calibrations are entered (i.e., n+1=2) dB=level.

Examples:

1) Existing cal file

   T37,C2,F3

2) To add new file or redefine old file with previously defined calibrations

   T37,C2,F4=1800.30,1815.05,200,400,U

3) To use new calibrations but not to redefine

   T37,C2,F3=1800,1900,200,400,H

   cals

It should be noted that calibrations are catalogued under tape and calibration number. Any redefinition of calibrations for any file under that tape and calibration number, redefines calibrations for all files.

Control Cards

Control cards are free form concatenations of option selections of the form

Option or Option = parameter list

(options are separated by commas)

Parameter lists have the following forms:

a) OFF turn the option off for all channels

b) none " " " on " " "

c) $n_1,\ldots,n_k$ turn the option off for channels n_i, off for other channels

d) hhmm.ss time

e) d_1 number

f) dB_1, dB_2 dB levels limits for dwell analysis

g) $t_1,\ldots,t_n$ times for dwell analysis

options	parameter list types	meaning	default
END		end of control cards	
CHANS	a,b,c	restrict analysis to these channels	1,2,...,10
CDF	a,b,c	CDF's on these channels	OFF
DWELL	a,b,c	dwell time analysis for these channels	OFF
MSG	a,b,c	message reliability statistics for these channels	OFF
DATA	a,b,c	plot data for these channels	OFF
SPECTRA	a,b,c	plot smoothed power spectra for these channels	OFF
RAW	a,b,c	plot raw power spectra for these channels	OFF
AUTO	a,b,c	perform autocorrelation for these channels	OFF
CROSS	a,b,c*	perform cross-correlation for these channels	OFF
CORR	e	correlation limit for plotting of auto and cross-correlations. CORR=0 - plot all CORR=2 - suppress plots	0.3
SECONDS	e	number of seconds (real time) in each period of analysis	900
PERIODS	e	number of periods to analyze	999
REWIND		rewind data tape	
SKIP	b,e	skip d,(or 0) files on data tape after skipping to end of current file if not already there	

options	parameter list types	meaning	default
START	d	real time start of data analysis	current real time on data tape or start of current data file
CLEAR		all analysis options and all channels off	
NTH	e	use every n'th point	1
DBS	f	dB range for dwell times and message reliability analysis	-10 to +5
TIMES	g	time ranges for dwell time and message reliability analysis	t_n t_{n+1} Δt .25 1 .25 1 6 .5 6 10 1 10 20 2 20 40 5 40 60 10 60 t_{max} all times in sec.

* Cross correlation channel list consists of sublists separated by semicolons. The first channel in the sublist is correlated with the remaining channels. The last sublist may be terminated by a comma or end of card.

For example:

```
CROSS=1,2,3;2,3,4
  or
CROSS=1,2,3;
2,3,4
  or
CROSS=1,2
3;2,3,4
```

will yield cross-correlations of channel 1 vs 2+3 and 2 vs 3+4, while

```
CROSS=1,2,3
2,3,4
```

will yield cross-correlations of 1 vs 2,3, and 4.

TITLE CARD

A title card is any card that cannot be mistaken for a calibration card or control card. Care should be taken not to use a control card option word as the first word of a title.

Processing begins after each title card is recognized.

Example:

To run 4 fifteen-minute data samples on channels 1,3,4 on data tape OS1, file three starting at 415. Statistics wanted are only print statistics including those for correlations. Further, one hour samples of smoothed spectra and autocorrelations, decimated 4 to 1 are wanted for the fourth file of the tape. Cross-correlations are wanted only for channel 1+2 versus the rest, and are to be plotted only if greater than 0.4. There are 5 channels on the tape. The calibrations are catalogued as tape 17, calibration 1, files 2 and 3. Plots are to be off line, red ink.

Deck

```
CANTOR, CM11000,T500.
VSN, TAPE1=050001.
REQUEST,TAPE1,HY,S.(OS0001/NORIN6)
ATTACH,SIG,SIGNALYSISX3828,ID=CANTOR.
CALL,I=SIG,P=OFFRED.
7/8/9
T17,C1,F2
PERIODS=4,SKIP=2,START=415,
CHANS=1,3,4,CDF,DWELL,MSG
AUTO,CROSS,CORR=2,END
TITLE FOR FIRST SAMPLE RUN
T17,C1,F3
```

```
PERIODS=999,SECONDS=3600
NTH=4,SKIP,CLEAR,SPECTRA,AUTO,
CROSS=1,2,3,4,5;2,3,4,5,CORR=0.4,END
TITLE FOR SECOND SAMPLE RUN
6/7/8/9
```

FOLLOWING THIS SECTION ARE:

CALIBRATION ERROR MESSAGES (3 pages)

ERROR MESSAGES

APPENDIX 1 - Catalogued Procedures on File SIGNALYSISX3828

APPENDIX 2 - Calibration File Format

APPENDIX 3 - Control Card Decoder

including

Sample Main Program
Functions
Sample Output

```
MAIN
CONTROL
T37,C2,F3=2113,2120,30,3300,0500,H
CHANNEL 1
137 MHZ
 221,   0
 215,   1
 208,   2
 201,   3
 193,   4
 186,   5
 179,   6
 171,   7
 164,   8
 156,   9
 149,  10
 141,  11
 133,  12
 125,  13
 117,  14
 109,  15
 101,  16
  94,  17
  87,  18
  79,  19
  73,  20
  67,  21
  61,  22
  55,  23
  50,  24
  45,  25
  40,  26
  36,  27
  33,  28
  30,  29
  28,  30
  27,  31
  26,  32
  25,  33
  24,  34
```

CALIBRATION ERROR MESSAGES (1 Of 3)

CHANNEL 1 POSSIBLE ERROR IN CALIBRATION

24	-34.
25	-33.
26	-32.
27	-31.
28	-30.
30	-29.
33	-28.
36	-27.
40	-26.
45	-25.
50	-24.
55	-23.
61	-22.
67	-21.
73	-20.
79	-19.
87	-18.
94	-17.
101	-16.
109	-15.
117	-14.
125	-13.
133	-12.
141	-11.
149	-10.
156	-9.
164	-8.
171	-7.
179	-6.
186	-5.
193	-4.
201	-3.
208	-2.
215	-1.
221	-0.

CALIBRATION ERROR MESSAGES (2 of 3)

```
CHANNEL 2
360 MHZ
215,0
198,1
181,2
165,3
148,4
133,5
118,6
103,7
89,8
76,9
65,12
56,11
50,12
46,13
42,14
39,15
37,16
35,17
34,18
33,20
32,22
31,24
-9
```

```
CHANNEL  2          ERROR IN CALIBRATION
   31   -24.
   32   -22.
   33   -20.
   34   -18.
   35   -17.
   37   -16.
   39   -15.
   42   -14.
   46   -13.
   50   -12.
   56   -11.
   65   -12.
   70    -9.
   89    -8.
  103    -7.
  118    -6.
  133    -5.
  148    -4.
  165    -3.
  181    -2.
  198    -1.
  215    -0.
STOP
```

CALIBRATION ERROR MESSAGES (3 Of 3)

ERROR MESSAGES	Further Explanation
REWIND,START=345,CDF,END NO TIME FOUND FOR DATA SEARCH	No tape specified before manipulation
T37,C2,F3. 3 10 FILE FULL OR CALS. NOT FOUND T37,C2,F3.	
T37,C2,F3 REWIND,START=345,END HIT END OF INFORMATION ON TAPE1	
T37,C2,F3 REWIND,START=1200,END HIT END OF FILE LOCKING ECS 12 0 0	
T37,C2,F3 PRIODS=3,SECONDS=300,CDF,END PARAMETERS OR CALS MISSING	Periods misspelled. Title card assumed
T37,C2,F3 PERIODS=3,SCONDS=300,CDF,END * PARAMETER ERROR IN FIELD ENDING WITH *.	

APPENDIX 1

Catalogued Procedures on File SIGNALYSISX3828.

```
*ONRED.
DISPOSE,PLOT,*PL.
ATTACH,LG1,DECOBINX2944,ID=CANTOR,MR=1.
COPYL,LG1,LGO,LG2.
UNLOAD,LG1,LGO.
ATTACH,PEN,ONLINEPEN.
LIBRARY,PEN.
ATTACH,TAPE10,CALIBX2944,ID=CANTOR,PW=CJC.
LG2.
EXTEND,TAPE10.
EXIT.
EXTEND,TAPE10.
```

```
*OFFRED.
DISPOSE,TAPE39,*LR.
ATTACH,LG1,DECOBINX2944,ID=CANTOR,MR=1.
COPYL,LG1,LGO,LG2.
UNLOAD,LG1,LGO.
ATTACH,PEN,OFFLINEPEN.
LIBRARY,PEN.
ATTACH,TAPE10,CALIBX2944,ID=CANTOR,PW=CJC.
LG2.
EXTEND,TAPE10.
EXIT.
EXTEND,TAPE10.
```

```
*OFFBLACK.
DISPOSE,TAPE39,*LL.
ATTACH,LG1,DECOBINX2944,ID=CANTOR,MR=1.
COPYL,LG1,LGO,LG2.
UNLOAD,LG1,LGO.
ATTACH,PEN,OFFLINEPEN.
LIBRARY,PEN.
ATTACH,TAPE10,CALIBX2944,ID=CANTOR,PW=CJC.
LG2.
EXTEND,TAPE10.
EXIT.
EXTEND,TAPE10.
```

```
*ONBLACK.
DISPOSE,PLOT,*OL.
ATTACH,LG1,DECDBINX2944,ID=CANTOR,MR=1.
COPYL,LG1,LGO,LG2.
UNLOAD,LG1,LGO.
ATTACH,PEN,ONLINEPEN.
LIBRARY,PEN.
ATTACH,TAPE10,CALIBX2944,ID=CANTOR,PW=CJC.
LG2.
EXTEND,TAPE10.
EXIT.
EXTEND,TAPE10.
```

```
*NOPLOT.
ATTACH,LG1,DECDBINX2944,ID=CANTOR,MR=1.
COPYL,LG1,LGO,LG2.
UNLOAD,LG1,LGO.
ATTACH,PEN,ONLINEPEN.
LIBRARY,PEN.
ATTACH,TAPE10,CALIBX2944,ID=CANTOR,PW=CJC.
LG2.
EXTEND,TAPE10.
EXIT.
EXTEND,TAPE10.
```

APPENDIX 2

Calibration File Format

Catalogued calibations reside on a CDC 6600 mass storage file. See the CDC FORTRAN Extended manual for general definitions and usage details. The defining parameters for a particular calibration are type number and calibration number, referred to hereafter as a calibration id. Each calibration id may have associated with it up to twenty files. Calibration id's are numerically indexed in the main file index in the order of receipt, excapt that additions or changes to an existing calibration id overwrite it. Up to one hundred calibration id's may be catalogued.

The following is a description of the calibration file structure.

Main Index Structure

Word	
1	Pointer to control record 1
2	Pointer to calibration subindex 1
2n-1	Pointer to control record n
2n	Pointer to calibration index n
2n+1	0
200	0

AD-A034 490 EMMANUEL COLL BOSTON MASS F/G 20/14
STUDY AND ANALYSIS OF TOTAL ELECTRON CONTENT AND SCINTILLATION --ETC(U)
OCT 76 S BASU, C J CANTOR, J JOHANSON F19628-76-C-0003
UNCLASSIFIED SCIENTIFIC-1 AFGL-TR-76-0260 NL

2 OF 2
AD
A034490

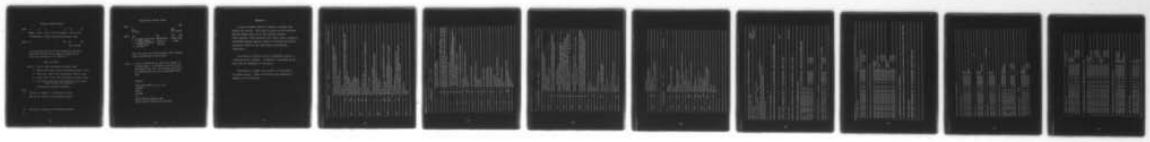

END
DATE
FILMED
2-77

Control Record Format

Word	1	2	3	7	8	12
	Tape#	Cal#	File id #1 (5 words)		File id #2	

Calibration id from calibration control card

Word	13	97	98	102
	. . . . . .		File id #20	

All variables in the control record are strictly positive floating point numbers except that a null file id consists of -999.0's.

File id Format

Word 1 - File # from calibration control card

2 - Start time (tape) from calibration control card

3 - End time (tape) from calibration control card

4 - Start time (real) from calibration control card

5 - End time (real) from calibration control card
(Time formats are hhmm.ss)

Calibration Subindex Structure

Word	
1	Pointer to channel 1 calibration record
2	Pointer to channel 2 calibration record
10	Pointer to channel 10 calibration record
11	0

Calibration Record Format

Word	1			256
	dBs 1 count		dBs 256 counts	
Word	257	258	259	260
	0 if signal decreases with counts. 1 if signal increases with count -1 see Note 1	#characters alpha in 259-260	Alpha from input	

dB's are $\leq$ for all counts except that original input calibrations are positive.

Note 1. A null calibration on input will result in setting $dB_i = i$. Calibrations should not be catalogued this way, but various statistics on uncalibrated data can be generated this way.

Example:

T999,C999,F999=t_1,t_2,r_1,r_2,H
1137MHZ
blank
2256MHZ
-9
DATA,SPECTRA,START=r_1,END
QUICK LOOK AT SPECTRA OF RAW DATA.

APPENDIX 3

As part of Signal Analysis Package, a control card decoder was written. This relies heavily on two functions NUM and IFIELD which are of more general interest. Taken together, these functions will scan a card, stripping off EDITOR defined sequence numbers if desired, and return individual fields on the card between user defined terminators.

The field is returned either as alphabetic array or a floating point variable. In addition, the length of the field and the terminator is available.

Following is a sample main program, the functions, and sample output. Usage instructions are contained in comments to the functions.

```
PROGRAM MAIN      74/74   OPT=1                              FTN 4.5+414

 1                PROGRAM MAIN(INPUT,TAPE6=INPUT,OUTPUT,TAPE5)
                  DIMENSION IBUFF(8),JBUFF(80),ITERM(4)
                  COMMON/IFLOXYZ/IT
                  DATA ITERM/1H,,1H=,0,0/
 5                REWIND 5
                  PRINT 100
              100 FORMAT(*1FOLLOWING IS INPUT CARD DECK. TERMINATORS ARE*
                 1,* COMMA AND EQUAL.*)
                1 READ(6,101)IBUFF
10            101 FORMAT(8A10)
                  IF(EOF(6))99,2
                2 WRITE(5,101)IBUFF
                  PRINT 109,IBUFF
              109 FORMAT(1X,8A10)
15                GO TO 1
               99 DO 3 I=1,2
                  IF(I.EQ.2)PRINT 102
              102 FORMAT(*1BLANK HAS BEEN ADDED AS A TERMINATOR.*)
                  REWIND 5
20                READ(5,101)IBUFF
                  N=0
                  NMAX=NUM(IBUFF,-80,JBUFF)
                5 NCHAR=IFLO1(JBUFF,IBUFF,N,NMAX,ITERM)
                  IF(IT.EQ.0)GO TO 3
25                IF(NCHAR)6,7,8
                7 PRINT 105,IT
                  GO TO 5
              105 FORMAT(* NULL FIELD TERMINATED BY "*,A1,1H")
                6 NCHAR=-NCHAR
30                PRINT 106,IT,NCHAR,IBUFF(1)
              106 FORMAT(* FLOAT FIELD TERMINATED BY "*,A1,1H"
                 1,I3,* CHARACTERS.*,F12.4)
                  GO TO 5
                8 NQ=(NCHAR+9)/10
35                PRINT 107,IT,NCHAR,(IBUFF(II),II=1,NQ)
              107 FORMAT(* ALPHA FIELD TERMINATED BY "*,A1,1H"
                 1,I3,* CHARACTERS.*,1X,8A10)
                  GO TO 5
                3 ITERM(3)=1H
40                STOP
                  END
```

```
      FUNCTION NUM        74/74   OPT=1                          FTN 4.5+414

      1                   FUNCTION NUM(IBUFF,N,JBUFF)
                          DIMENSION IBUFF(8),JBUFF(80)
                      C
                      C   FUNCTION NUM TAKES A "CARD" IN A10 FORMAT IN IBUFF,
      5               C   PLACES IT IN JBUFF IN A1 FORMAT IN JBUFF AND RETURNS THE NUMBER
                      C   OF CHARACTERS LESS TRAILING BLANKS
                      C   PLACES IT IN JBUFF IN A1 FORMAT IN JBUFF AND RETURNS THE NUMBER
                      C   OF CHARACTERS LESS TRAILING BLANKS
                      C
     10               C   IBUFF=INPUT CARD A10 FORMAT
                      C   N=NUMBER OF CHARACTERS IN IBUFF(TYPICALLY 80).
                      C     IF N IS NEGATIVE, EDITOR FORMAT SEQUENCE NUMBERS IN 73-80
                      C     ARE REMOVED IF THE PROGRAM DETERMINES THAT AN EDITOR
                      C     FORMAT CARD WAS INPUT.
     15               C   JBUFF=OUTPUT CARD IMAGE IN A1 FORMAT
                      C
                      C   NUM=NUMBER OF CHARACTERS LESS TRAILING BLANKS
                      C
                          NN=IABS(N)
     20                   DECODE(NN,100,IBUFF)(JBUFF(I),I=1,NN)
                      100 FORMAT(80A1)
                     +    NNN=NN
                      C
                      C   STRIP TRAILING BLANKS
     25               C
                          DO 1 I=1,NN
                          IF(JBUFF(NNN).NE.1H )GO TO 2
                      1   NNN=NNN-1
                      2   CONTINUE
     30                   NUM=NNN
                      C
                      C   EDITOR FORMAT CHECKS
                      C
                          IF(N.GT.0)GO TO 99
     35                   IF(NNN.NE.78)GO TO 99
                      C
                      C   SEQUENCE NUMBER CHECK
                      C
                          DO 3 I=73,78
     40                   J=JBUFF(I)
                          IF(J.GE.1H0.AND.J.LE.1H9)GO TO 3
                          GO TO 99
                      3   CONTINUE
                      C   CARD IS EDITOR FORMAT
     45                   NN=72
                          GO TO 4
                      99  PRINT 102,(JBUFF(I),I=1,NNN)
                      102 FORMAT(/1H0,80A1)
                          PRINT 100
     50                   RETURN
                          END
```

```
      FUNCTION IFIELD   74/74   OPT=1                    FTN 4.5+414
      FUNCTION IFIELD(JBUFF,ABUFF,N,NMAX,ITERM)
      DIMENSION JBUFF(80),ITERM(80),IFMT(3)
      DIMENSION ABUFF(8)
      COMMON/IFLDXYZ/L
      DATA IFMT/2H(F,1H ,3H.0)/
C
C     FUNCTION IFIELD SCANS A CARD AND RETURNS A FIELD,ALPHABETIC
C     OR NUMERIC, TERMINATED BY USER DEFINED TERMINATORS.
C
C           CALLING SEQUENCE
C     JBUFF=INPUT ARRAY, A1 FORMAT.
C     ABUFF=OUTPUT, EITHER ALPHA (A10) OR FLOATING POINT.
C           ALSO USED AS INPUT BUFFER FOR ENTRY IFLD1.
C     N=STARTING POSITION IN ARRAY JBUFF, SHOULD BE SET TO
C       ZERO ORIGINALLY BY MAIN PROGRAM, MAINTAINED BY IFIELD.
C     NMAX=MAXIMUM NUMBER OF CHARACTERS. OUTPUT OF FUNCTION NUM
C     ITERM=ARRAY OF TERMINATION CHARACTERS, LAST ONE MUST BE ZERO.
C     EXAMPLE: DATA ITERM/1H,,1H             ,1H ,0/
C
C           ENTRY POINTS
C     IFIELD-DO NOT READ NEXT CARD IF N>NMAX
C     IFLD1-READ NEXT CARD IF NECESSARY (END OF CARD TERMINATES A
C           FIELD IN ANY CASE).
C
C     FUNCTION VALUE IS THE NUMBER OF CHARACTERS IN THE FIELD, POSITIVE
C     IF ALPHABETIC, NEGATIVE IF FLOATING POINT, 0 IF NULL OR END OF
C     COMMON BLOCK /IFLDXYZ/CONTAINS THE FIELD TERMINATOR. END OF
C     CARD TERMINATOR IS A FORCED COMMA, END OF FILE IS ZERO.
C
      IFLG=0
      GO TO 25
      ENTRY IFLD1
      IFLG=1
   25 NN=0
      M=N+1
      MM=M
      IF(M.GT.NMAX)GO TO 66
C
C     ILEAD IS LEADING BLANK SWITCH
C     INUM IS ALPHA/NUMERIC SWITCH
      ILEAD=0
      INUM=0
      DO 1 I=M,NMAX
      N=N+1
      L=JBUFF(I)
C     LEADING BLANK CHECK
      IF(ILEAD.NE.0.OR.L.NE.1H )GO TO 4
      GO TO 1
    4 ILEAD=1
C     TERMINATOR CHECK
```

```
                    DO 2 J=1,80
                    IF(ITERM(J).EQ.0)GO TO 5
                    IF(L.EQ.ITERM(J))GO TO 3
                2   CONTINUE
55              C   NUMERIC CHECK
                5   IF(L.GE.1H0.AND.L.LE.1H9)GO TO 1
                    IF(L.EQ.1H..OR.L.EQ.1H-)GO TO 1


FUNCTION IFIELD    74/74   OPT=1                    FTN 4.5+414    3

                    INUM=1
                1   CONTINUE
60              C   END OF CARD ON FALL THROUGH
                    L=1H,
                    N=N+1
                3   NN=N-M
                C   NN=NUMBER OF CHARACTERS
65                  IF(NN.EQ.0)GO TO 6
                    NN1=N-1
                    ENCODE(NN,100,ABUFF(1))(JBUFF(I),I=M,NN1)
                    IF(INUM.NE.0)GO TO 5
                C   GET F FORMAT
70                  ENCODE(10,101,IFMT(2))NN
              100   FORMAT(80A1)
              101   FORMAT(I10)
                    DECODE(NN,IFMT,ABUFF(1))ABUFF(1)
                    NN=-NN
75            6     IFIELD=NN
              105   FORMAT(1X,8A10)
                    RETURN
                66  IF(IFLG.EQ.0)GO TO 6
                C   READ NEXT CARD
80                  READ(5,106)ABUFF
              106   FORMAT(8A10)
                    IF(EOF(5))61,67
                C   NOTE CHECK FOR EDITOR CARDS
                67  NMAX=NUM(ABUFF,-80,JBUFF)
85                  N=0
                    GO TO 25
                61  L=0
                    GO TO 6
                    END
```

```
FOLLOWING IS INPUT CARD DECK. TERMINATORS ARE COMMA AND EQUAL.
THIS IS AN EDITOR CARD                                                  000100
THIS IS NOT                                                             100
NOR IS THIS                                                             000100XX
SHOW MULTIPLE TERMINATORS,,,,1,2,3
SHOW MULTIPLE BLANKS     1,2,3
LONG BLANK LEAD                                  7.2,5.978,2.3
REWIND,START=315,CDF=1,2,3,SPECTRA,DATA=3,3.0,3.
NON-COMMA TERMINATOR AS LAST CHARACTER=
END OF CARD DECK

THIS IS AN EDITOR CARD

ALPHA FIELD TERMINATED BY "," 22 CHARACTERS. THIS IS AN EDITOR CARD

THIS IS NOT                                                             100

ALPHA FIELD TERMINATED BY "," 75 CHARACTERS. THIS IS NOT

NOR IS THIS                                                             000100XX

ALPHA FIELD TERMINATED BY "," 80 CHARACTERS. NOR IS THIS

SHOW MULTIPLE TERMINATORS,,,,1,2,3

ALPHA FIELD TERMINATED BY "," 25 CHARACTERS. SHOW MULTIPLE TERMINATORS
NULL  FIELD TERMINATED BY ","
NULL  FIELD TERMINATED BY ","
NULL  FIELD TERMINATED BY ","
FLOAT FIELD TERMINATED BY ","  1 CHARACTERS.      1.0000
FLOAT FIELD TERMINATED BY ","  1 CHARACTERS.      2.0000
FLOAT FIELD TERMINATED BY ","  1 CHARACTERS.      3.0000

SHOW MULTIPLE BLANKS     1,2,3

ALPHA FIELD TERMINATED BY "," 26 CHARACTERS. SHOW MULTIPLE BLANKS     1
FLOAT FIELD TERMINATED BY ","  1 CHARACTERS.      2.0000
FLOAT FIELD TERMINATED BY ","  1 CHARACTERS.      3.0000
```

```
LONG BLANK LEAD                                7.2,5.978,2.3

ALPHA FIELD TERMINATED BY "," 44 CHARACTERS. LONG BLANK LEAD
FLOAT FIELD TERMINATED BY "," 5 CHARACTERS.      5.9780
FLOAT FIELD TERMINATED BY "," 3 CHARACTERS.      2.3000

REWIND,START=315,CDF=1,2,3,SPECTRA,DATA=3,3.0,3.

ALPHA FIELD TERMINATED BY "," 6 CHARACTERS. REWIND
ALPHA FIELD TERMINATED BY "=" 5 CHARACTERS. START
FLOAT FIELD TERMINATED BY "," 3 CHARACTERS.    315.0000
ALPHA FIELD TERMINATED BY "=" 3 CHARACTERS. CDF
FLOAT FIELD TERMINATED BY "," 1 CHARACTERS.      1.0000
FLOAT FIELD TERMINATED BY "," 1 CHARACTERS.      2.0000
FLOAT FIELD TERMINATED BY "," 1 CHARACTERS.      3.0000
ALPHA FIELD TERMINATED BY "," 7 CHARACTERS. SPECTRA
ALPHA FIELD TERMINATED BY "=" 4 CHARACTERS. DATA
FLOAT FIELD TERMINATED BY "," 1 CHARACTERS.      3.0000
FLOAT FIELD TERMINATED BY "," 3 CHARACTERS.      3.0000
FLOAT FIELD TERMINATED BY "," 2 CHARACTERS.      3.0000

NON-COMMA TERMINATOR AS LAST CHARACTER=

ALPHA FIELD TERMINATED BY "=" 38 CHARACTERS. NON-COMMA TERMINATOR AS LAST CHARACTER

END OF CARD DECK

ALPHA FIELD TERMINATED BY "," 16 CHARACTERS. END OF CARD DECK
```

BLANK HAS BEEN ADDED AS A TERMINATOR.

THIS IS AN EDITOR CARD

ALPHA FIELD TERMINATED BY " " 4 CHARACTERS. THIS
ALPHA FIELD TERMINATED BY " " 2 CHARACTERS. IS
ALPHA FIELD TERMINATED BY " " 2 CHARACTERS. AN
ALPHA FIELD TERMINATED BY " " 6 CHARACTERS. EDITOR
ALPHA FIELD TERMINATED BY "," 4 CHARACTERS. CARD

THIS IS NOT 100

ALPHA FIELD TERMINATED BY " " 4 CHARACTERS. THIS
ALPHA FIELD TERMINATED BY " " 2 CHARACTERS. IS
ALPHA FIELD TERMINATED BY " " 3 CHARACTERS. NOT
FLOAT FIELD TERMINATED BY "," 63 CHARACTERS. 100.0000

NOR IS THIS 00010000XX

ALPHA FIELD TERMINATED BY " " 3 CHARACTERS. NOR
ALPHA FIELD TERMINATED BY " " 2 CHARACTERS. IS
ALPHA FIELD TERMINATED BY " " 4 CHARACTERS. THIS
ALPHA FIELD TERMINATED BY "," 68 CHARACTERS.

SHOW MULTIPLE TERMINATORS,,,,1,2,3

ALPHA FIELD TERMINATED BY " " 4 CHARACTERS. SHOW
ALPHA FIELD TERMINATED BY " " 8 CHARACTERS. MULTIPLE
ALPHA FIELD TERMINATED BY "," 11 CHARACTERS. TERMINATORS
NULL FIELD TERMINATED BY ","
NULL FIELD TERMINATED BY ","
NULL FIELD TERMINATED BY ","
FLOAT FIELD TERMINATED BY "," 1 CHARACTERS. 1.0000
FLOAT FIELD TERMINATED BY "," 1 CHARACTERS. 2.0000
FLOAT FIELD TERMINATED BY "," 1 CHARACTERS. 3.0000

SHOW MULTIPLE BLANKS 1,2,3

ALPHA FIELD TERMINATED BY " " 4 CHARACTERS. SHOW
ALPHA FIELD TERMINATED BY " " 8 CHARACTERS. MULTIPLE
ALPHA FIELD TERMINATED BY " " 6 CHARACTERS. BLANKS
FLOAT FIELD TERMINATED BY "," 5 CHARACTERS. 1.0000
FLOAT FIELD TERMINATED BY "," 1 CHARACTERS. 2.0000
FLOAT FIELD TERMINATED BY "," 1 CHARACTERS. 3.0000

```
LONG BLANK LEAD                                    7.2,5.978,2.3

ALPHA FIELD TERMINATED BY " "  4 CHARACTERS. LONG
ALPHA FIELD TERMINATED BY " "  5 CHARACTERS. BLANK
ALPHA FIELD TERMINATED BY " "  4 CHARACTERS. LEAD
FLOAT FIELD TERMINATED BY "," 28 CHARACTERS.       7.2000
FLOAT FIELD TERMINATED BY ","  5 CHARACTERS.       5.9780
FLOAT FIELD TERMINATED BY ","  3 CHARACTERS.       2.3000


REWIND,START=315,CDF=1,2,3,SPECTRA,DATA=3,3.0,3.

ALPHA FIELD TERMINATED BY ","  6 CHARACTERS. REWIND
ALPHA FIELD TERMINATED BY "="  5 CHARACTERS. START
FLOAT FIELD TERMINATED BY ","  3 CHARACTERS.     315.0000
ALPHA FIELD TERMINATED BY "="  3 CHARACTERS. CDF
FLOAT FIELD TERMINATED BY ","  1 CHARACTERS.       1.0000
FLOAT FIELD TERMINATED BY ","  1 CHARACTERS.       2.0000
FLOAT FIELD TERMINATED BY ","  1 CHARACTERS.       3.0000
ALPHA FIELD TERMINATED BY ","  7 CHARACTERS. SPECTRA
ALPHA FIELD TERMINATED BY "="  4 CHARACTERS. DATA
FLOAT FIELD TERMINATED BY ","  1 CHARACTERS.       3.0000
FLOAT FIELD TERMINATED BY ","  3 CHARACTERS.       3.0000
FLOAT FIELD TERMINATED BY ","  2 CHARACTERS.       3.0000


NON-COMMA TERMINATOR AS LAST CHARACTER=

ALPHA FIELD TERMINATED BY " "  9 CHARACTERS. NON-COMMA
ALPHA FIELD TERMINATED BY " " 10 CHARACTERS. TERMINATOR
ALPHA FIELD TERMINATED BY " "  2 CHARACTERS. AS
ALPHA FIELD TERMINATED BY " "  4 CHARACTERS. LAST
ALPHA FIELD TERMINATED BY "="  9 CHARACTERS. CHARACTER


END OF CARD DECK

ALPHA FIELD TERMINATED BY " "  3 CHARACTERS. END
ALPHA FIELD TERMINATED BY " "  2 CHARACTERS. OF
ALPHA FIELD TERMINATED BY " "  4 CHARACTERS. CARD
ALPHA FIELD TERMINATED BY ","  4 CHARACTERS. DECK
```